Synthesis and Fluorescent Labeling of Functional Silica Nanochannels

---

Dissertation

zur

Erlangung der naturwissenschaftlichen Doktorwürde (Dr. sc. nat.)

vorgelegt der

Mathematisch-naturwissenschaftlichen Fakultät

der

Universität Zürich

von

Jan Hinrich Ramm

aus Deutschland

Promotionskomitee

Prof. Dr. Heinz Berke (Vorsitz)

Dr. Dominik Brühwiler (Leitung der Dissertation)

Prof. Dr. Roger Alberto

Zürich, 2010

Kurzfassung

Eine Anwendung von mesoporösen Silica-Materialien für Wirkstofftransport, Sensorik, Katalyse oder Logikelemente beinhaltet zumeist eine Funktionalisierung der Oberfläche unter Beibehaltung einer möglichst definierten Porengrössenverteilung. Für sophistizierte Systeme wird darüber hinaus häufig eine Multifunktionalisierung angestrebt. Bifunktionalisierte Materialien vom Typ SBA-15 basierend auf einer Iodpropylgruppe und einer weiteren funktionellen Gruppe wurden über einen in situ Syntheseweg hergestellt. Stellvertretend für mögliche Zielmoleküle wurde eine selektive Umsetzung mit zwei lumineszierenden Molekülen erzielt, die anhand der entsprechenden Emissionssignale detektiert wurden. Eine Modifizierung der gängigen MCM-41 und SBA-15 Materialien mit Nil Rot wurde über unterschiedliche Synthesewege sowie über Physisorption erzielt. Die polaritätssensitive Emission von Nil Rot wurde zur Detektion von Oberflächenpolaritäten für unterschiedlich funktionalisierte Silica-Materialien ausgenutzt. Ähnliche Untersuchungen wurden mittels Adsorption von Molekülen, welche einen twisted intramolecular charge transfer (TICT) Zustand ausbilden können, durchgeführt. Beispielhaft für die Perspektiven als Sensor-Materialien zeigten Proben von kovalent gebundenem Nil Rot eine Abhängigkeit des Emissionsmaximums gegenüber Lösungsmitteln verschiedener Polarität.

Eine kovalente Verankerung des photochromen Spiropyran wurde sowohl über einen in-situ als auch über einen postpräparativen Weg vollzogen. Die Bildung der unterschiedlichen Isomere wurde in Abhängigkeit des eingestrahlten UV und Vis Lichtes sowie des pH Wertes untersucht und mit den Edukten in Lösung verglichen. Unter dem Gesichtspunkt der Erzeugung eines durch einen externen Impuls gesteuerten Wirkstofftransportsystems, wurde ein Modellsystem auf Basis des intensiv fluoreszierenden Resorufin Anions entwickelt, dessen Freisetzung aus MCM-41 durch eine erhöhte Lumineszenzintensität in Lösung detektiert werden kann.

Einzelne Nanopartikel (quantum dots) vom Typ CdSe/ZnS wurden in funktionalisiertes mesoporöses Silica eingelagert und erste Untersuchungen bezüglich der Konzentration sowie der Lage in den Kanälen wurden vorgenommen.

Abstract

An application of mesoporous silica based materials for drug delivery systems, sensor systems, catalysis or logic gates comprises mostly a functionalization of the surface by retention of a defined pore size distribution. For sophisticated systems, multifunctionalization is typically required. Bifunctional SBA-15 type materials based on iodopropyl and a further functional group were synthesized by an in situ route. Representative for potential target molecules, a selective conversion of a bifunctionalized mesoporous silica was achieved by reaction with luminescent labels which were detected by the corresponding emission signals. Modification of the MCM-41 and SBA-15 type mesoporous silica materials with nile red was accomplished by different synthesis pathways, as well as by physisorption. The polarity sensitive emission of nile red was exploited for the detection of the surface polarity of various functionalized mesoporous silicas. Similar studies were conducted by the adsorption of molecules with twisted intramolecular charge transfer (TICT) states. Covalently attached nile red samples showed a dependence of the emission maximum on the solvent polarity, exemplifying the potential of such materials for sensing applications.

Covalent attachment of photochromic spiropyran was accomplished by an in situ and a postsynthetic route. The formation of the different isomers was investigated in dependence of irradiation with UV and Vis light as well as the pH value and compared to the educts. Under the aspect of developing a drug delivery system controlled by an external stimulus, a model system based on the fluorescent resorufin anion was prepared. Desorption of resorufin from MCM-41 can be detected by an increased luminescence intensity in solution.

Single nanoparticles (quantum dots) of CdSe/ZnS were included in functionalized mesoporous silica and first studies concerning their concentration and arrangement in the channels were conducted.

Acknowledgment

While working on my dissertation at the ACI of the university of Zürich I obtained various support, wherefore I want to express my gratitude to the following persons:

I am very grateful to Dr. Dominik Brühwiler for the supervision of my thesis. It was very convenient and fruitful to interact in an uncomplicated way, by which I always received time for questions and discussions.

Prof. Dr. Heinz Berke is thanked for the chairing of my defence and acting as the representative for my dissertation before the faculty.
For acting as a surveyor of my thesis I would like to thank Prof. Dr. Roger Alberto.

For the financial support the Swiss National Science Foundation (Project 200020-117591) and the European Commission through the Human Potential Program (Marie Curie RTN Nanomatch, Grant No. MRTN-CT-2006-035884) are thanked.

I highly appreciated the good and helpful atmosphere in the working group also apart of work. Therefore I would like to thank all former and actual group members: Hanna, Christian, Le-Quyenh, André, Christina, Zhao, Christophe, Igor, Nando and Thomas.
For interesting, helpful and also distracting discussions at lunch and coffee time or just by meeting at the institute floor, at celebrations, or at sports all former and actual members of the ACI are thanked.

Thanks to Anna is given for the pleasant cooperation and the analysis of quantum dot loaded silica samples at Tübingen.
Christina is thanked for her work in the synthesis of co-condensed spiropyran samples.

For their competent help at various technical problems and for the measurement of various elemental analyses and NMR spectra I am grateful to Balz, Hans-Peter, Heinz and Thomas.

Hard to honour enough, but in every way most important was the support I gained apart from university. Therefore I sincerely thank my family and all my friends for their encouragement and also the distraction from work if needed.

Table of contents

Introduction **1**

Theory **5**

2.1 Mesoporous silica **6**

2.1.1 Synthesis 6

2.1.2 Functionalization 14

Grafting 14

Co-Condensation 17

Comparison of grafting and co-condensation 18

External surface grafting 18

2.1.3 Labeling with luminescent molecules 19

2.1.4 Photoreactive systems 20

2.2 Nitrogen sorption **21**

Results **31**

3.1 Silica host **32**

3.2 Synthesis of bifunctionalized mesoporous silica with iodopropyl groups **33**

High iodopropyl content 36

Conclusion 38

3.3 Inclusion of Resorufin **39**

3.3.1 Adsorption 39

3.3.2 Release 42

Conclusion 45

3.4 Functionalization with Nile Red **46**

3.4.1 Introduction 46

3.4.2 Inclusion of nile red 48

3.4.3 Detection of surface polarity 50

3.4.4 Covalent attachment 53

3.4.5 Co-condensation of nile red ... 58

Conclusion ... 63

3.5 Coupling of organic dyes to iodopropyl functionalized SBA type silica ... 64

3.5.1 Coupling of nile red ... 64

3.5.2 Hybrid materials by functionalization with different fluorescent dyes ... 66

Conclusion ... 69

3.6 Adsorption of TICT molecules ... 70

Conclusion ... 73

3.7 Functionalization with spiropyran ... 74

3.7.1 Introduction ... 74

3.7.2 Grafting ... 75

3.7.3 Co-condensation ... 77

3.7.4 Pore size analysis ... 78

3.7.5 Photochemical properties ... 80

Absorption ... 82

Emission ... 83

3.7.6 Emission of solid sample ... 86

Conclusion ... 88

3.8 Adsorption of quantum dots ... 89

Conclusion ... 97

Conclusion/Outlook ... 99

Experimental ... 103

5.1 Synthesis of mesoporous silicas ... 104

5.1.1 Synthesis of MCM-41 ... 104

Template removal ... 104

5.1.2 Synthesis of SBA-15 ... 104

Template removal ... 105

5.1.3 Large pore SBA-15 ... 105

5.2 Functionalization of mesoporous silica ... 106

5.2.1 Propyltrimethylammonium chloride ... 106
5.2.2 Aminopropyl ... 106
5.2.3 Bromopropyl ... 106
5.2.4 Octadecyl ... 107
5.2.5 Propionitrile ... 108
5.2.6 Carboxyl ... 108
5.2.7 Silylation ... 109

5.3 Synthesis of organic dyes ... 110

5.3.1 Synthesis of nile red ... 110
5.3.1.1. 5-Diethylamino-2-nitrosophenol (DNP) ... 110
5.3.1.2. 9-Diethylamino-2-hydroxy-5*H*-benzo[*a*]phenoxazin-5-one (HNR) ... 111
5.3.1.3. 9-Diethylamino-5-oxo-5*H*-benzo[*a*]phenoxazin-2-yl-(5-carboxy)-pentanoate ... 112
5.3.2 Synthesis of spiropyran ... 113
5.3.2.1. 1-(3-Carbomethoxypropyl)-3,3-dimethyl-2-methyleneindoline ... 113
5.3.2.2. 1´-(3-Carbomethoxypropyl)-3´,3´-dimethyl-6-nitrospiro[2*H*-1]benzopyran-2,2´-indoline (SPCOOMe) ... 114
5.3.2.3. 1´-(3-Carboxypropyl)-3´,3´-dimethyl-6-nitrospiro-[2*H*-1]-benzopyran-2,2´-indoline (SPCOOH) ... 115

5.4 Grafting of fluorescent dyes to the silica surface ... 116

5.4.1 Coupling with spiropyran ... 116
5.4.2 Grafting of nile red by different linking groups ... 116
5.4.2.1. Ether bond ... 116
5.4.2.2. Amide bond ... 116
5.4.2.3. Ester bond ... 117
5.4.3 Coupling of fluorescein isothiocyanate ... 117

5.5 Co-Condensation ... 118

5.5.1 Spiropyran co-condensed in MCM-41 ... 118
5.5.1.1. Coupling of spiropyran with APTES ... 118
5.5.1.2. Co-condensation ... 118
5.5.1.3. Extraction ... 118

5.5.2 SBA with iodopropyl groups ... 119

5.5.3 HNR co-condensed in SBA-15 ... 119

5.6 Adsorption from solution/dispersion ... 120

5.6.1 Nile red ... 120

5.6.2 Resorufin ... 120

5.6.3 Dimethylaminobenzonitrile (DMABN) ... 120

5.6.4 4,4´-Diaminodiphenyl sulfone (DAPS) ... 121

5.6.5 CdSe/ZnS quantum dots ... 121

5.7 Determination of dye contents ... 122

5.7.1 Dissolving in $NaOH_{(aq)}$ ... 122

5.7.1.1. HNR modified silica ... 122

5.7.1.2. Fluorescein isothiocyanate modified silica ... 122

5.7.1.3. Resorufin loaded silica ... 122

5.7.2 Extraction in ethanol ... 123

5.7.2.1. Resorufin loaded silica ... 123

5.7.2.2. Nile red loaded silica ... 123

5.8 Instrumentation ... 124

Nitrogen sorption ... 124

IR ... 124

Elemental analysis ... 124

UV/Vis ... 124

^{13}C-NMR and ^{1}H-NMR ... 125

SEM ... 125

Luminescence ... 125

Confocal microscopy ... 125

Appendix ... 127

List of abbreviations ... 128

Publications and conference contributions ... 131

Curriculum Vitae ... 133

Chapter 1

Introduction

Materials with large surface areas are of particular interest due to their high potential catalytic activity. New nanostructures offer larger surface areas than traditional bulk materials. The synthesis can be achieved by creating either small particles or by designing materials with large void space compared to the amount of bulk material. Highly dispersed metal catalysts or quantum dots are examples of the first group, whereas microporous and mesoporous materials such as large surface inorganic oxides, carbons and silicas belong to the second.

Porous structures offer additional advantages compared to nanosized particles, due to their ability to either include molecules inside their voids or selectively exclude them by chemical and sterical properties. Zeolites, which are applied in many fields, occur in nature and the synthesis was pioneered by Union Carbide in the 1950´s.[1] Pore surfaces up to about 900 m²/g could be reached. Zeolites are limited to the microporous range and typically feature pore sizes between 3 Å and 13 Å.

An example for rather newly developed porous materials with large surface areas are carbon nanotubes (CNT´s) which were first observed in 1991 in the carbon soot of electrodes after arc discharge.[2] After the discovery of CNT´s, the reports on potential applications of CNT´s skyrocketed. This is seen among other things by the large amount of articles concerning the topic. In some cases, surface areas of 1000 m²/g are possible depending on synthesis methods and modifications,[3] although typical surface areas are much lower and pore size distributions are broad. Additionally, porous carbons should also be mentioned, as they constitute a wide research field as well.[4]

Besides this, the M41S family, a mesoporous silica class based on an entirely different synthesis strategy, was reported in 1992.[5] Independently, Yanagsawa et al. developed the FSM-16 family in 1990.[6] These syntheses were conducted by using a liquid crystal template for the formation of nanochannels. Surface areas of around 1000 m²/g were obtained and therefore the materials were highly interesting for catalytic applications. Compared to

[1] D. W. Breck, W. G. Eversole, R. M. Milton, T. B. Reed, T. L. Thomas, *J. Am. Chem. Soc.* **1956**, *78*, 5963; T. B. Reed, D. W. Breck, *J. Am. Chem. Soc.* **1956**, *23*, 5972.
[2] S. Iijima, *Nature* **1991**, *354*, 56.
[3] S.-H. Tsai, C.-T. Shiu, S.-H. Lai, H.-C. Shih, *Carbon* **2002**, *40*, 1597.
[4] A. Stein, Z. Wang, M. A. Fierke, *Adv. Mat.* **2009**, *21*, 265; L. Chengdu, L. Zuojiang, D. Sheng, *Angew. Chem. Int. Ed.* **2008**, *47*, 3696; R. Ryoo, S. H. Joo, M. Kruk, M. Jaroniec, *Adv. Mater.* **2001**, *13*, 677; Y. Wan, Y. Shi, D. Zhao, *Chem. Mater.* **2007**, *20*, 932.
[5] J. S. Beck, J. C. Vartuli, W. J. Roth, M. E. Leonowicz, C. T. Kresge, K. D. Schmitt, C. T. W. Chu, D. H. Olson, E. W. Sheppard, *J. Am. Chem. Soc.* **2002**, *114*, 10834; C. T. Kresge, M. E. Leonowicz, W. J. Roth, J. C. Vartuli, J. S. Beck, *Nature* **1992**, *359*, 710.
[6] T. Yanagsawa, T. Shimizu, K. Kuroda, C. Kato, *Bull. Chem. Soc. Jpn.* **1990**, *63*, 988.

zeolites, the pore diameter is increased to the mesoporous range. Although the framework of the materials is not crystalline, the pore size is well defined as, e.g., in contrast to CNT´s. Soon after this initial work, other mesoporous silicas based on a templating approach were reported (e.g. SBA-15[7]). Synthetic pathways and material properties such as morphology, surface areas and pore sizes have been thoroughly investigated leading to a variety of systems which cover the mesopore range between 2 and 30 nm.[8]

Other mesoporous materials were prepared by using the same principle,[9] including different kinds of metal oxides (aluminia-,[10] zirconia-, titania-,[11,12] niobia-,[13,14] tin-,[15] manganese oxide[16] and others),[15,17,18] metal sulfides,[19,20] metal phosphates,[21,22] metals,[23,24,25] polymers and carbon.[26] Despite these efforts, there are still issues which need further investigation, concerning, e.g., hydrothermal stability, utilization as thin films or improvements in the regulation of pore size and surface according to the required demands.

The fact that the properties of mesoporous silicas generally can be controlled by manipulating the surface with modification of different silanes is particularly challenging and inspiring. This offers a huge palette of possibilities for the chemist to construct a system for his actual demands. Therefore, the functionalization of the nanochannels or the silica structure is a highly investigated topic.[27,28] Various potential applications benefit from these possibilities.

---

[7] D. Zhao, Q. Huo, J. Feng, B. F. Chmelka, G. D. Stucky, *J. Am. Chem. Soc.* **1998**, *120*, 6024.
[8] Y. Wan, D. Zhao, *Chem. Rev.* **2007**, *107*, 2821.
[9] Y. Wan, H. Yang, D. Zhao, *Acc. Chem. Res.* **2006**, *39*, 423.
[10] A. B. Stephen, J. P. Thomas, *Angew. Chem. Int. Ed.* **1996**, *35*, 1102.
[11] M. A. David, Y. Y. Jackie, *Angew. Chem. Int. Ed.* **1995**, *34*, 2014.
[12] K. L. Frindell, J. Tang, J. H. Harreld, G. D. Stucky, *Chem. Mater.* **2004**, *16*, 3524.
[13] M. A. David, Y. Y. Jackie, *Angew. Chem. Int. Ed.* **1996**, *35*, 426.
[14] T. Sun, J. Y. Ying, *Nature* **1997**, *389*, 704.
[15] P. Yang, D. Zhao, D. I. Margolese, B. F. Chmelka, G. D. Stucky, *Chem. Mater.* **1999**, *11*, 2813.
[16] Z.-R. Tian, W. Tong, J.-Y. Wang, N.-G. Duan, V. V. Krishnan, S. L. Suib, *Science* **1997**, *276*, 926.
[17] Q. Huo, D. I. Margolese, U. Ciesla, P. Feng, T. E. Gier, P. Sieger, R. Leon, P. M. Petroff, F. Schüth, G. D. Stucky, *Nature* **1994**, *368*, 317.
[18] X. Zhou, T. Conradsson, M. Klingstedt, M. S. Dadachov, M. O´Keffee, *Nature* **2005**, *437*, 716.
[19] P. V. Braun, P. Osenar, S. I. Stupp, *Nature* **1996**, *380*, 325.
[20] M. J. MacLachlan, N. Coombs, G. A. Ozin, *Nature* **1999**, *397*, 681.
[21] M. Tiemann, M. Fröba, *Chem. Mater.* **2001**, *13*, 3211.
[22] U. Ciesla, S. Schacht, G. D. Stucky, K. K. Unger, F. Schüth, *Angew. Chem. Int. Ed.* **1996**, *35*, 541.
[23] G. S. Armatas, M. G. Kanatzidis, *Nature* **2006**, *441*, 1122.
[24] D. Sun, A. E. Riley, A. J. Cadby, E. K. Richman, S. D. Korlann, S. H. Tolbert, *Nature* **2006**, *441*, 1126.
[25] G. S. Attard, P. N. Bartlett, N. R. B. Colemann, J. M. Elliott, J. R. Owen, J. H. Wang, *Science* **1997**, *278*, 838.
[26] M. Yan, G. Dong, Z. Fuqiang, S. Yifeng, Y. Haifeng, L. Zheng, Y. Chengzhong, T. Bo, Z. Dongyuan, *Angew. Chem. Int. Ed.* **2005**, *44*, 7053.
[27] A. Stein, B. J. Melde, R. C. Schroden, *Adv. Mater.* **2000**, *12*, 1403.
[28] A. Vinu, K. Z. Hossain, K. Ariga, *J. Nanosci. Nanotech.* **2005**, *5*, 347.

Examples are the modifications with metals or organic moieties for catalysis, adsorbents for heavy metals, inclusion of pharmaceutical compounds, optical applications and sensing or immobilisation of biomolecules.[29,30,31,32,33]

This work focuses on the functionalization of the nanochannel surface by different synthetic approaches and on the subsequent adsorption and attachment of fluorescent molecules. The specific introduction of a fluorescent moiety can provide information on the accessibility of functional groups and their environment in the nanochannels, offering perspectives in the field of sensing applications. Furthermore, the possibility to change the nanochannel properties by an external stimulus such as irradiation is offered by the attachment of adequate luminescent moieties.

[29] Q. Yang, J. Liu, L. Zhang, C. Li, *J. Mater. Chem.* **2009**, *19*, 1945; A. Corma, H. Garcia, *Adv. Synth. Catal.* **2006**, *348*, 1391; J. M. Thomas, R. Raja, *J. Organomet. Chem.* **2004**, *689*, 4110.
[30] L. F. Giraldo, B. L. López, L. Pérez, S. Urrego, L. Sierra, M. Mesa, *Macromol. Symp.* **2007**, *258*, 129.
[31] Y. Klichko, M. Liong, E. Choi, S. Angelos, A. E. Nel, J. F. Stoddart, F. Tamanoi, J. I. Zink, *J. Am. Ceram. Soc.* **2009**, *92*, S2.
[32] L. Pasqua, S. Cundari, C. Ceresa, G. Cavaletti, *Curr. Med. Chem.* **2009**, *16*, 3054; I. I. Slowing, J. L. Vivero-Escoto, C.-W. Wu, V. S.-Y. Lin, *Adv. Drug Delivery Rev.* **2008**, *60*, 1278.
[33] S. A. El-Safty, *J. Mater. Sci.* **2009**, *44*, 6764.

Chapter 2

Theory

2.1 Mesoporous silica

2.1.1 Synthesis

A definition for mesoporous materials is given by IUPAC as materials with pore sizes between 2 and 50 nm. Mesoporous silicas, which offer distinct pore sizes between approximately 2 and 30 nm, nearly fill this range and fall in between microporous materials, such as zeolites, nanotubes, micelles, on one side and large pore sized mesopores up to 50 nm and macroporous materials such as anodic alumina or colloid arrays on the other side (Figure 1).

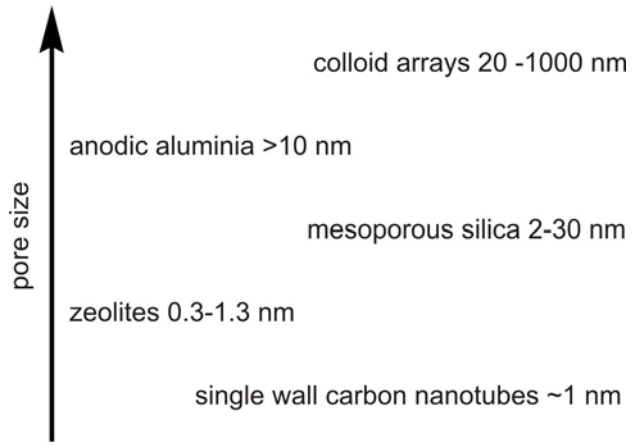

Figure 1 Pore size range of typical porous materials.

Mesoporous silica materials have attracted increasing interest in the last 20 years. The initiation of a considerable research effort was the discovery of the M41S family[34] by the Mobil Corporation in 1992 which has resulted in the development of various new syntheses and applications for silica based materials. Six years later, another milestone was achieved as SBA-15 (Santa Barbara Amorphous type material) was reported by researchers of the University of California at Santa Barbara.[35]

Pillard clays with mesopores have been investigated extensively since 1980. However, broad pore size distributions (PSD´s) and disordered, rectangular pores, which are not fully opened, are typically obtained.[36] An important improvement resulted from the use of a template to form the mesopores in a hydrothermal synthesis. Advantageous, compared to other traditional

[34] J. S. Beck, J. C. Vartuli, W. J. Roth, M. E. Leonowicz, C. T. Kresge, K. D. Schmitt, C. T. W. Chu, D. H. Olson, E. W. Sheppard, *J. Am. Chem. Soc.* **2002**, *114*, 10834; C. T. Kresge, M. E. Leonowicz, W. J. Roth, J. C. Vartuli, J. S. Beck, *Nature* **1992**, *359*, 710.
[35] D. Zhao, Q. Huo, J. Feng, B. F. Chmelka, G. D. Stucky, *J. Am. Chem. Soc.* **1998**, *120*, 6024.
[36] A. Corma, *Chem. Rev.* **1997**, *97*, 2373.

inorganic material syntheses like that of zeolites performed at high temperature or pressure, are the relatively mild reaction conditions.

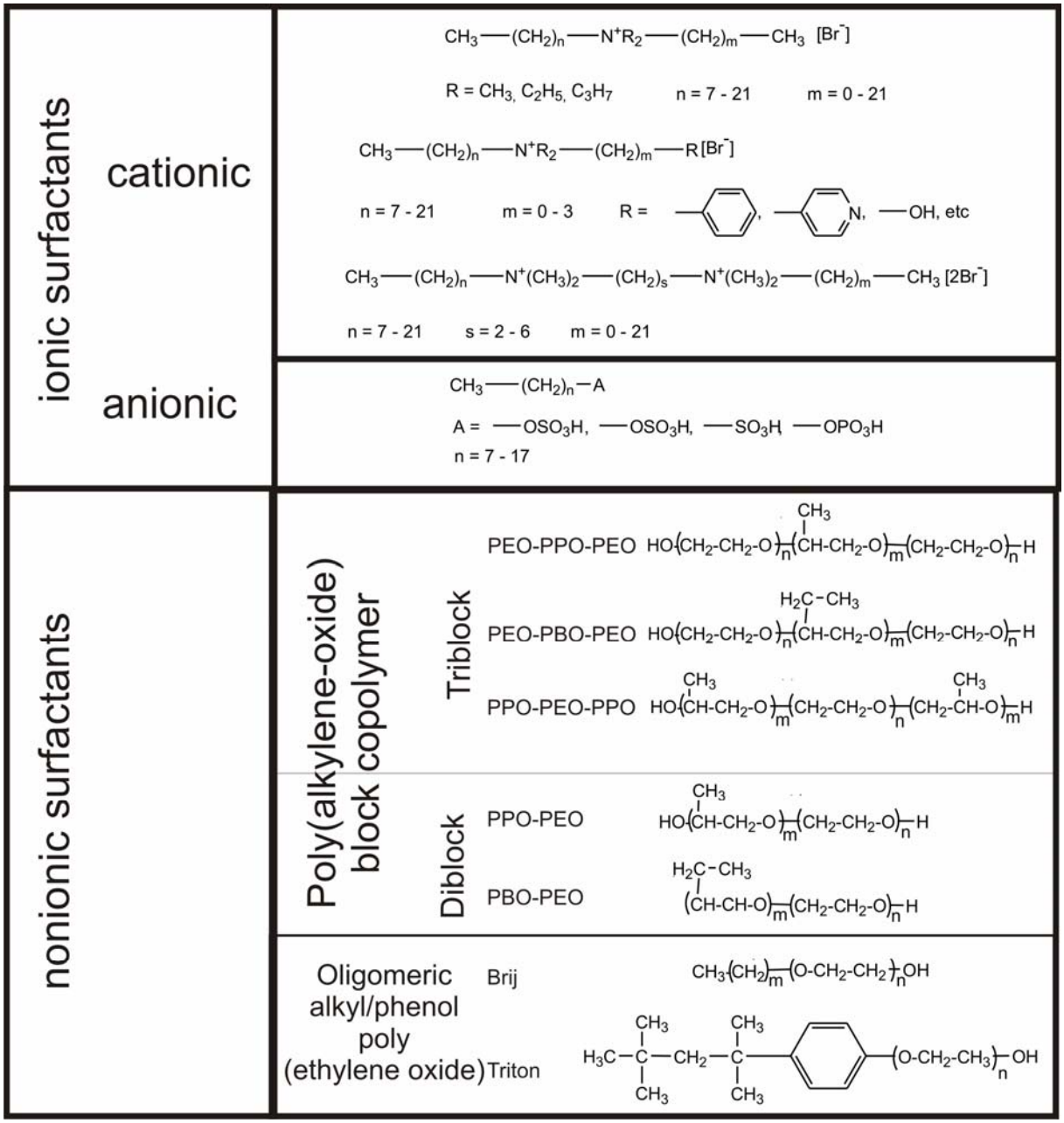

Table 1 Selection of typical surfactants.

Cetyltrimethylammonium bromide (CTAB) was one of the first surfactants used as a template. Many other structure-directing agents (SDA´s) have been reported since. An overview of the most common SDA´s is given in Table 1. A basic differentiation can be introduced by dividing into anionic, neutral and cationic surfactants. Anionic surfactants are relatively rare due to the repulsive interactions with the anionic silica species present in basic

media. However, examples of aminosilanes or quaternary aminosilanes as a co-structure-directing agent (CSDA) in order to overcome the repulsive effect are given by Che et al.[37]

For the formation of the mesoporous structure, the interactions between surfactant and inorganic species are crucial. A classification was given by Huo et al. [38,39] who defined the following possible combinations of cationic and anionic surfactants S^+, S^-, inorganic precursors I^+, I^- and also of counter ions X^+, X^- as mediators: S^+I^-, S^-I^+, $S^+X^-I^+$, $S^-X^+I^-$. In addition, neutral surfactants (S°) can be used to generate $S°H^+X^-I^+$ and S°I° interactions. The ionic structures are attracted by Coulomb interactions, whereas the non-ionic moieties are stabilized by hydrogen bonding (Figure 2).

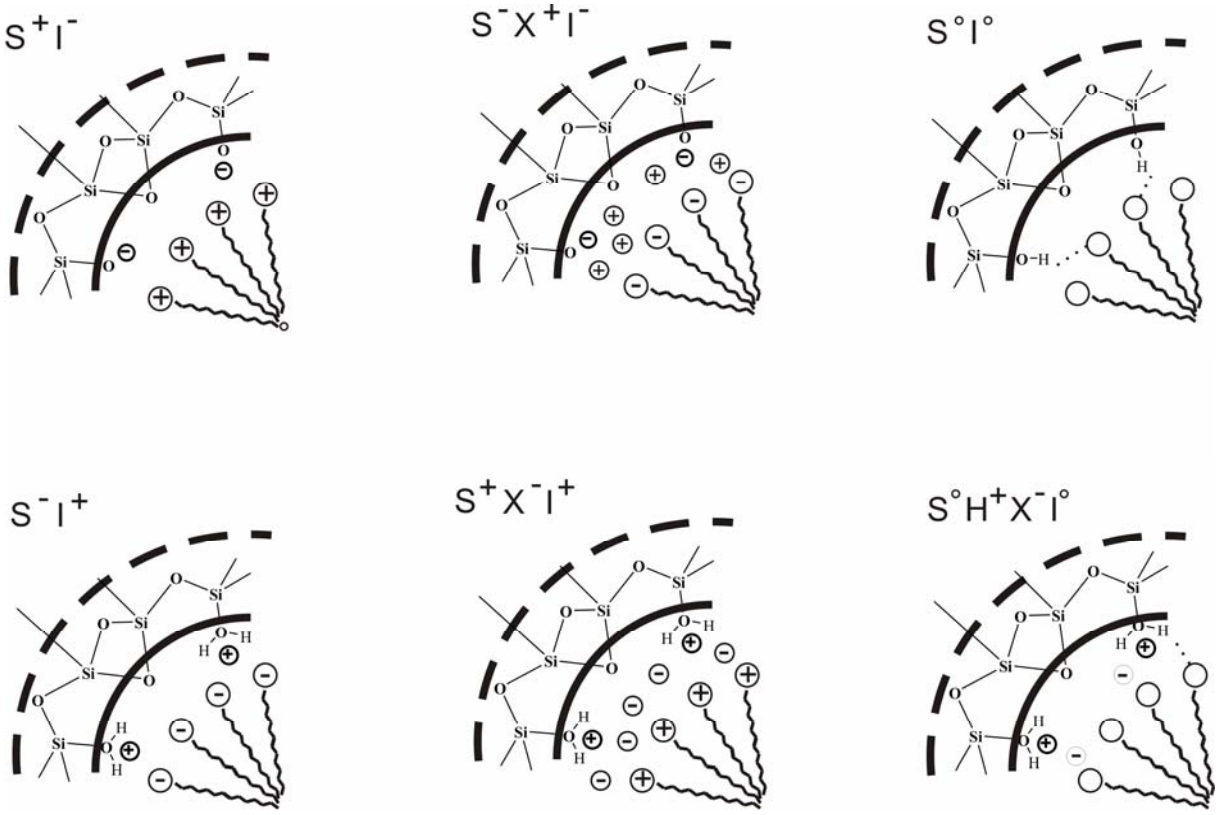

Figure 2 Interaction types between silica precursor and SDA.

The general formation mechanism by an initial liquid crystal templating (LCT) approach was first formulated by Mobil scientists.[40] Later, two main pathways, namely a cooperative self-assembly and a "true" LCT process, were proposed. The latter is using a real semi-liquid-

[37] S. Che, A. E. Garcia-Bennett, T. Yokoi, K. Sakamoto, H. Kunieda, O. Terasaki, T. Tatsumi, *Nat. Mater.* **2003**, *2*, 801.
[38] Q. Huo, D. I. Margolese, U. Ciesla, P. Feng, T. E. Gier, P. Sieger, R. Leon, P. M. Petroff, F. Schüth, G. D. Stucky, *Nature* **1994**, *368*, 317.
[39] Q. Huo, D. I. Margolese, U. Cesla, D. G. Demuth, P. Feng, T. E. Gier, P. Sieger, A. Firouzi, B. F. Chmelka, F. Schüth, G. D. Stucky, *Chem. Mater.* **1994**, *6*, 1176.
[40] J. S. Beck, J. C. Vartuli, W. J. Roth, M. E. Leonowicz, C. T. Kresge, K. D. Schmitt, C. T. W. Chu, D. H. Olson, E. W. Sheppard, S. B. McCullen, J. B. Higgins, J. L. Schlenker, *J. Am. Chem. Soc.* **1992**, *114*, 10834.

crystal mesophase, which needs a sufficiently high concentration of surfactants in order to form a liquid crystal phase. The silica is growing around this template and forms the structure of the liquid crystal mesophase. Compared to the cooperative self-assembly, relatively high surfactant concentrations are needed in order to form stable micelle structures leading generally to the formation of mesostructures with relatively small curvature. The cooperative self-assembly process emanates from the interactions between silicates and surfactants. For ionic surfactants, a mechanism was proposed by Huo et al.[38] Initially, interactions between surfactants and silicate species occur which are driven by Coulomb forces. The silicate species polymerize and change the charge density. This in turn influences the arrangement of the surfactants. The process is therefore driven by the cooperative effects of both silicate and surfactant. The final mesophase is the ordered 3-D arrangement with the lowest interface energy. Studies on non-ionic surfactants were conducted by Ruthstein et al. who investigated the formation of SBA-15 with in-situ measurements.[41,42] They found a continuous transformation from spheroidal micelles into threadlike micelles by addition of TMOS. The silicate species adsorb and polymerize at the interface and simultaneously reduce their curvature, which leads to the formation of threadlike micelles.

In conclusion, the decisive parameter for the formation of the mesoporous material is the interaction of surfactants and inorganic precursor. This can be expressed by the free energy after a formula from Monnier and Huo et al.[43,44]

$$\Delta G = \Delta G_{inter} + \Delta G_{wall} + \Delta G_{intra} + \Delta G_{sol} \qquad (1)$$

where ΔG_{inter} is the free energy between inorganic walls and micelles, ΔG_{wall} is the structural free energy of the inorganic framework, ΔG_{intra} represents the van der Waals forces between the surfactants in the micelles and ΔG_{sol} gives the free energy of the soluted species. A highly negative value of ΔG_{inter} is therefore most desirable in order to achieve a mesoporous structure.

A hydrothermal pathway is used for the synthesis of mesoporous silica, following a reaction in solution at convenient temperatures. The surfactant has to be dissolved in water as the

[41] S. Ruthstein, V. Frydman, S. Kababya, M. Landau, D. Goldfarb, *J. Phys. Chem. B* **2003**, *107*, 1739.
[42] S. Ruthstein, J. Schmidt, E. Kesselman, Y. Talmon, D. Goldfarb, *J. Am. Chem. Soc.* **2006**, *128*, 3366.
[43] Q. Huo, D. I. Margolese, U. Ciesla, D. G. Demuth, P. Feng, T. E. Gier, P. Sieger, A. Firouzi, B. F. Chmelka, *Chem. Mater.* **1994**, *6*, 1176.
[44] A. Monnier, F. Schüth, Q. Huo, D. Kumar, D. Margolese, R. S. Maxwell, G. D. Stucky, M. Krishnamurty, P. Petroff, A. Firouzi, M. Janicke, B. F. Chmelka, *Science* **1993**, *261*, 1299.

commonly used solvent. The silicate precursors are subsequently added and undergo hydrolysis. A sol of oligomers is formed which are interacting with the surfactants and polycondensation occurs, inducing the precipitation from a gel. This first step is relatively fast and occurs in about 5 min after addition of the silicate source in case of ionic surfactants. For non-ionic surfactants, as used for the formation of SBA-15, longer precipitation times of about 30 min are required. The synthesis can be accomplished in acidic or in basic solution. In both cases, the pH value plays an important role, due to its influence on the condensation rate. Under basic conditions, a pH between 9.5 and 12.5 is used, at which polymerization and cross-linking of the silicate are reversible leading to the formation of a distinct mesoporous structure. The standard synthesis of SBA-15 is achieved under acidic conditions using a solution of about 2 M HCl. Lower pH excessively increases the condensation rate and results in unspecific structures, whereas higher pH reduces the precipitation.

To form an ordered mesostructure and allow further reorganization, the mixture is stirred for some time (normally some hours). A temperature in the range of -10 to 130 °C can be used. Usually a RT treatment is applied for most synthesis, as for the standard synthesis of MCM-41 and SBA-15 used in this work.

The hydrothermal treatment, which can continue for days, follows the reaction in solution, in order to complete the condensation and to form an ordered mesostructure. Temperatures are typically in the range of 80 to 150 °C. Higher temperatures are not recommended due to a degradation of the periodicity and the decomposition of the surfactants. The hydrothermal treatment is crucial to refine the mesoporous properties of the product. The mesostructures undergo reorganization, growth and crystallization.

Two main routes of removing the organic template exist, either by solvent extraction or by calcination. Although calcination reduces the amount of silanol groups, it allows a complete template removal and is achieved with relatively small synthetic effort. However, extraction can be done under much more moderate conditions and offers therefore advantages as will be discussed later.

Characterisation of porous silicas is accomplished on one hand by the determination of the pore diameter and the pore wall thickness and on the other hand by the symmetry of the mesostructure. Variation of the synthesis conditions leads to a variety of different compounds. The amount and type of the SDA, the addition of compounds which affect the micelle formation, and the temperature play an eminent role for obtaining the desired final mesostructure. In order to predict the influence of the surfactant on the product, specific

parameters are utilized. In particular these are the packing parameter *g*, which is defined as the volume of surfactant hydrophobic chains plus cosolvent (*V*) divided by the effective hydrophilic head group area at the aqueous micelle surface (a_0) and the kinetic surfactant tail length (*l*) ($g = V/a_0*l$) or the hydrophilic/hydrophobic volume ratios *Vh/Vl*, which are used to estimate the resulting structure. A lower packing factor or higher hydrophilic part, which means higher volume ratios, favours the alignment of micelles with high curvature, whereas for high packing factor and low *Vh/Vl*, structures with lower curvature and ultimately lamellar structures are favoured. In this sense, spherical, cylindrical, 3D cylindrical and lamellar micelles are formed by lowering the micelle curvature to result in a variety of structures from cubic (P3m) to hexagonal ($p6^3/mmc$), 2D hexagonal (p6mm), cubic ($Ia\bar{3}d$) and finally lamellar. Increasing the amount of surfactants affects the micelle structure in a similar way. Table 2 gives an overview of typical structures and the associated surfactants.

The pore size is mainly controlled by the size of the hydrophobic parts of the micelles and therefore particularly by the chain length. Smaller micelles generally result in smaller pore sizes. However, although this system fits very well for simple cationic surfactants such as CTAB, also other parameters have to be taken into account. For the synthesis of SBA-15 with P123 for example, the temperature and also the time of the hydrothermal treatment can influence the pore sizes in a remarkable way, ranging from 4.6 to 11.4 nm.[45] A considerable effect can be assigned to the hydrophilic parts of P123 which are known to induce the formation of microporosity, particularly at low synthesis temperature. An explanation is given by a dehydration of the PEO heads for higher temperatures. The reduced hydrophilic part of the SDA causes a reduced interaction between PEO chains of nearby micelles and an increased effective size of the micelles as interactions between silicate species and SDA are decreased. The obtained material features therefore larger pore sizes and thinner pore walls with reduced or no microporosity.[46,47]

[45] A. Galarneau, H. Cambon, F. Di Renzo, R. Ryoo, M. Choi, F. Fajula, *New J. Chem.* **2003**, *27*, 73.
[46] A. Nossoy, E. Haddad, F. Guenneau, A. Galarneau, F. Di Renzo, F. Fajula, A. Gedeon, *J. Phys. Chem. B* **2003**, *107*, 12456.
[47] A. Galarneau, H. Cambon, F. Di Renzo, F. Fajula, *Langmuir* **2001**, *17*, 8328.

	space group	materials	surfactants
2D	p6mm	MCM-41 FSM-16 SBA-15	CTAB P123
	cmm	SBA-8	CTAB
	layered	MCM-50 KSW-2	CTAB CTACl
3D	$Fm\bar{3}m$	FDU-12 KIT-5	F127
	$Im\bar{3}m$	SBA-16	F127
	$Pm\bar{3}n$	SBA-1	SBA-6
	$Pm\bar{3}m$	SBA-11	Brij 56
	$Fd\bar{3}m$	FDU-2	$C_{m\text{-}2\text{-}3\text{-}1}$(m = 14, 16. 18)*
	$P6_3/mmc$	SBA-12	Brij 76
	$Ia\bar{3}d$	MCM-48 FDU-5	CTAB P123

*Tri-headed-quaternary ammonium alkyl chain

Table 2 Overview of known silica mesostructures designed by LCT.

Another important method of pore size tuning is by the addition of swelling agents. A huge variety of compounds have been used for this purpose. Generally, the added compounds are included in the micelles, where they cause an enlargement. By this method, pore sizes of up to 30 nm could be produced, although the pore size distribution was broadened significantly.[48] Relatively distinct pore sizes up to 20 nm can be synthesized by addition of the frequently used TMB as a swelling agent.[49]

A demanding topic is the tailoring of the morphology and size of the particles. Uniformly sized spheres are for example desirable as column packing materials for chromatographic separation and controlled delivery, films in catalysis or monoliths for certain optical applications.[50,51,52,53]

[48] D. Zhao, J. Feng, Q. Huo, N. Melosh, G. H. Fredrickson, B. F. Chmelka, G. D. Stucky, *Science* **1998**, *279*, 548.
[49] L. Wang, T. Qi, Y. Zhang, J. Chu, *Microporous Mesoporous Mater.* **2006**, *91*, 156.
[50] T. Martin, A Galarneau, F. Di Renzo, D. Brunel, F. Fajula, *Chem. Mater.* **2004**, *16*, 1725; M. Mesa, L. Sierra, B. López, A. Ramirez, J.-L. Guth, *Solid State Sci.* **2003**, *5*, 1303; A. Galarneau, J. Iapichella, D. Brunel, F.

However, the preparation of distinct morphologies is difficult as it is affected by the shape of the surfactants, hydrolysis and condensation of silicate species and possible addition of inorganic salts, swelling agents, cosolvents or cosurfactants. Figure 3 gives two examples of well defined morphologies, namely hexagonal fibers[54] and spheres (5.1.3)

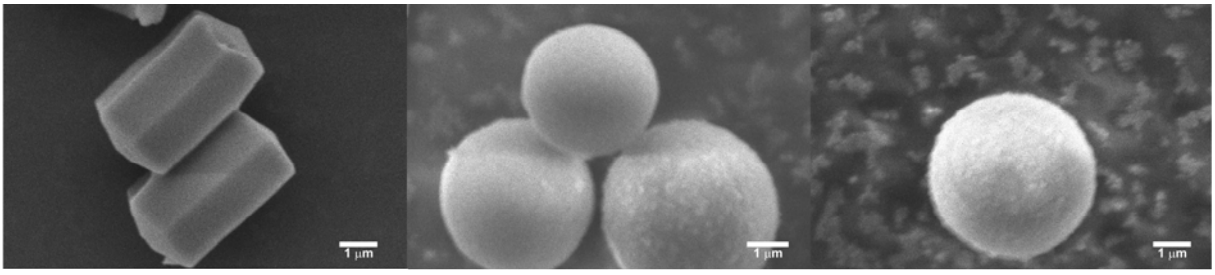

Figure 3 SEM images of hexagonal (left) and spherical (middle and right) mesoporous silica.

This thesis is focused mainly on SBA-15 and MCM-41. Therefore, a brief characterisation of the products obtained by the standard synthesis is summarized here. Both are 2D mesostructures with p6mm space group. Depending on the synthesis conditions, MCM-41 exhibits generally pore sizes in the range of 1.6 to 4.2 nm and SBA-15 from 4.6 to 11.4 nm. While MCM-41 consists only of mesopores, micropores can be present in SBA-15. The pore walls of SBA-15, which are between 20 Å and 40 Å for higher synthesis temperature, are typically thicker than those of MCM-41 which shows a pore wall thickness between 8 Å and 12 Å. This is also reflected in a higher stability of SBA-15 against hydrolysis. BET surface areas were found to be between 700-800 m²/g for SBA-15[55] and ~1000m²/g for MCM-41.[56]

Fajula, Z. Bayram-Hahn, K. Unger, G. Puy, C. Demesmay, J.-L. Rocca, *J. Sep. Sci.* **2006**, *29*, 844; A. Katiyar, N. G. Pinto, *Small* **2006**, *2*, 644.
[51] H. Yang, Q. Shi, B. Tian, S. Xie, F. Zhang, Y. Yan, B. Tu, D. Zhao, *Chem. Mater.* **2003**, *15*, 536.
[52] H. Yang, N. Coombs, I. Sokolov, G. A. Ozin, *Nature* **1996**, *381*, 589.
[53] P. Feng, X. Bu, G. D. Stucky, D. J. Pine, *J. Am. Chem. Soc.* **2000**, *122*, 994.
[54] N. Gartmann, D. Brühwiler, *Angew. Chem. Int. Ed.* **2009**, *48*, 6354.
[55] A. Galarneau, H. Camion, F. Di Renzo, F. Fajula, *Langmuir* **2001**, *17*, 8328.
[56] M. Kruk, M. Jaroniec, Y. Sakamoto, O. Terasaki, R. Ryoo, C. H. Ko, *J. Phys. Chem. B* **1999**, *104*, 292.

2.1.2 Functionalization

Extensive research efforts on the functionalization of mesoporous silica have resulted in a considerable amount of scientific articles and reviews.[57] The goal is to obtain specifically designed properties by the incorporation of functional groups which are often organic. The possible applications are diverse and are concerned for example with drug delivery systems, inclusion of biomolecules, sensing, smart devices or light sensitive devices.[58]

Two general ways exist for the introduction of functional groups to the silica surfaces as is depicted in Figure 4: Grafting and co-condensation. Grafting is based on a postsynthetic treatment, whereas functionalization by co-condensation is achieved by a one pot synthesis. Besides, periodic mesoporous organosilica (PMO) can be synthesized by embedding organic groups into the silica framework, which is generally affecting the silica mesostructure itself instead of activating the surface for further synthetic modifications.[59]

Grafting

Mesoporous silica contains abundant free silanol groups. Five kinds of SiOH groups were shown to be present by IR measurements: isolated, three different kinds of hydrogen bonded silanol groups,[60] as well as geminal SiOH groups.[61] Grafting exploits these free silanol groups on the surface. After hydrothermal synthesis, grafting with alkoxy- $(R'O)_3SiR$, chlorosilanes Cl_3SiR or silazanes $HN(SiR_3)_2$ leads to a functionalization with the organic group R. Alkoxysilanes are less reactive than chlorosilanes and therefore often easier to control. The reactivity of the alkoxysilanes also depends on the R´ group. Normally, methoxy- and ethoxysilanes are used but also larger alkyl rests are possible. The reactivity is generally decreased with increasing alkyl chain length.

---

[57] K. Moller, T. Bein, *Chem. Mater.* **1998**, *10*, 2950; A. Vinu, K. Z. Hossain, K. Ariga, *J. Nanosc. Nanotechnol.* **2005**, *5*, 347; A. Stein, B. J. Melde, R. C. Schroden, *Adv. Mater.* **2000**, *12*, 1403; A. B. Descalzo, R. Martinez-Manez, R. Sancenon, K. Hoffmann, K. Rurack, *Angew. Chem. Int. Ed.* **2006**, *45*, 5924.

[58] L. Basabe-Desmonts, D. N. Reinhoudt, M. Crego-Calama, *Chem. Soc. Rev.* **2007**, *36*, 993; M. Vallet-Regí, F. Balas, D. Arcos, *Angew. Chem. Int. Ed.* **2007**, *46*, 7548; L. F. Giraldo, B. L. López, L. Pérez, S. Urrego, L. Sierra, M. Mesa, *Macromol. Symp.* **2007**, *258*, 129; F. Lu, S.-H. Wu, Y. Hung, C.-Y. Mou, *Small* **2009**, *5*, 1408; T. Asefa, A. N. Otuonye, G. Wang, E. A. Blair, R. Vathyam, K. Denton, *Adsorption* **2009**, *15*, 287; L. Wang, W. Zhao, W. Tan, *Nano Res.* **2008**, *1*, 99; V. Ajayan, M. Masahiko, A. Katsuhiko, *J. Nanosc. Nanotechnol*. **2006**, *6*, 1510; Y. Klichko, M. Liong, E. Choi, S. Angelos, A. E. Nel, J. F. Stoddart, F. Tamanoi, J. I. Zink, *J. Am. Ceram. Soc.* **2009**, *92*, S2.

[59] F. Hoffmann, M. Cornelius, J. Morell, M. Fröba, *J. Nanosci. Nanotechnol.* **2006**, *6*, 265; T. Tani, N. Mizoshita, S. Inagaki, *J. Mater. Chem.* **2009**, *19*, 4451.

[60] C. Jiesheng, L. Qinghua, X. Ruren, X. Fengshou, *Angew. Chem. Int. Ed.* **1996**, *34*, 2694.

[61] X. S. Zhao, G. Q. Lu, A. K. Whittaker, G. J. Millar, H. Y. Zhu, *J. Phys. Chem. B* **1997**, *101*, 6525.

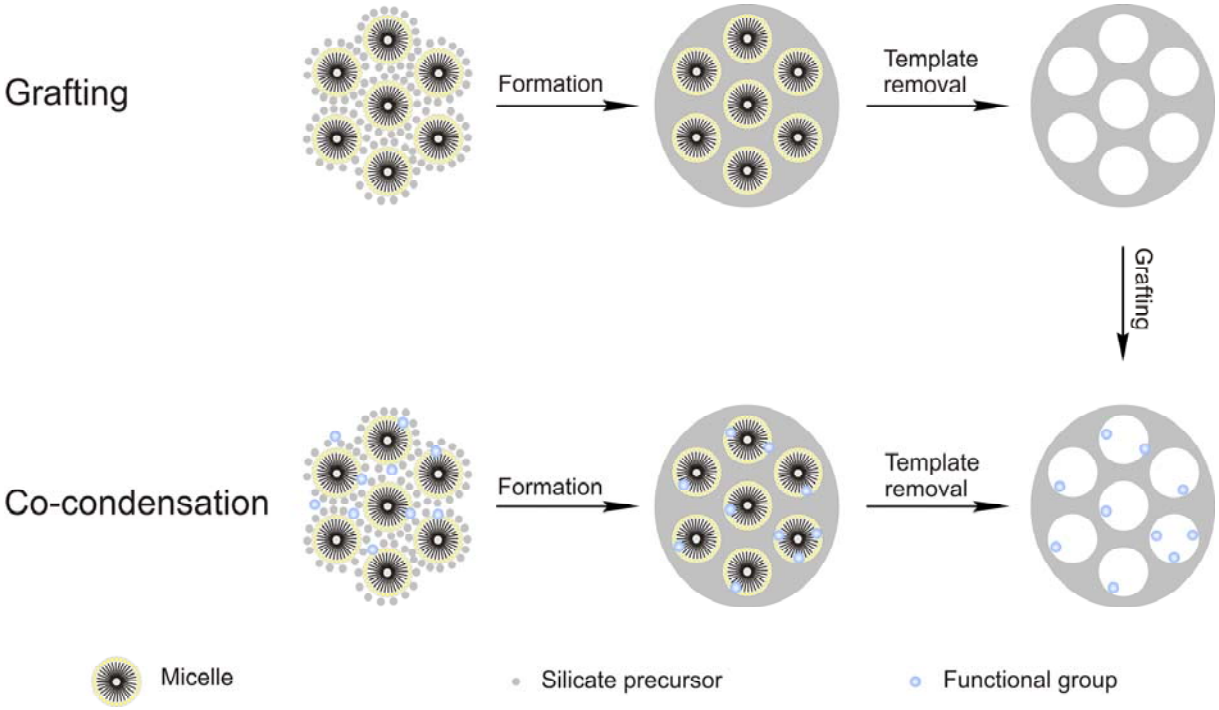

Figure 4 Scheme of grafting and co-condensation.

Many different groups have been introduced by the grafting approach. Figure 5 gives an overview of functional groups created by direct or secondary modification.

Grafting with alkyl groups of different length is a frequently employed method. Depending on the grafting amount and the characteristics of the alkyl chain, the hydrophilic surface of the silica is changed successively to hydrophobic, which can be exploited for the adsorption of diverse kinds of unpolar target molecules as for example drug molecules.[62] Silylation reactions, implying a complete reaction of the available silanol groups, were accomplished by using an excess of a highly reactive alkylsilane, which further resulted in an increased stability of the mesostructured silica against water vapor[63] and a high adsorption capacity for certain drug molecules as for example for 4-nonylphenol.[64,65] For this purpose, chlorosilanes are often used due to their increased reactivity compared to alkoxysilanes.

The introduction of an amino group is a popular first step towards functionalized mesoporous silica, offering possibilities for further coupling reactions at relatively mild conditions. Amide bonds by reaction with an organic acid are frequently used due to reaction conditions at RT forming a relatively stable connection which is very common in biological systems.

---

[62] J. C. Doadrio, E. M. B. Sousa, I. Izquierdo-Barba, A. L. Doadrio, J. Perez-Pariente, M. Vallet-Regi, *J. Mater. Chem.* **2006**, *16*, 462.
[63] T. Shigeno, M. Nagao, T. Kimura, K. Kuroda, *Langmuir* **2002**, *18*, 8102.
[64] K. Inumaru, J. Kiyoto, S. Yamanaka, *Chem. Commun.* **2000**, 903.
[65] K. Inumaru, Y. Inoue, S. Kakii, T. Nakano, S. Yamanaka, *Phys. Chem. Chem. Phys.* **2004**, *6*, 3133.

Thiol groups are often introduced as they are promising candidates for complexation with heavy metal ions such as mercury or gold.[66,67,68,69] Hg^{2+} has been selectively adsorbed in the presence of other metal ions and application for the removal of mercury from waste water has therefore been suggested.[70] Amino and thiol functionalizations have been used for the complexation of a variety of metal ions such as Ag^{+}, Cd^{2+}, Cu^{2+}, Hg^{2+}, Zn^{2+}, Cr^{3+}, Ni^{2+}, Pd^{2+}, Pt^{2+} [71] and also arsenate or chromate, making it useful for the remediation of drinking water.[72] A further interesting class of mesoporous materials is obtained by the addition of halogens. Especially bromo- and iodo groups are known as good leaving groups and can be used for the formation of alkylated amino groups, ester or ether bonds.

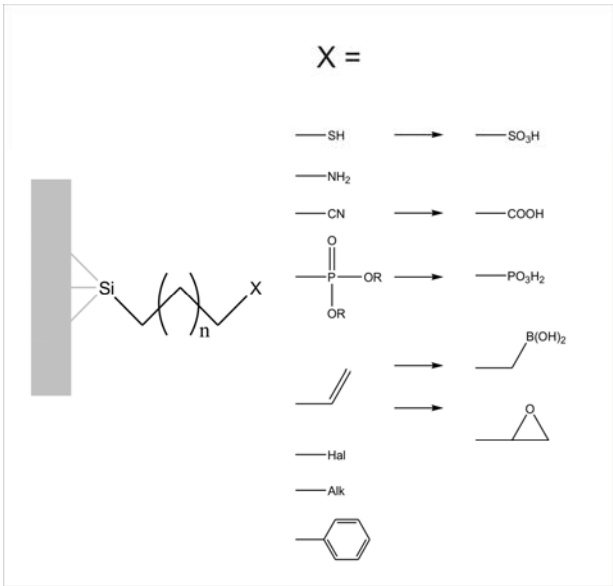

Figure 5 Functional groups introduced to mesoporous silica.

Functionalization with cyano groups has been reported, which can be oxidized to the carboxylic acid after treatment with sulfuric acid.[73] The introduction of double bonds[74] also offers many further reaction pathways as for example ozonisation to the epoxide and further

[66] R. I. Nooney, M. Kalyanaraman, G. Kennedy, E. J. Maginn, *Langmuir* **2000**, *17*, 528.
[67] A. Ghosh, C. Ranjan Patra, P. Mukherjee, M. Sastry, R. Kumar, *Microporous Mesoporous Mater.* **2003**, *58*, 201.
[68] Y. Guari, C. Thieuleux, A. Mehdi, C. Reye, R. J. P. Corriu, S. Gomez-Gallardo, K. Philippot, B. Chaudret, *Chem. Mater.* **2003**, *15*, 2017; Y. Guari, C. Thieuleux, A. Mehdi, C. Reye, R. J. P. Corriu, S. Gomez-Gallardo, K. Philippot, B. Chaudret, R Dutartre, *Chem. Commun.* **2001**, 1374.
[69] X. Feng, G. E. Fryxell, L. Q. Wang, A. Y. Kim, J. Liu, K. M. Kemner, *Science* **1997**, *276*, 923.
[70] S. M. Evangelista, E. De Olivera, G. R. Castro, L. F. Zara, A. G. S. Prado, *Surface Science* **2007**, *601*, 2194.
[71] S. Mattigod, G. E. Fryxell, X. Feng, J. Liu, in *3rd Eingineering-Foundation Conference on Process and Reagents for Metal Separations- Metal Separation Technologies Beyond 2000* edited by K. C. Liddell, D. J. Chaiko, Minerals, Metals & Materials Soc, Kahuku, Hi **1999**, pp. 71-79; S. A. El-Safty, *J. Mater. Sci.* **2009**, *44*, 6764.
[72] G. E. Fryxell, J. Liu, T. A. Hauser, Z. Nie, K. F. Ferris, S. Mattigod, M. Gong, R. T. Hallen, *Chem. Mater.* **1999**, *11*, 2148.
[73] K. Y. Ho, G. Mc Kay, K. L. Yeung, *Langmuir* **2003**, *19*, 3019.
[74] M. H. Lim, C. F. Blanford, A. Stein, *Chem. Mater.* **1998**, *10*, 467; C. E. Fowler, S. L. Burkett, S. Mann, *Chem. Commun.* **1997**, 1769.

reaction to a glycol or reaction with borane to a terminal alcohol. Simple phosphates can be prepared[75] and for example be hydrolyzed to phosphoric acids.

Co-Condensation

Co-condensation or so called one pot synthesis is an alternate pathway for a functionalization. It comprises an in situ reaction of functional silanes in a LCT process. Hence, functional groups are directly incorporated into the silica structure and are already present at the beginning of the synthesis. The same silanes as for the postsynthetic method can be used, although compounds sensitive to basic or acidic conditions, depending on the synthesis procedure, have to be avoided. After the hydrothermal synthesis, the surfactant has to be removed, which is usually accomplished by an extraction procedure since calcination would destroy the organic moieties. Compared to grafting, one step less is required as shown in Figure 4.

An interesting variation is a self-templating approach where the functional group is designed as an amphiphilic molecule which is used as a surfactant itself.[76,77] By a variation of this method, cleavage of the hydrophobic part of the surfactant at a later stage can form the functional group (Lizard template method).[78] By combining surfactant and functional molecule very dense packing of functional groups has been achieved, although the surfactant synthesis must be sophisticated in order to generate the appropriate mesopores.

[75] R. J. P. Corriu, A. Mehdi, C. Reyé, *C. R. Acad. Sci. Paris* **1999**, *t2*, 35.
[76] S. Atsushi, K. Kazuyuki, *Angew. Chem. Int. Ed.* **2003**, *42*, 4057.
[77] E. Ruiz-Hitzky, S. Letaief, V. Prévot, *Adv. Mater.* **2002**, *14*, 439.
[78] Q. Zhang, K. Ariga, A. Okabe, T. Aida, *J. Am. Chem. Soc.* **2004**, *126*, 988.

Comparison of grafting and co-condensation

Both synthesis strategies exhibit specific advantages. The grafting reaction can make use of extracted as well as calcined material. For extraction, problems due to template residues can occur. In the case of co-condensed material, incorporation of the organic group into the pore wall can arise depending largely on the chemical properties and interaction of the precursors with the micelles. This leads to a decrease of the reactive group content on the surface.
Grafting, on the other hand, is problematic when an uniform distribution of the functional groups is desired. Functionalization often occurs on the external surface or on the pore entrances, especially in cases where diffusion through the pore network is hindered. This effect can be exploited for the controlled access to pores by photoreactive groups (see below).

External surface grafting

For many tasks, a different functionalization of the rather small external and the inner surface is desirable. Some techniques have been developed to achieve this goal. Usually, a premodification of the external surface is carried out under the assumption that all the available external silanol groups are converted. Afterwards, the appropriate molecules can be introduced to the pore surface.
One possibility is the use of chlorosilane species such as diphenyldichlorosilane (DPDCS) in a sufficient amount relative to the external silanol groups. Due to the high reactivity, diffusion into the pores is prevented and mostly the outer surface is functionalized.[79] However, partial incorporation and channel entrance functionalization has to be assumed. Another method is the functionalization of the material before the template removal. In this case, diffusion in the channels is blocked by the template. For small precursors, this method is only partially successful. For small groups, the possibility of entering the channels or at least the channel entrances is still given.[54]

[79] D. S. Shephard, W. Zhou, T. Maschmeyer, J. M. Matters, C. L. Roper, S. Parsons, B. F. G. Johnson, M. J. Duer, *Angew. Chem. Int. Ed.* **1998**, *37*, 2719.

2.1.3 Labeling with luminescent molecules

Inclusion of luminescent species into mesoporous silica by functionalization or adsorption generates promising properties for the development of optical applications. Sensors, pigments, optical data storage devices, solar cells, photocatalysis, models for drug delivery systems (DDS) or the examination of the surface functionalization itself are examples for fields where such materials are of interest.

Generally, adsorption can be achieved by different pathways. The adsorption from a concentrated solution is most common, but also incipient wetness impregnation or inclusion from the gas phase are feasible.[80]

Mesoporous silica MCM-41 is an excellent host for dye adsorption, as demonstrated by the incorporation of rhodamine-B by Yamashita et al.[81] However, if applications as sensing systems are aspired, an immobilization (fixation) of the fluorescent dye on the surface is indispensable. One of the first examples is the functionalization with co-condensed 3-(2,4-dinitrophenylamino)propyl.[82] High porosity and high transparency in the visible are excellent properties of mesoporous silica based optical sensors.

Organic dyes with distinct sensing properties can be transferred to mesoporous silica by coupling to the surface via an attached functional group. Exploiting these surface functions, different types of pH, humidity or gas sensing silicas were developed. A pH sensor was prepared by reaction of fluorescein isothiocyanate with 3-aminopropyltriethoxysilane (APTES) modified silica. The strong luminescence at pH values of about 11 is reduced drastically by lowering the pH.[83,84] Oxygen sensors were developed by means of co-condensed $[Ru(bpy)_3]^{2+}$ based derivatives.[85] A sensor for primary amines was synthesized by using a pore surface anchored *o*-phthalic hemithioacetal group. Primary amines reacted to fluorescent isoindole products, which could be detected.[86] External surface grafting was performed in order to regulate the penetration of molecules.[87] Similar to materials based on

[80] J. Santamaría-González, J. Mérida-Robles, M. Alcántara-Rodríguez, P. Maireles-Torres, E. Rodríguez-Castellón, A. Jiménez-López, *Catal. Lett.* **2000**, *64*, 209.
[81] H. Yamashita, A. Tanaka, M. Nishimura, K. Koyano, T. Tatsumi, M. Anpo in *Mesoporous Molecular Sieves 1998, Vol. 117: Studies in Surface and Catalysis,* edited by L. Bonneviot, F. Béland, C. Danumah, S. Giasson, S. Kaliaguine, Elsevier Science Publ B V, Amsterdam, **1998**, pp. 551.
[82] C. E. Fowler, B. Lebeau, S. Mann, *Chem. Commun.* ***1998***, 1825.
[83] H. Fan, Y. Lu, A. Stump, S. T. Reed, T. Baer, R. Schunk, V. Perez-Luna, G. P. Lopez, C. J. Brinker, *Nature* **2000**, *405*, 56.
[84] G. Wirnsberger, B. J. Scott, G. D. Stucky, *Chem. Commun.* **2001**, 119.
[85] H. Zhang, B. Li, B. Lei, W. Li, *J. Luminescence* **2008**, *128*, 1331.
[86] V. S. Y. Lin, C.-Y. Lai, J. Huang, S.-A. Song, S. Xu, *J. Am. Chem. Soc.* **2001**, *123*, 11510.
[87] D. R. Radu, C.-Y. Lai, J. W. Wiench, M. Pruski, V. S. Y. Lin, *J. Am. Chem. Soc.* **2004**, *126*, 1640.

zeolites,[88] humidity sensing materials can be synthesized by exploiting the photophysical properties of dyes such as nile red (3.5).

2.1.4 Photoreactive systems

The functionalization with photoreactive molecules is a particular challenge, offering the possibility to change the properties of the mesoporous material by light irradiation. One of the most interesting examples is the anchoring of coumarin at the channel entrances of MCM-41 by external surface grafting. Irradiation in the UV (~250 nm) causes a dimerisation of two coumarin molecules in a 2+2 cycloaddition which leads to a closure of the channels. A controlled release of incorporated drug molecules was demonstrated by irradiation with UV and Vis (>310 nm) light which causes an opening of the channels.[89]

Another example is given by the functionalization with azobenzene, which can switch between trans and cis state. The material was obtained by co-condensation with 4-(3-triethoxysilylpropylureido)azobenzene by evaporation induced self assembly (EISA). Due to the different sizes of trans and cis form, a changeable pore size was claimed.[90]

Photochromic molecules such as spiropyrans, which can undergo ring opening under irradiation in the UV, are frequently investigated and the fixation on mesoporous silica is studied, as is shown in chapter 3.7. Other ring opening molecules like spirooxazines[91] and dihydroazulenes[92] show promise for the anchoring to mesoporous silica as well, although they have up to now rarely been employed for that particular purpose.

[88] I. Pellejero, M. Urbiztondo, D. Izquierdo, S. Irusa, I. Salinas, M. P. Pina, *Ind. Eng. Chem. Res.* **2006**, *46*, 2335.
[89] N. K. Mal, M. Fujiwara, Y. Tanaka, T. Taguchi, M. Matsukata, *Chem. Mater.* **2003**, *15*, 3385; N. K. Mal, N. Fujiwara, Y. Tanaka, *Nature* **2003**, *421*, 350.
[90] N. Liu, Z. Chen, D. R. Dunphy, Y.-B. Jiang, R. A. Assink, C. J. Brinker, *Angew. Chem. Int. Ed.* **2003**, *42*, 1731; Y. F. Lu, R. Ganguli, C. A. Drewien, M. T. Anderson, C. J. Brinker, W. L. Gong, Y. X. Guo, H. Soyez, B. Dunn, M. H. Huang, J. I. Zink, *Nature* **1997**, *389*, 364.
[91] Y. Fu, H. Chen, D. Qiu, Z. Wang, X. Zhang, *Langmuir* **2002**, *18*, 4989; G. Wirnsberger, B. J. Scott, B. F. Chmelka, G. D. Stucky, *Adv. Mater.* **2000**, *12*, 1450; S. Yagi, N. Minami, J. Fujita, Y. Hyodo, H. Nakazumi, T. Yazawa, T. Kami, A. H. Ali, *Chem. Commun.* **2002**, 2444.
[92] V. De Waele, U. Schmidhammer, T. Mrozek, J. Daub, E. Riedle, *J. Am. Chem. Soc.* **2002**, *124*, 2438.

2.2 Nitrogen sorption

Nitrogen sorption is one of the most important methods for the characterisation of porous materials. An introduction is given in order to establish the various possibilities for identifying mesoporous silicas.

Adsorption by porous materials is a long known phenomenon and first quantitative studies were done in the late 18´th century on certain forms of charcoal.[93] The first reported isotherms were measured by van Bemmelen in 1881.[94] Freundlich in 1907[95] was one of the first who appreciated the role of the surface and proposed an empirical equation (1926). A radical change was brought about by the first papers of Langmuir (1916, 1917, 1918),[96] who pointed out that the formation of a monolayer is involved in the adsorption process. Further important advance was achieved by Brunauer, Emmett and Teller (BET), who extended the theory and developed an equation by taking multilayer adsorption into account.[97] Isotherm equations of Freundlich, Langmuir and BET are given in the following equations and the corresponding isotherms are shown in Figure 6.

Freundlich equation: $n = k\,p^{1/m}$ (2)

where n is the specific amount of gas adsorbed at the equilibrium pressure p; k and m are constants with $m>1$.

Langmuir equation: $\theta = bp/(1+bp)$ (3)

where $\theta = N^a/N^s$ is the ratio of occupied sites N^a and available independent sites N^s for localized adsorption; b is the adsorption coefficient given by

$$b = K \exp(E/RT) \quad (4)$$

where K is a constant and E the positive value of the adsorption energy.

[93] F. Rouquerol, J. Rouquerol, K. Sing, *Adsorption by powders and porous solids*, Academic Press, London, San Diego, **1999**, pp. 2.
[94] S. D. Forrester, C. H. Giles, *Chem. & Ind*. **1972**, 318.
[95] H. Freundlich, *Z. Phys. Chem.* **1907**, *57*, 385.
[96] I. Langmuir, *J. Am. Chem. Soc.* **1916**, *38*, 221; I. Langmuir, *J. Am. Chem. Soc.* **1917**, *39*, 1848; I. Langmuir, *J. Am. Chem. Soc.* **1918**, *40*, 1361;
[97] S. Brunauer, P. H. Emmett, E. Teller, *J. Am. Chem. Soc.* **1938**, *60*, 309.

Linear form of the BET equation:

$$\frac{p}{n(p_0 - p)} = \frac{1}{n_m C} + \frac{C-1}{n_m C} * \frac{p}{p_0} \qquad (5)$$

with n_m being the amount of adsorbed gas for a monolayer and p/p_0 as the relative pressure. C is a constant proportional to E_1:

$$C \sim (E_1\text{-}E_L/RT) \qquad (6)$$

where E_1 is the positive value of energy at the first adsorption layer. E_L is the liquefaction energy of the adsorptive and R the gas constant. The term E_1-E_L was described as the net molar energy of adsorption.

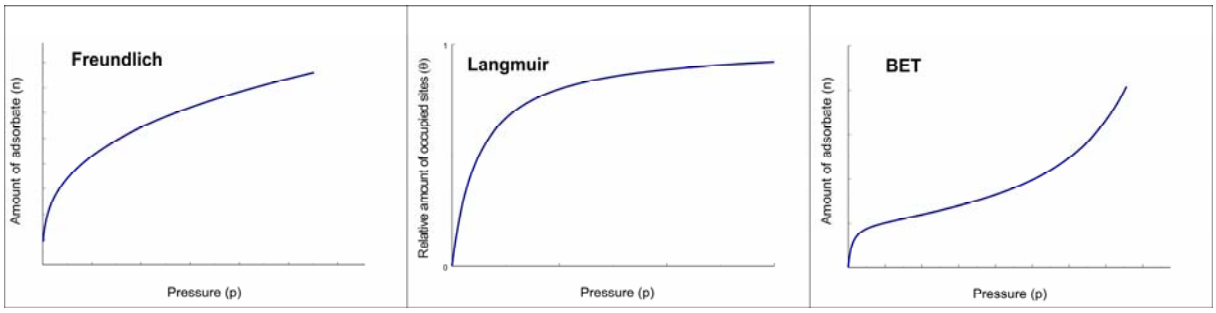

Figure 6 Typical isotherms after the theories of Freundlich, Langmuir and BET.

Physisorption isotherms can be arranged in six classes following the IUPAC definition as shown in Figure 7.

The Type I isotherm seems to obey the Langmuir equation over a wide pressure range. It rises sharply at low pressures and then reaches a plateau. However, the plateau is normally not assigned to a complete monolayer adsorption, as in the Langmuir theory, since it is normally found for microporous samples with small external surface for restricted multilayer adsorption.

Isotherms of Type II show unrestricted monolayer-multilayer adsorption and are common for macroporous or non-porous adsorbents. The point B at the beginning of the linear part in the middle section is indicative of complete monolayer coverage.

Type III isotherms are convex towards the pressure axis over the entire pressure range, typical for very weak interactions between adsorbent and adsorbate. A point B as in Type II is not existent for these curves. Type IV and V are representing mesoporous solids. Both exhibit a hysteresis loop, the lower branch representing the adsorption and the higher branch the

desorption isotherm. Type V is convex at low pressure due to weak interactions between adsorbent and adsorbate.

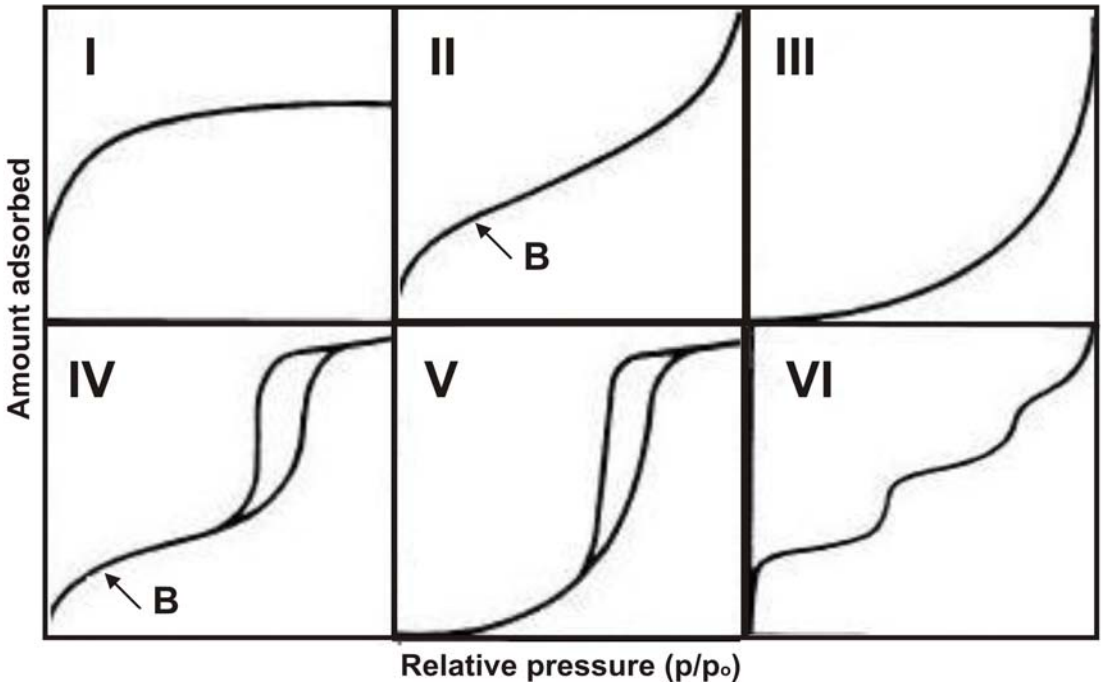

Figure 7 Isotherm types according to IUPAC.[98]

Different adsorptives are used for the measurement of sorption isotherms, with liquid nitrogen being the most frequent. However, due to the presence of a quadrupolar moment, which can result in increased interactions with the heterogeneous surface of zeolites, argon is often used in this case. For mesoporous samples, the use of argon at 77 K is limited since the temperature is below the triple point and pore condensation vanishes for pore diameters above approximately 12 nm. Carbon dioxide, on the other hand, can be used at higher temperatures, which enhances the diffusion properties in highly microporous systems. As a drawback, only a limited range of micropores can be measured under the normal setup.[99]

Type VI isotherms are associated with layer by layer deposition and are relatively rare.

Hysteresis loops can be arranged in different groups and provide information on the pore shapes which can be cylindrical, slit shaped, wedge shaped with open ends, wedge shaped with narrow necks or ink-bottle form.

[98] K. S. W. Sing, D. H. Everett, R. A. W. Haul, L. Moscou, R. A. Pierotti, J. Rouquerol, T. Siemieniewska, *Pure Appl. Chem.* **1985**, *57*, 603.
[99] J. C. Groen, L. A. A. Pfeffer, J. Pérez-Ramírez, *Microporous Mesoporous Mater.* **2003**, *60*, 1.

For mesoporous samples, Type IV isotherms are most frequently encountered. As shown in Figure 7, point B is indicating complete monolayer formation. By using the low pressure part of the isotherm, the BET theory gives a good description for mesoporous systems and the specific surface area can be calculated as follows:

$$\alpha = n_m N \sigma \qquad (7)$$

Where α is the surface area, N the Avogadro constant and σ the average area occupied by each molecule. For nitrogen adsorption at 77 K, a value of 0.162 nm² is used, assuming a hexagonal close packed monolayer.[98] The value of n_m can be obtained by generating a linear plot of $1/n[(p_0/p)-1]$ against p/p_0 by consideration of the linear BET equation. Only the linear part of this BET plot can be utilized for the calculation of the surface area. This is typically the case at a relative pressure between 0.05 to 0.35, which is, after monolayer formation and before mesopore filling. The slope C-$1/n_mC$ and the intercept $1/n_mC$ provide values for n_m which are used in equation (5).

The C value indicates the interactions between the adsorbate and the adsorbent. Nitrogen adsorption of calcined mesoporous silicas, such as MCM-41 or SBA-15, typically gives C values between 80 and 110. A high C value is indicative of a well defined localized monolayer. Low C values, on the other hand, are due to weak interactions. Use of regular C values in the BET equation results in isotherms of Type II shape, whereas by decreasing the C value below 2, Type III isotherms are obtained.

Some restrictions have to be considered when using the BET method. It has to be ensured that only mesopores are present, since micropores will lead to incorrect values. Monolayer-multilayer physisorption does not always occur in strict accordance with the BET model. Therefore, the calculated value for n_m has to be used carefully. The energetic heterogeneity of most surfaces and adsorbate-adsorbate interactions can play a significant role that is incompatible with the BET theory. Type VI isotherms are not described as well, since separate adsorption of more than one layer is not defined by the BET theory.

The t-plot method and the α_S-plot method are frequently used empirical methods for the determination of the surface areas and for assessing microporosity. They are based on referring the porous sample to a non-porous reference sample with the same surface structure.

The t-plot method is exploiting the statistical thickness t of an adsorbed multilayer, which is defined as

$$t = n / n_m * d \quad (8)$$

where d is the effective thickness of a monolayer. In this context, it is beneficial that the multilayer adsorption is not very much affected by the surface structure in contrast to the monolayer adsorption. Therefore, the thickness t of the multilayer depends essentially on the equilibrium pressure. A t-plot is created by plotting the amount adsorbed, n, against t, the standard multilayer thickness of the reference non-porous material at the corresponding p/p_0. Differences between sample and reference result in non-linearity. The slope $s = n/t$ represents the surface area by including the molar mass M and the density ρ of the adsorbate:

$$\alpha(t) = M / \rho * s \quad (9)$$

The limitation of this method is that it relies on the monolayer capacity of the reference material and is therefore dependent on the validity of the BET theory for the analysis of the reference material.

The α_S-plot method overcomes this problem by taking an adsorbed amount n_S at pre-selected relative pressure, which is usually $(p/p_0)_S = 0.4$. The reduced adsorption n/n_S is expressed as α_S. Similar to the t-plot, the adsorbed amount of the investigated sample n_{inv} against α_S of the reference sample gives the α_S-plot and the surface area can be calculated by means of the slope $s = n_{inv}/\alpha_S$:

$$\alpha = \alpha_{ref} * s / n_{ref,\,0.4} \quad (10)$$

where α_{ref} and $n_{ref,\,0.4}$ are the BET specific surface area and the adsorbed amount at a relative pressure of 0.4 of the reference adsorbent. The method is especially helpful to detect microporosity, in which case the intercept with the ordinate can be used to calculate the micropore volume. An intercept of zero indicates the absence of micropores, as is the case for MCM-41.[100] However, complications can arise due to the fact that the method is dependent on the nature of the reference material.

[100] M. Kruk, M. Jaroniec, R. Ryoo, J. M. Kim, *Microporous Mater.* **1997**, *12*, 93.

The pore volume is generally determined by taking the liquid volume of an adsorptive at a predetermined relative pressure. For calculating the total pore volume $p/p_0 \geq 0.95$ is normally used. This method is sufficiently accurate, given that no macropores are present which would be filled at a relative pressure near 1. Furthermore, the adsorbed amount on the external surface should be negligible.

The distribution of pore volume with respect to the pore size is called pore size distribution (PSD). The determination of PSD is a very useful tool to describe porous materials. For mesopores, the most popular computational method for the calculation of the PSD is the method developed by Barrett, Joyner and Halenda (BJH), which is based on the Kelvin equation and corrected for multilayer adsorption.[101] Other existing so called "classical" methods are likewise based on the Kelvin equation:

$$r_K = -2\gamma V_m / [RT \ln (p/p_0)] \qquad (11)$$

where γ is the surface tension of the adsorptive, V_m is the molar volume of the adsorptive, R the gas constant, T the boiling point of the adsorptive, p/p_0 the relative pressure and r_K the Kelvin radius of the pore. This equation is used to describe the capillary condensation in porous systems. The radius r_K describes the radius which is given by the meniscus of the condensate in the pores and which is connected by addition of the adsorbed multilayer thickness (t) with the pore size. For complex systems, the contact angle between condensate and multilayer adsorption has to be taken into account as well. The theory of capillary condensation is used by the classical methods to calculate pore sizes. This also includes some simplifications/assumptions:

- the Kelvin equation can be used over the complete mesopore range;
- the contact angle is zero and therefore the meniscus curvature is controlled by the pore size and shape;
- the pores are rigid and well defined;
- the distribution is only confined to the mesopore range;
- the filling of a given pore does not depend on its location within the network;
- the adsorption on the pore walls proceeds in exactly the same way as on a corresponding open surface.

[101] E. P. Barrett, L. G. Joyner, P. H. Halenda, *J. Am. Chem. Soc.* **1951**, *73*, 373.

Since the formation of a condensate with a corresponding meniscus is only possible for large enough pores, the method can only be applied for mesopores. Moreover, it has to be kept in mind that for pores smaller than about 10 nm and especially for pores near the limit of capillary condensation, a significant underestimation up to over 20 % of the pore size can occur when using the BJH method[102]. For micropore calculations, semi-empirical methods such as the Horvath-Kawazoe (HK)[103] model for slit shaped pores and the Saito-Foley (SF)[104] model for cylindrical pores are used.

Beyond this, new models based on non-linear density functional theory (NLDFT) and also molecular simulations such as Monte Carlo simulation and molecular dynamics have been developed for the calculation of PSD of silicas.[105] The DFT method has been applied for the characterization of many porous systems such as micro- and mesoporous carbons, silicas and zeolites using cylindrical or slit-pore models with different adsorptives. Application of this model further confirmed the underestimated pore sizes of the classical approaches (BJH, HK and SF). Especially for complex porous materials, a combination of the methods is often required to achieve a thorough characterisation.

Mesoporous materials typically show hysteresis associated with capillary condensation. As a relatively rare example, MCM-41 with a pore size around 4 nm exhibits a reversible isotherm with no hysteresis, because the pore size is at the border of the validity of capillary condensation. The nitrogen isotherms of typical samples of MCM-41 and SBA-15 are shown in Figure 8. The pore size distribution of MCM-41 is underestimated by around 1 nm due to the calculation with the BJH method. Furthermore, the difference in terms of hysteresis is shown, as SBA-15 samples typically exhibit broad hysteresis loops.

[102] A. Galarneau, D. Desplantier, R. Dutartre, F. Di Renzo, *Microporous Mesoporous Mater.* **1999**, *27*, 297.
[103] G. Horváth, K. Kawazoe, *J. Chem. Eng. Jap.* **1983**, *16*, 470.
[104] A. Saito, H. C. Foley, *Microporous Mater.* **1995**, *3*, 531; A. Saito, H. C. Foley, *AIChE J.* **1991**, *37*, 429.
[105] L. D. Gelb, K. E. Gubbins, R. Radhakrsihnan, M. Sliwinka-Bartowiak, *Rep. Prog. Phys.* **1999**, *62*, 1573; A. V. Neimark, P. I. Ravikovitch, M. Gruen, F. Schüth, K. K. Unger, *J. Colloid Interface Sci,* **1998**, *207*, 159; P. I. Ravikovitch, D. Wie, W. T. Church, G. L. Haller, A. V. Neimark, *J. Phys. Chem. B* **1997**, *101*, 3671.

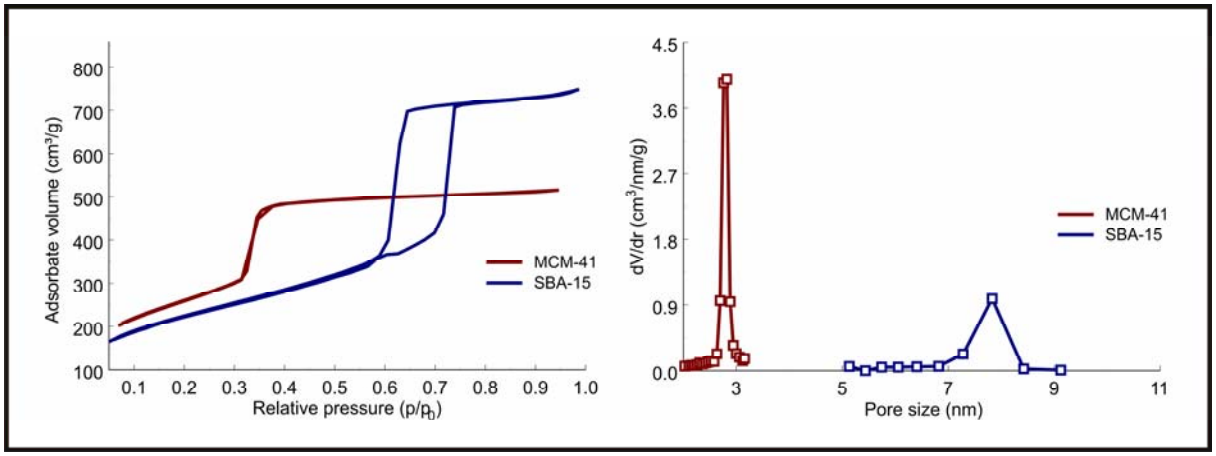

Figure 8 Nitrogen sorption isotherms (left) and pore size distributions (right) of typical samples of MCM-41 and SBA-15. The distributions were calculated by BJH using the respective adsorption isotherms.

Two major contributing factors influencing the appearance of hysteresis can be identified: (1) the adsorption by the development of a metastable multilayer and therefore an associated delay in the capillary condensation and (2) the entrapment of condensate through network percolation, thus delaying the desorption process. The type of hysteresis is associated with the shape of the pores (cylindrical, slit shaped, wedge shaped with open and narrow neck and ink bottle). IUPAC identifies four major types of hysteresis loops as depicted in Figure 9.[106] For a narrow distribution of uniform pores, as for the cylindrical pores of SBA-15, type H1 loops are expected. H2 loops are found for interconnected networks with pores of different size and shape. H3 and H4 type loops are typical for slit- or wedge shaped pores, with the pore size distribution for H4 being mainly in the micropore range.

[106] K. S. W. Sing, D. H. Everett, R. A. W. Haul, L. Moscou, R. A. Pierotti, J. Rouquerol, T. Siemieniewska, *Pure Appl. Chem.* **1985**, *57*, 603.

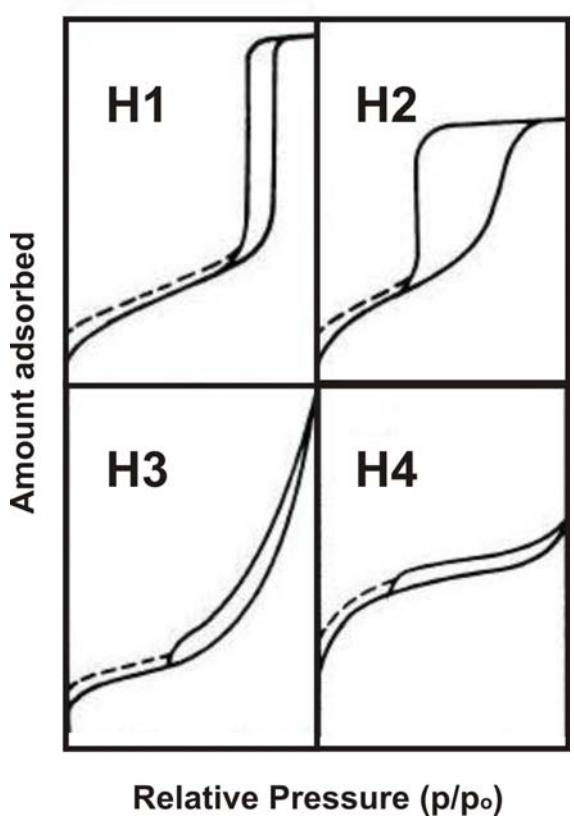

Figure 9 IUPAC classification of hysteresis loops.

Classical methods, in particular BJH, are widely used for the characterisation of porous materials. In any case, specific effects have to be considered to ensure correct interpretation of the results. For the evaluation of mesoporous materials, the tensile strength effect (TSE) is a particular pitfall. The TSE manifests itself by a forced closure of the hysteresis loop upon desorption. Due to this effect, a peak is observed in the PSD calculated from the desorption isotherm. TSE is a result of the threshold zone between the area where desorption and adsorption appear at similar pressures for pores <~4 nm and, on the other side, for pores >~4 nm, which show hysteresis. In the critical pressure range between these two regimes, there seems to be an instability of the hemispherical meniscus during the desorption, which can be observed by a forced closure of the desorption branch. This effect can even be more pronounced if pore network effects exist and desorption of larger pores has to occur through smaller pores. Plugged mesopores show a similar influence on the desorption branch.[107] For these reasons, the adsorption isotherm often gives a more accurate description of the PSD of mesopores.

[107] P. Van Der Voort, P. O. Ravikovitch, K. P. De Jong, A. V. Neimark, A. H. Janssen, M. Benjelloun, E. Van Bavel, P. Cool, B. M. Weckhuysen, E. F. Vansant, *Chem. Commun.* **2002**, 1010.

The pore diameter can also be determined by X-ray diffraction (XRD) using the fact that mesoporous samples diffract in the low angle range up to about 2 θ = 10°. This offers an analytical method which is independent of theoretical models such as the capillary condensation or NLDFT. For honeycomb structures such as SBA-15 and MCM-41, the pore diameter ω can be calculated by the primary pore volume V_p, the lattice spacing d_{100} (d) and the density of the pore walls (ρ):[108]

$$\omega = cd\sqrt{\left(\frac{\rho V_p}{1+\rho V_p}\right)} \tag{12}$$

with $c = (8/(3^{1/2}\pi))^{1/2}$. Knowledge of the lattice spacing also allows the determination of the pore wall thickness t_w by using the repeat distance for hexagonal systems $a = 2 * d / \sqrt{3}$.

$$t_w = a - \omega = d\left[\frac{2}{\sqrt{3}} - c\sqrt{\left(\frac{\rho V_p}{1+\rho V_p}\right)}\right] \tag{13}$$

Pore wall thickness and pore size measurements based on XRD and nitrogen sorption can feature a significant absolute error. SBA-15 was frequently investigated in this regard, as pore wall thickness, pore size and the occurrence of microporosity strongly depend on the synthesis conditions. Microporosity was thereby generally detected by means of the α_S–plot method and pore wall thickness and pore size by using the XRD and the nitrogen adsorption data.[109,110]

[108] M. Kruk, M. Jaroniec, R. Ryoo, J. M. Kim, *Microporous Mater.* **1997**, *12*, 93.
[109] A. Galarneau, H. Cambon, F. Di Renzo, F. Fajula, *Langmuir* **2001**, *17*, 8328.
[110] M. Kruk, M. Jaroniec, *Chem. Mater.* **2000**, *12*, 1961.

Chapter 3

Results

3.1 Silica host

A wide variety of mesoporous silica exists (chapter 2) which would allow a combination with fluorescent entities. Due to their defined structural characteristics and wide range of synthesis conditions, an outstanding position can be ascribed to SBA-15 and MCM-41 type silica, which are employed as host materials for luminescent guests in this thesis.

The properties of the calcined standard materials (5.1.1, 5.1.2) obtained from nitrogen sorption are given in Table 3. The pore sizes were calculated either by means of BJH or DFT, for which generally the adsorption branch was utilized. Nearly the entire mesoporous range can be covered, achieving pore sizes between around 2 and 25 nm by either using different synthesis conditions or reducing the pore size by post-synthetic functionalization. Large pore sizes between 15 and 25 nm were synthesized by adding a swelling agent (1,3,5-trimethylbenzene (TMB)). For SBA-15 samples in particular, the occurrence of microporosity has to be considered.

Material	Pore size[a] [nm]	Pore size[b] [nm]	Microporosity	S_{BET}[c] [m^2/g]	V_{tot}[d] [cm^3/g]
MCM-41	2.75-2.85	3.9-4.0	No	~900	0.7-0.8
SBA-15	~7.3	~7.3	Yes	~800	~1.1

Table 3 Nitrogen adsorption data of typical used SBA-15 and MCM-41 silica materials;
[a] calculated by the BJH method using the adsorption isotherm;
[b] calculated by the DFT method using the adsorption isotherm;
[c] Total BET surface area;
[d] Total pore volume calculated from the adsorption isotherm at $p/p_0 = 0.95$.

3.2 Synthesis of bifunctionalized mesoporous silica with iodopropyl groups

Bifunctionalized mesoporous silica has recently attracted increased interest in the fields of catalysis,[111] adsorption,[112] and sensing.[113] A variety of functional group pairs have been explored, including sulfonic acid/amino,[114] sulfonic acid/mercapto,[115] amino/carboxyl,[116] mercapto/acetylacetonato,[117] and amino/phenyl.[118] Among the many functional groups that have been incorporated into mesoporous silica, the iodopropyl group stands out as a particularly interesting option in terms of the intriguing possibilities for further modification by means of nucleophilic substitution. Alauzun et al. have shown that the direct synthesis of iodopropyl-functionalized SBA-15 type materials is successful, if HCl is replaced by HI to avoid the formation of chloropropyl groups.[119] Based on this procedure and with regard to the functionalization with fluorescent molecules, the direct synthesis of bifunctionalized mesoporous silica containing iodopropyl as primary functional group was investigated. Additional organic groups can for example be envisaged to provide channels with increased hydrophobicity, which for many applications might be more desirable than the environment created by the abundant surface hydroxyl groups common to mesoporous silica based materials after removal of the SDA.[120]

The inclusion of different functional groups into mesoporous silica is most conveniently accomplished by a co-condensation approach, as postsynthetic modification often leads to a

[111] S. Huh, H.-T. Chen, J. W. Wiench, M. Pruski, V. S.-Y. Lin, *J. Am. Chem. Soc.* **2004**, *126*, 1010; S. Huh, H.-T. Chen, J. W. Wiench, M. Pruski, V. S.-Y. Lin, *Angew. Chem. Int. Ed.* **2005**, *44*, 1826; I. K. Mbaraka, B. H. Shanks, *J. Catal.* **2005** *229*, 365.
[112] T.-H. Kim, M. Jang, J. K. Park, *Microporous Mesoporous Mater.* **2008**, *108*, 22.
[113] V. S.-Y. Lin, C.-Y. Lai, J. Huang, S.-A. Song, S. Xu, *J. Am. Chem. Soc.* **2001**, *123*, 11510; M. Comes, M. D. Marcos, R. Martínez-Máñez, F. Sancenón, J. Soto, L. A. Villaescusa, P. Amorós, D. Beltrán, *Adv. Mater.* **2004**, *16*, 1783; A. B. Descalzo, K. Rurack, H. Weisshoff, R. Martínez-Máñez, M. D. Marcos, P. Amorós, K. Hoffmann, J. Soto, *J. Am. Chem. Soc.* **2005**, *127*, 184.
[114] R. K. Zeidan, S.-J. Hwang, M. E. Davis, *Angew. Chem. Int. Ed.* **2006**, *45,* 6332.
[115] E. L. Margelefsky, A. Bendjériou, R. K. Zeidan, V. Dufaud, M. E. Davis, *J. Am. Chem. Soc.* **2008**, *130*, 13442.
[116] S. R. Hall, C. E. Fowler, B. Lebeau, S. Mann, *Chem. Commun.* **1999**, 201.
[117] R. Mouawia, A. Mehdi, C. Reyé, R. Corriu, *New J. Chem.* **2006**, *30*, 1077.
[118] S. R. Hall, C. E. Fowler, B. Lebeau, S. Mann, *Chem. Commun.* **1999**, 201.
[119] J. Alauzun, A. Mehdi, C. Reyé, R. Corriu, *New J. Chem.* **2007**, *31*, 911.
[120] Y. Kuwahara, K. Maki, Y. Matsumara, T. Kamegawa, K. Mori, H. Yamashita, *J. Phys. Chem. C* **2009**, *113*, 1552; Y. Zhu, T. E. Müller, J. A. Lercher, *Adv. Funct. Mater.* **2008**, *18*, 3427; A. B. Descalzo, M. D. Marcos, C. Monte, R. Martínez-Máñez, K. Rurack, *J. Mater. Chem.* **2007**, *17*, 4716; K. Inumaru, T. Ishihara, Y. Kamiya, T. Okuhara, S. Yamanaka, *Angew. Chem. Int. Ed.* **2007**, *46*, 7625; J. A. Melero, J. Iglesias, J. M. Arsuaga, J. Sainz-Pardo, P. de Frutos, S. Blazquez, *J. Mater. Chem.* **2007**, *17*, 377; J. C. Doadrio, E. M. B. Sousa, I. Izquierdo-Barba, A. L. Doadrio, J. Perez-Pariente, M. Vallet-Regí, *J. Mater. Chem.* **2006,** *16*, 462; F. Omota, A. C. Dimian, A. Bliek, *Appl. Catal. A* **2005**, *294*, 121; A. Matsumoto, K. Tsutsumi, K. Schumacher, K. K. Unger, *Langmuir* **2002**, *18*, 4014; A. Bhaumik, T. Tatsumi, *Catal. Lett.* **2000**, *66*, 181.

preferential functionalization of the most accessible sites (external surface and pore entrances).[121] However, the quality of the porous inorganic-organic hybrid materials resulting from co-condensation depends on the nature of the respective alkoxysilane precursors. Having an organic group that is sufficiently hydrophobic to interact with the core of the micelles is often advantageous. The quality of the bifunctional material in terms of a narrow pore size distribution depends therefore strongly on the respective organosilane precursor.

The nitrogen sorption isotherms of samples synthesized with an iodopropyltrimethoxysilane/alkyltrimethoxysilane (IPTMS/RTMS) ratio of 1:10 are shown in Figure 10. The corresponding PSD´s are given in Figure 11 with additional characterization data compiled in Table 4. Comparison with the monofunctionalized sample (Ip) reveals that the addition of methyltrimethoxysilane (MTMS) to the synthesis mixture does not cause a significant change in the porosity of the material (Ip/Me). The course of the respective adsorption isotherm at a relative pressure above 0.80 even suggests that Ip/Me features less secondary mesoporosity. This observation is supported by the pore volumes calculated at relative pressures of 0.98 and 0.80. In the case of Ip/Me, the total pore volume V_{tot} (p/p_0 = 0.98) is 1.27 cm^3/g, whereas $V_{0.80}$ (p/p_0 = 0.80) amounts to 1.02 cm^3/g. For Ip, the difference between these two values is significantly larger (V_{tot} = 1.65 cm^3/g, $V_{0.80}$ = 0.86 cm^3/g). The presence of the methyl groups in Ip/Me furthermore leads to a decrease of the C_{BET} value (Table 4), indicating a less polar surface.[122]

Compared to Ip and Ip/Me, co-condensation of IPTMS with isobutyltrimethoxysilane (IBTMS) or phenyltrimethoxysilane (PTMS) produced samples with smaller pore diameter (Ip/iBu and Ip/Ph) and, particularly in the case of Ip/Ph, a less defined PSD. Interestingly, the sample synthesized with octyltrimethoxysilane (OTMS) (Ip/Oc) does not possess defined mesopores, whereas the sample prepared with octadecyltrimethoxysilane (ODTMS) (Ip/Od) features a comparatively well-defined PSD with a maximum at 9.1 nm. Irrespective of the employed RTMS, C_{BET} values are lower than for the sample synthesized in the absence of a RTMS additive.

[121] H. Salmio, D. Brühwiler, *J. Phys. Chem. C* **2007**, *111*, 923; N. Gartmann, D. Brühwiler, *Angew. Chem. Int. Ed.* **2009**, *48*, 6354; T. Yokoi, H. Yoshitake, T. Tatsumi, *J. Mater. Chem.* **2004**, *14*, 951; M. H. Lim, A. Stein, *Chem. Mater.* **1999**, *11*, 3285.

[122] M. F. Ottaviani, A. Moscatelli, D. Desplantier-Giscard, F. Di Renzo, P. J. Kooyman, B. Alonso, A. Galarneau, *J. Phys. Chem. B* **2004**, *108*, 12123; D. Brunel, A. Cauvel, F. Di Renzo, F. Fajula, B. Fubini, B. Onida, E. Garrone, *New J. Chem.* **2000**, *24*, 807; L. Jelinek, E. Kováts, *Langmuir* **1994**, *10*, 4225.

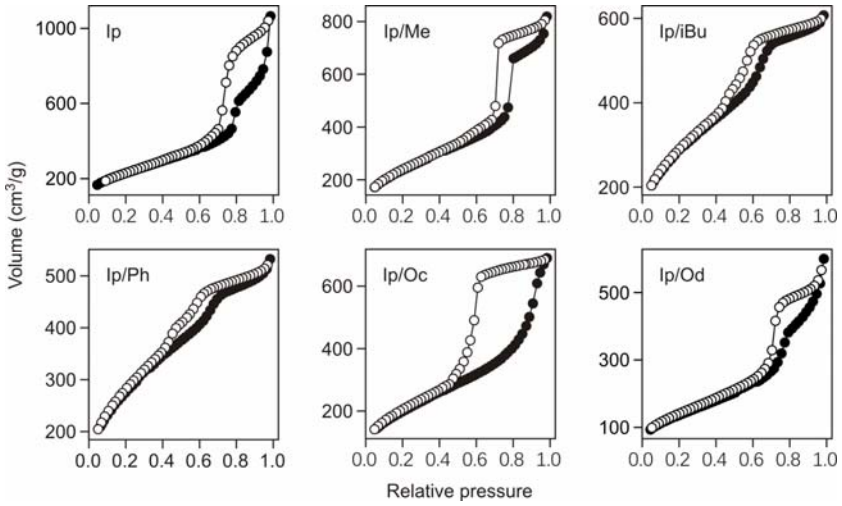

Figure 10 Nitrogen adsorption (●) and desorption isotherms (○) of monofunctionalized (Ip) and bifunctionalized mesoporous iodopropyl-silica.

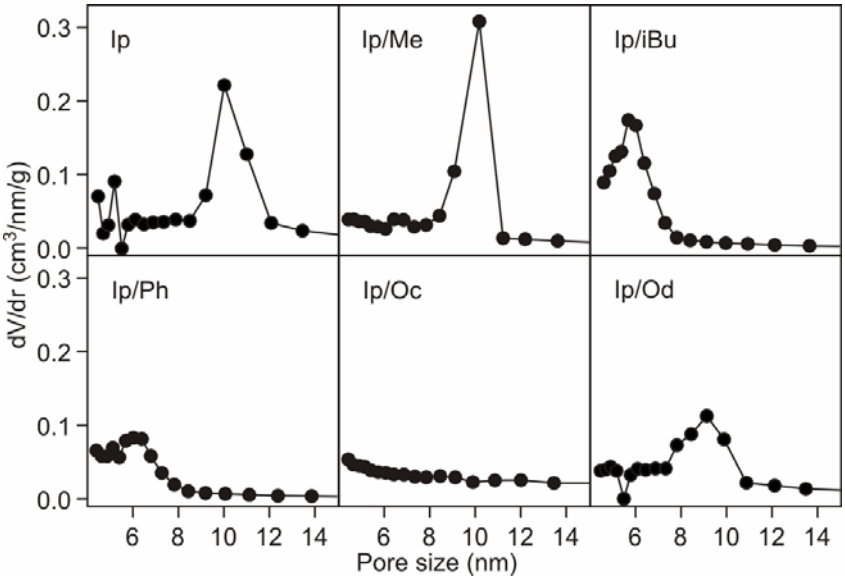

Figure 11 Pore size distributions of monofunctionalized (Ip) and bifunctionalized mesoporous iodopropyl-silica calculated (by BJH) from the adsorption isotherms shown in Figure 10.

The determination of the absolute amount of incorporated R moieties is complicated by a slight esterification of the silica surface upon extraction of the SDA with ethanol.[123] The values given in Table 4 were obtained by taking Ip as a reference. In accordance with the relative amounts of RTMS and IPTMS in the synthesis mixture, the n(R)/n(I) ratios in the final products are reasonably close to 10. More importantly, it can be concluded that the presence of a RTMS additive does not cause a significant change of the amount of incorporated iodopropyl moieties. In all cases, scanning electron microscopy images showed

[123] C. C. Ballard, E. C. Broge, R. K. Iler, D. S. St. John, J. R. McWhorter, *J. Phys. Chem.* **1961**, *65*, 20; T. Kimura, K. Kuroda, Y. Sugahara, K. Kuroda, *J. Porous Mater.* **1998**, *5*, 127.

particles with irregular morphology and sizes ranging from 2 µm to larger aggregates of ca. 50 µm.

Sample	R	n(IPTMS) [mmol]	n(RTMS) [mmol]	n(I)[a] [mmol/g]	n(R)[b] [mmol/g]	d_{BJH}[c] [nm]	S_{BET}[d] [m^2/g]	C_{BET}	V_{tot}[e] [cm^3/g]
Ip	–	0.15	0	0.09	0	10.0	832	95	1.65
Ip/Me	methyl	0.15	1.5	0.09	0.83	10.2	862	79	1.27
Ip/iBu	isobutyl	0.15	1.5	0.07	1.16	5.8	1057	61	0.94
Ip/Ph	phenyl	0.15	1.5	0.08	1.06	6.0	1010	76	0.82
Ip/Oc	octyl	0.15	1.5	0.06	0.66	–	798	56	1.07
Ip/Od	octadecyl	0.15	1.5	0.05	0.73	9.1	503	63	0.93
Ip-1.1	–	1.12	0	0.53	0	6.7	865	83	0.84
Ip-1.1/Me	methyl	1.12	1.5	0.53	0.52	5.9	969	62	0.95

Table 4 Structural properties of the functionalized samples.

[a] Iodine content from elemental analysis.

[b] Estimated from the carbon content obtained from elemental analysis.

[c] Average pore size calculated from the adsorption isotherm by the BJH method.

[d] Total BET surface area.

[e] Total pore volume (calculated at $p/p_0 = 0.98$).

High iodopropyl content

In terms of the PSD, the best results were obtained with MTMS as an additive (Figure 11). Therefore the same synthesis with an increased amount of IPTMS (samples Ip-1.1 and Ip-1.1/Me) was conducted. The 7.5-fold increase of the IPTMS concentration led to a substantially smaller pore size, whereas an identical amount of non-crosslinkable iodopropane did not show such an effect (Figure 12). Interestingly, the pore size difference between Ip-1.1 and Ip is retained after removal of the grafted iodopropyl moieties by calcination (Figure 13), thus indicating that the presence of IPTMS has a significant effect on the condensation of the silica framework.

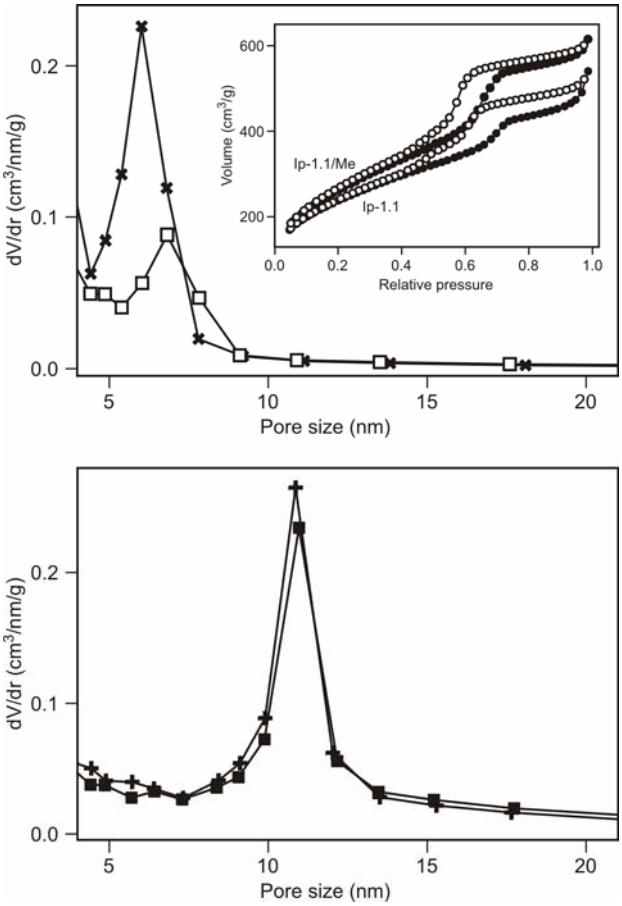

Figure 12 Top: Pore size distributions of Ip-1.1 (1.12 mmol of IPTMS, □) and Ip-1.1/Me (1.12 mmol of IPTMS and 1.5 mmol of MTMS, ×). The corresponding nitrogen sorption isotherms are shown in the inset. Bottom: Pore size distributions of a sample prepared without IPTMS/RTMS (+) and a sample synthesized with addition of 1.12 mmol of iodopropane (■).

The bifunctionalized sample Ip-1.1/Me is superior to the monofunctionalized sample Ip-1.1 in terms of containing a minimum relative amount of secondary mesopores. This is in agreement with the results obtained from the corresponding samples synthesized with a smaller concentration of IPTMS (Ip and Ip/Me). The addition of MTMS obviously does not affect the incorporation of IPTMS into the silica framework, as indicated by the iodo contents of Ip-1.1 and Ip-1.1/Me (Table 4).

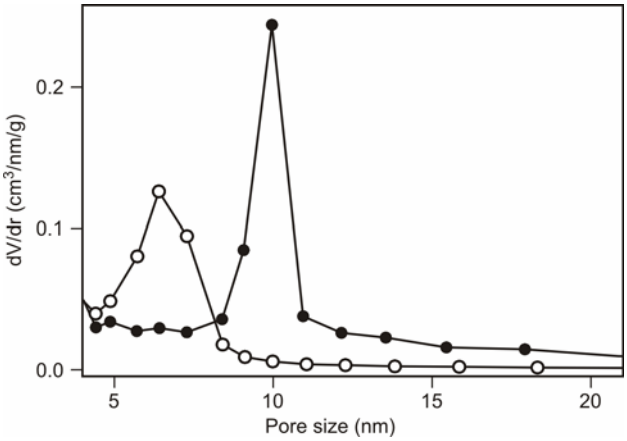

Figure 13 Pore size distribution of Ip-1.1 (○) and Ip (●) after removal of the iodopropyl moieties by calcination.

Conclusion

IPTMS and RTMS were successfully co-condensed with TEOS in the presence of Pluronic P123 as a structure-directing agent to yield bifunctionalized mesoporous silica. The best results in terms of a narrow PSD were obtained with R = methyl which seemed to be even superior to purely IPTMS co-condensed silica. As evident from the low C_{BET} values, the inclusion of alkyl moieties causes a change in surface properties, thus opening possibilities to tailor the environment of the iodopropyl sites.

3.3 Inclusion of Resorufin

3.3.1 Adsorption

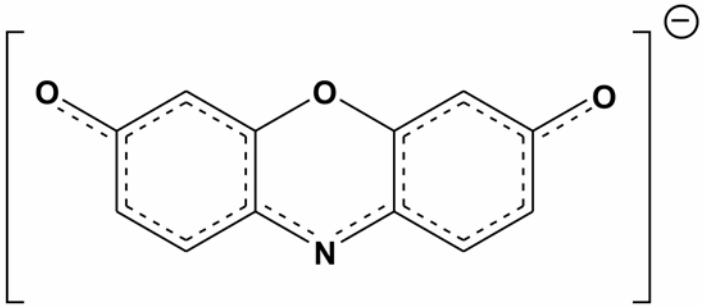

Figure 14 Resorufin anion.

The use of mesoporous materials as drug delivery systems is of great current interest.[124] In this context, the possibility of an incorporation of the resorufin anion (Res^-) in MCM-41 was investigated. In contrast to the microporous system of zeolites which is complicating an inclusion due to the anionic framework, it is worth mentioning that for mesoporous silica an adequate environment for an inclusion can be generated by postsynthetic modification. The potential advantage of Res^- as a drug model lies in the possibility of measuring release kinetics in situ by luminescence spectroscopy. Previous experiments with Res^- showed a strong quenching of the luminescence when the dye was incorporated into zeolite L[125], which could be exploited, since for a release from the channels the luminescence signal increases again. Res^- is a strongly fluorescent molecule with a quantum yield of $\Phi_F = 0.74$[126] and 0.83[127] in water at pH = 9.5 and 10, respectively. However, it has to be considered that by switching to acidic conditions the quantum yield is reduced due to the formation of resorufin (ResH).[126] Below pH 3 nearly no fluorescence is detected. As a consequence, a certain pH value has to be selected for the detection.

MCM-41 synthesised by procedure 5.1.1 was used as host material, exhibiting a relatively small pore size (with respect to other mesoporous silica materials) of about 2.8 nm (calculated by the BJH method). For the incorporation of an anion, the channels were

[124] K. Inumaru, J. Kiyoto, S. Yamanaka, *Chem. Commun.* **2000**, 903; C. Charnay, S. Bégu, C. Tourné-Péteilh, L. Nicole, D. A. Lerner, J. M. Devoisselle, *Eur. J. Pharm. Biopharm.* **2004**, *57*, 533 ; M. Vallet-Regi, A. Ramila, R. P. del Real, J. Pérez-Pariente, *Chem. Mater.* **2000**, *13*, 308; A. Bogershausen, S. J. Pas, A. J. Hill, H. Koller, *Chem. Mater.* **2006**, *18*, 664; Q. Yang, S. Wang, P. Fan, L. Wang, Y. Di, K. Lin, F.-S. Xiao, *Chem. Mater.* **2005**, *17*, 5999; B. Munoz, A. Ramila, J. Perez-Pariente, I. Diaz, M. Vallet-Regi, *Chem. Mater.* **2002**, *15*, 500.
[125] D. Brühwiler, N. Gfeller, G. Calzaferri, *J. Phys. Chem. B* **1998**, *102*, 2923.
[126] C. Bueno, M. L. Villegas, S. G. Bertolott, C. M. Previtali, M. G. Neumann, M. V. Encinas, *Photochem. Photobiol.* **2002**, *76*, 385.
[127] H. A. Montejano, M. Gervaldo, S. G. Bertolotti, *Dyes and Pigments* **2005**, *64*, 117.

functionalized with trimethoxysilylpropyl(trimethyl)ammonium chloride TMSTAC (5.2.1). The positively charged ammonium groups allow exchange of chloride ions with Res^-. The grafted amount was varied between 50 µL and 1000 µL TMSTAC per g (MCM-41) (0.2 - 3.8 mmol/g).

As a side effect of the higher functionalization degree, the average pore size is reduced. This is confirmed by nitrogen sorption measurements (Figure 15, Table 5). For 1000 µL TMSTAC/g (MCM-41), only a flat line is visible due to the scale of the ordinate.

#	TMSTAC [µL/g(MCM-41)]	Pore size[a] [nm]	V_P[b] [cm³/g]
M-1	0	2.8	0.73
MT-2	100	2.5	0.49
MT-3	200	2.4	0.66
MT-4	300	2.4	0.39
MT-5	400	2.3	0.52
MT-6	1000	~2.2	0.01

Table 5 Nitrogen adsorption data of TMSTAC modified MCM-41;
[a] Pore size calculated by the BJH method using the adsorption branch;
[b] Primary pore volume at a relative pressure of 0.4.

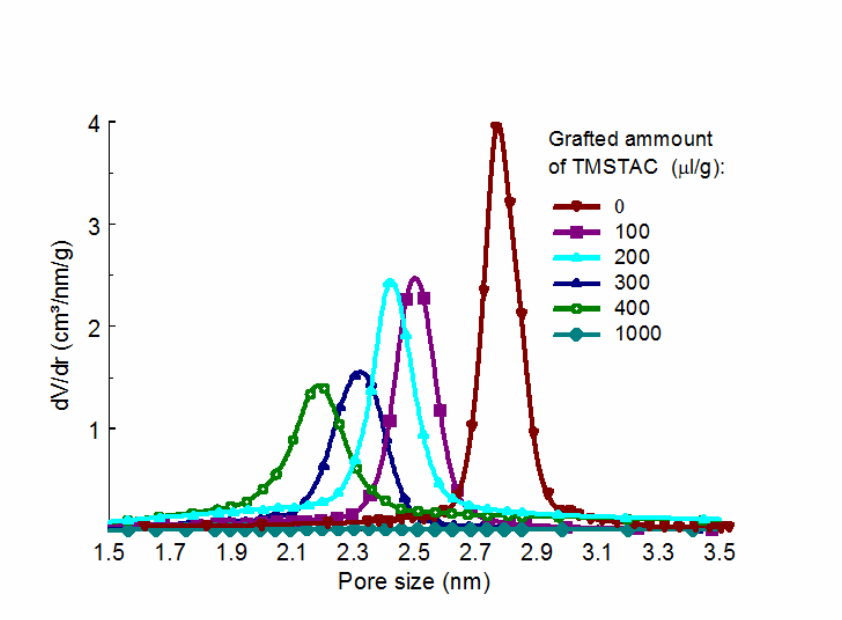

Figure 15 Pore size distribution of MCM-41 samples with different amounts of grafted TMSTAC.

Subsequent ion exchange leads to the inclusion of Res^- (5.6.2) and provides therefore a model for a controlled drug release (Figure 16). This procedure was conducted under mild

conditions at RT by dispersing the functionalised MCM-41 in a stock solution of Res^- (in 1-butanol; 0.4 - 0.5 mmol/L).

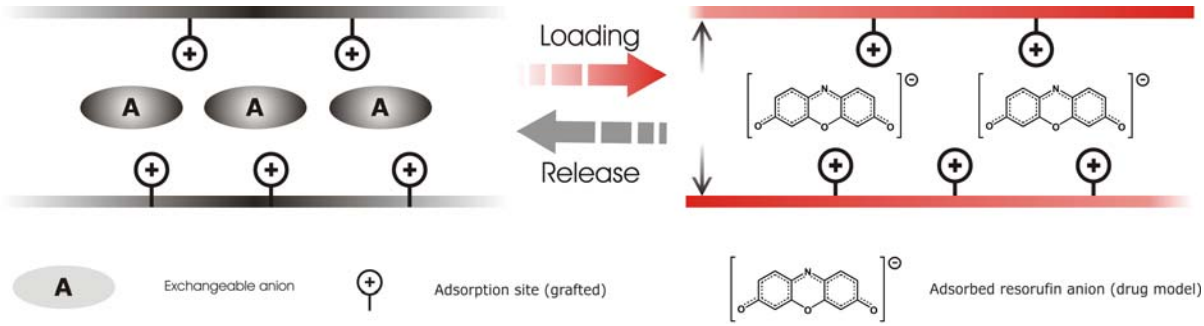

Figure 16 Controlled loading and release of Res^-.

The amount of adsorbed Res^- was determined either by extraction in an aqueous sodium chloride solution (for small Res^- amounts) (5.7.2.1) or by dissolving the silica sample in 0.02 N NaOH (for large Res^- amounts) (5.7.1.3). The absorption spectra were measured and Res^- loadings of 0.2 to 30 µmol/g (Table 6) were determined. A typical absorption and emission spectrum of Res^- in 0.02N NaOH is given in Figure 17.

#	TMSTAC [µL/g(MCM-41)]	TMSTAC [µmol/g(MCM-41)]	Intensity at 584 nm	Res^- loading [µmol/g(MCM-41)]
M-1	0	0	6	~0
MT-2	100	377	87	7
MT-3	200	753	186	16
MT-4	300	1130	930	19
MT-5	400	1507	460	13
MT-6	1000	3767	42	~0

Table 6 Res^- uptake in dependence of the amount of TMSTAC.

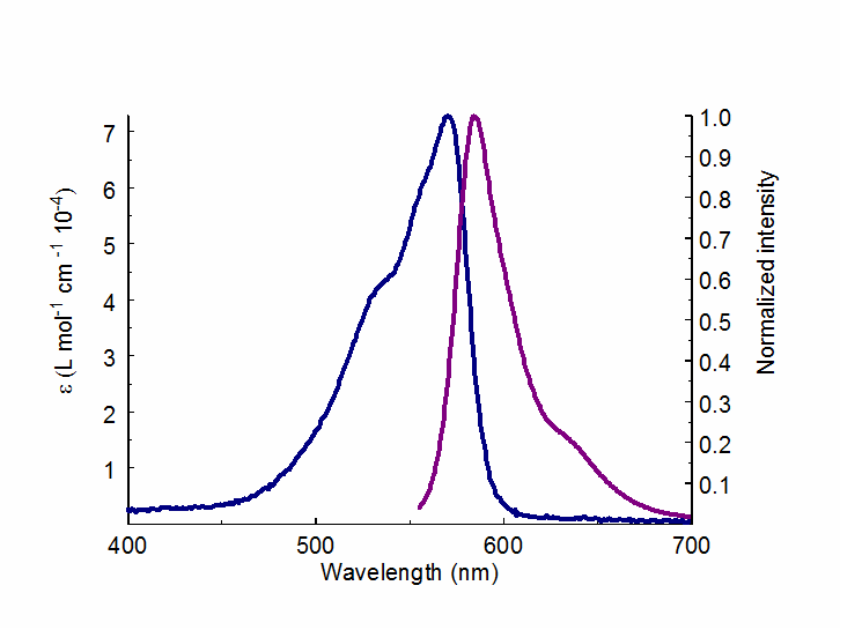

Figure 17 Absorption and emission spectra of Res^- in 0.02 N $NaOH_{(aq)}$. Excitation was performed at 535 nm.

The intensity of the measured luminescence spectra depends strongly on the amount of grafted TMSTAC groups. A relatively high loading with a distinct pore size distribution was achieved at around 300 µL TMSTAC / g (MCM-41). A higher TMSTAC group content leads to blocking of the pores and therefore also to a reduced uptake capacity, whereas small TMSTAC amounts do not provide sufficient ammonium chloride groups for the ion exchange. Table 6 gives an overview of Res^- uptake. The same loading conditions were used for each sample, since variations, such as in the amount of used silica sample, result in significant variation of the uptake. In the absence of the ammonium groups, no uptake of Res^- was observed (M-1). The Res^- amounts for M-1 as a "blank" sample and MT-6 as a sample with blocked pores are below the detection limit of the UV/Vis method and also fluorescence measurements did not show significant intensity.

Upon washing, a significant amount of adsorbed molecules was removed, yielding a maximum amount of about 40 % of included Res^-.

3.3.2 Release

In order to obtain a delivery profile, the dye release of the samples was investigated (Figure 18). In analogy to Ref. 125, the release was followed by fluorescence spectroscopy. A cuvette was filled with a weighed amount (typically about 4.5 mg) of the Res^- loaded silica and 3 mL

of solvent was added. After a certain time for equilibration of the emission signal, the release was triggered by addition of 0.5 mL of a sodium chloride solution with different concentrations (usually between 0.2 and 2 mol/L). A significant increase in the intensity was detected after the addition, which indicated the release from the channels. A blank test without the silica material pointed out that the addition of sodium chloride solution had no effect on the luminescence intensity.

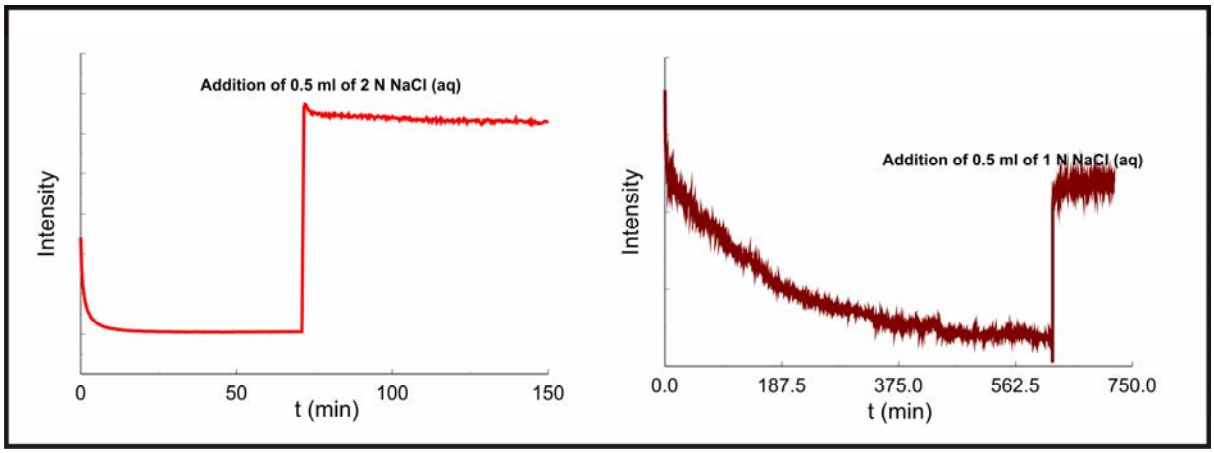

Figure 18 Release profile of Res^- in ethanol (left) and water (right) (λ_{Ex} = 535 nm; λ_{Em} = 585 nm).

A strong initial decrease of the fluorescence intensity is observed directly after the addition of the solvent. This was initially assumed to be a stirring and aggregation effect. Nevertheless, an investigation of a possible solvent effect was undertaken by comparing a "dry"-(stored at 60 °C for several hours) and a "wet" sample. The latter was prepared by storage under an atmosphere with high humidity by keeping it in a closed container over a saturated solution of potassium nitrate (ca. 93 % humidity at 25 °C). Subsequent luminescence measurements of the "dry" and "wet" sample revealed a significantly reduced luminescence for the "wet" state (Figure 19). An influence of water on the luminescent intensity was already detected for tris-(2,2´-bipyridine)-ruthenium(II) complexes incorporated in FSM type silica.[128] In this case, adsorption of water led to an increase in the intensity due to a reduced aggregation. This effect seems unlikely for the inclusion of Res^- which shows a contrary behaviour. Instead, a possible explanation can be given by a partial protonation of Res^- to ResH, which features strongly reduced fluorescence intensity at the wavelength of detection. Protonation can be achieved by reaction with silanol groups which will form on the surface by the adsorption of water. It was also shown that this process is partially reversible, since a subsequent drying of the "wet" sample at 60 °C led to an increase of the luminescent intensity.

[128] M. Ogawa, T. Nakamura, J.-I. Mori, K. Kuroda, *J. Phys. Chem. B* **2000**, *104*, 8554.

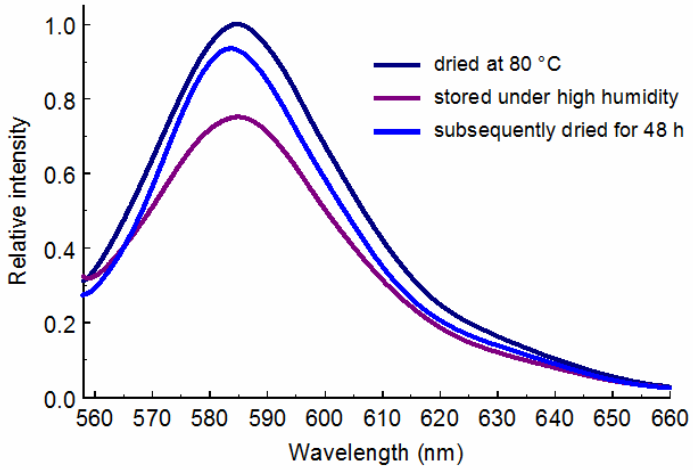

Figure 19 Fluorescence spectra of a "dry" and a "wet" Res˙ sample (λ_{Ex} = 535 nm).

A comparison of the initial drop of the luminescence intensity by using a "wet" and a "dry" sample for the time-dependent luminescence measurements resulted in a more stable signal for the "wet" sample, which confirmed the effect as being mainly solvent dependent (Figure 20).

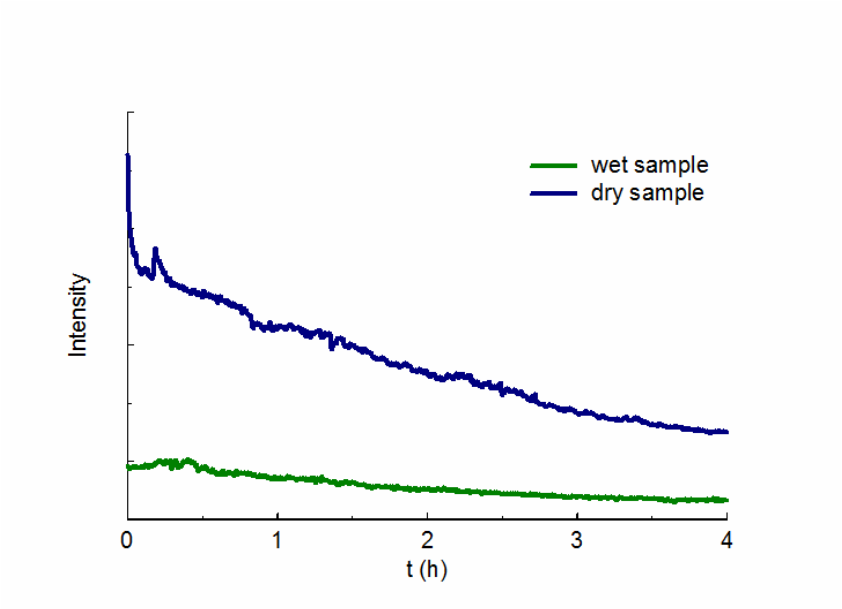

Figure 20 Fluorescence signal for a „wet" and a „dry" sample in water (λ_{Ex} = 535 nm; λ_{Em} = 585 nm).

Conclusion

The release of anionic dyes from functionalized MCM-41 was investigated by the incorporation of Res^- as a model compound for a drug delivery system. The loading from solution was shown to be depending on the amount of grafted TMSTAC which defines the amount of positive surface charges as well as the pore size. Further measurements on the release of Res^- should therefore also focus on possible effects of the amount of grafted TMSTAC. Monitoring of the release process by luminescence detection was established as an adequate method, although humidity was shown to have a distinct influence on the emission.

A mesoporous material with stimuli-responsive gates in combination with the monitoring of Res^- by fluorescence spectroscopy is expected to provide valuable information on the release kinetics of such delivery systems.

3.4 Functionalization with Nile Red

3.4.1 Introduction

Applications of nile red (NR) are mostly found in biological and medical research due to its ability to indicate lipids,[129] to stain proteins[130] or to detect the ligand-binding to enzymes[131] by fluorescence. NR is assigned to the class of angular benzo[*a*]phenoxazines (Figure 21).

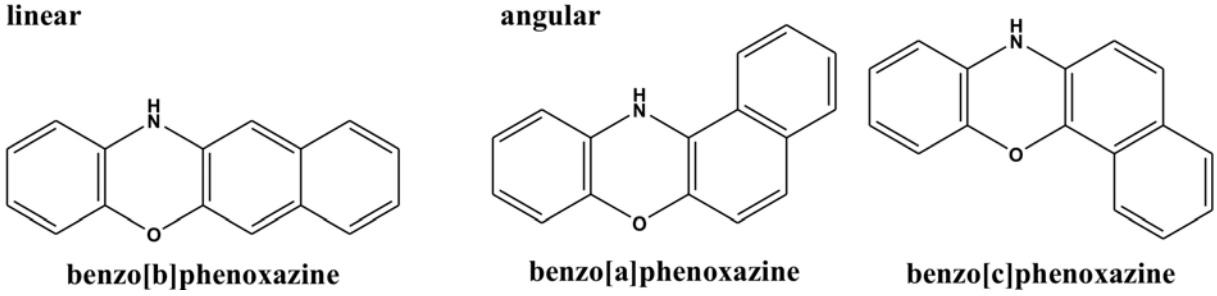

Figure 21 Benzophenoxazine structural isomers.

Electron accepting and/or donating substituents on the benzophenoxazine core can lead to compounds with interesting photophysical properties.[132] NR features on one side an electron donating diethylamino substituent and on the other an electron accepting carbonyl group which results in interesting fluorescent properties (Figure 22). Reasonably high fluorescence quantum yields in apolar solvents and long wavelength emission offer intriguing properties for fluorescent probing applications. NR shows good photochemical stability and has been proposed as a laser dye.[133]

[129] P. Greenspan, S. D. Fowler, *J. Lipid Res.* **1985**, *26*, 781; H. Morjani, N. Aouali, R. Belhoussine, R. J. Veldman, T. Levade, M. Manfait, *Int. J. Cancer* **2001**, *94*, 157; A. M. Klinkner, P. J. Bugelski, C. R. Waites, C. Louden, T. K. Hart, W. D. Kems, *J. Histochem. Cytochem.* **1997**, *45*, 743.
[130] D. L. Sackett, J. Wolff, *Anal. Biochem.* **1987**, *167*, 228; J.-R. Daban, *Electrophoresis* **2001**, *22*, 874; M. Sutter, S. Oliveira, N. N. Sanders, B. Lucas, A. van Hoek, M. A. Hink, A. Visser, S. C. De Smedt, W. E. Hennink, W. Jiskoot, *J. Fluoresc.* **2007**, *17*, 181.
[131] S. B. Ruvinov, X.-J. Yang, K. D. Parris, U. Banik, S. A. Ahmed, E. W. Miles, D. L. Sackett, *J. Biol. Chem.* **1995**, *270*, 6357.
[132] J. Jose, K. Burgess, *Tetrahedron* **2006**, *62*, 11021; J. Jose, K. Burgess, *J. Org. Chem.* **2006**, *71*, 7835.
[133] D. Basting, D. Ouw, F. P. Schäfer, *Opt. Commun.* **1976**, *18*, 260.

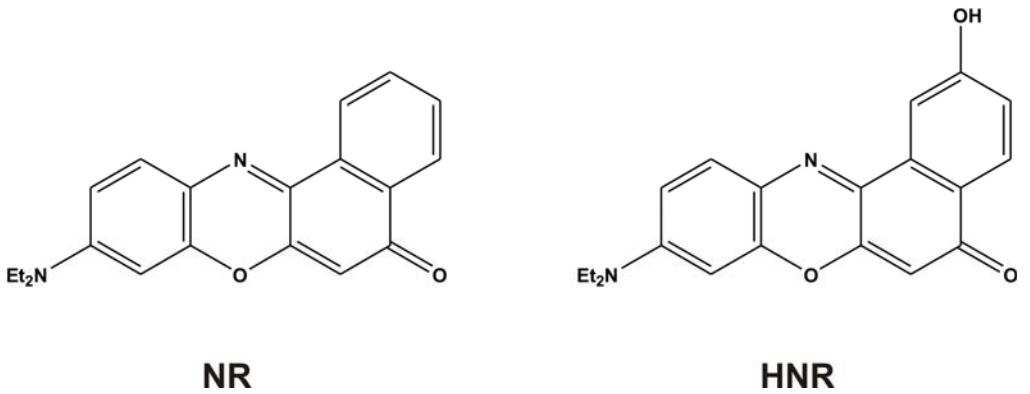

Figure 22 Structures of nile red (NR) and 2-hydroxy nile red (HNR).

The solubility in water is poor, but is increased for more apolar solvents. Due to its distinct solvatochromic effect, NR was investigated in various liquids and used for the description of solvent strength.[134] Polar solvents, featuring reduced solubility, cause a bathochromic shift, but also a considerable decrease of the luminescence quantum yield is observed.[132,135]

Due to the intriguing properties of NR, many functionalized derivatives were synthesized in order to investigate the fluorescence behaviour, to increase the solubility in aqueous media or to enable a linking reaction as a fluorescent label. Briggs et al. were therefore investigating the 9-diethylamino-2-hydroxy-5H-benzo[*a*]phenoxazine-2-one or 2-hydroxy nile red (HNR) (Figure 22), which was shown to exhibit stronger fluorescence compared to the 1-hydroxy derivative.[136] Based on the synthesis of the 1- and 2-hydroxy derivatives,[137] a carboxyl group was introduced via the 2-position, resulting in a potential fluorescent label for biomolecules.

A modification of mesoporous silica with NR offers the possibility to probe the environment around the NR binding sites. Moreover, the functionalized silica can be used to detect different solvents or gases.[138] Inclusion in comparable structures in the microporous range (zeolites) was realized for the detection of humidity[139] or solvents.[140] The modification with NR can further provide evidence concerning the surface polarity.

---

[134] J. F. Deye, T. A. Berger, A. G. Anderson, *Anal. Chem.* **2002**, *62*, 615.
[135] O. Valdes-Aguilera, D. Neckers, *Acc. Chem. Res.* **1989**, *22*, 171.
[136] M. S. J. Briggs, I. Bruce, J. N. Miller, C. J. Moody, A. C. Simmonds, E. Swann, *J. Chem. Soc., Perkin Trans. 1* **1997**, 1051.
[137] N. N. Alekseev, A. Ya. Gorelenko, N. N. Vasilév, *Otkrytiya, Izobret., Prom. Obraztsy, Tovarnye Znaki* **1984**, *31*, 66; *Chem. Abstr.* **1984**, *101*, 230, 551.
[138] A. B. Descalzo, M. Dolores Marcos, C. Monte, R. Martínez-Mánez, K. Rurack, *J. Mater. Chem*. **2007**, *17*, 4716.
[139] I. Pellejero, M. Urbiztondo, D. Izquierdo, S. Irusta, I. Salinas, M. P. Pina, in *Conference on Advanced Membrane Technol. III Membrane Engineering for Process Intensification*, Amer. Chem. Soc., Cetraro, Italy, **2006**, pp. 2335.
[140] M. Urbiztondo, S. Irusta, R. Mallada, M. P. Pina, J. Santamaría, *Desalination*, **2006**, *200*, 601.

3.4.2 Inclusion of nile red

Probing the silica surface of functionalized MCM-41 was attempted by exploiting the polarity sensitive properties of NR. Inclusion was realized by adsorption from a dye solution (5.6.1). Pentane was found to be an excellent solvent for this purpose since the low solubility of NR led to a relatively efficient inclusion into the silica channels. More polar solvents such as ethanol, though offering much higher concentrations of NR, gave only small loadings. The high solubility of NR in ethanol was exploited for the determination of the loading by extraction (5.7.1).

The unmodified silica surface is relatively polar due to the presence of silanol groups. In contrast, a hydrophobic surface can be created by grafting of alkyltrialkoxysilanes. However, first experiments resulted only in a slight increase of the hydrophobicity, as detected by luminescence measurements of the NR loaded samples. Better results were obtained by using highly reactive chlorosilanes at increased temperature and in presence of amines (5.2.7.1/5.2.7.2/5.2.7.3). Monochlorosilanes were used for these reactions to exclude the possibility of generating additional silanol groups due to conversion of unreacted alkoxy- or chlorosilanes as illustrated in Figure 23.

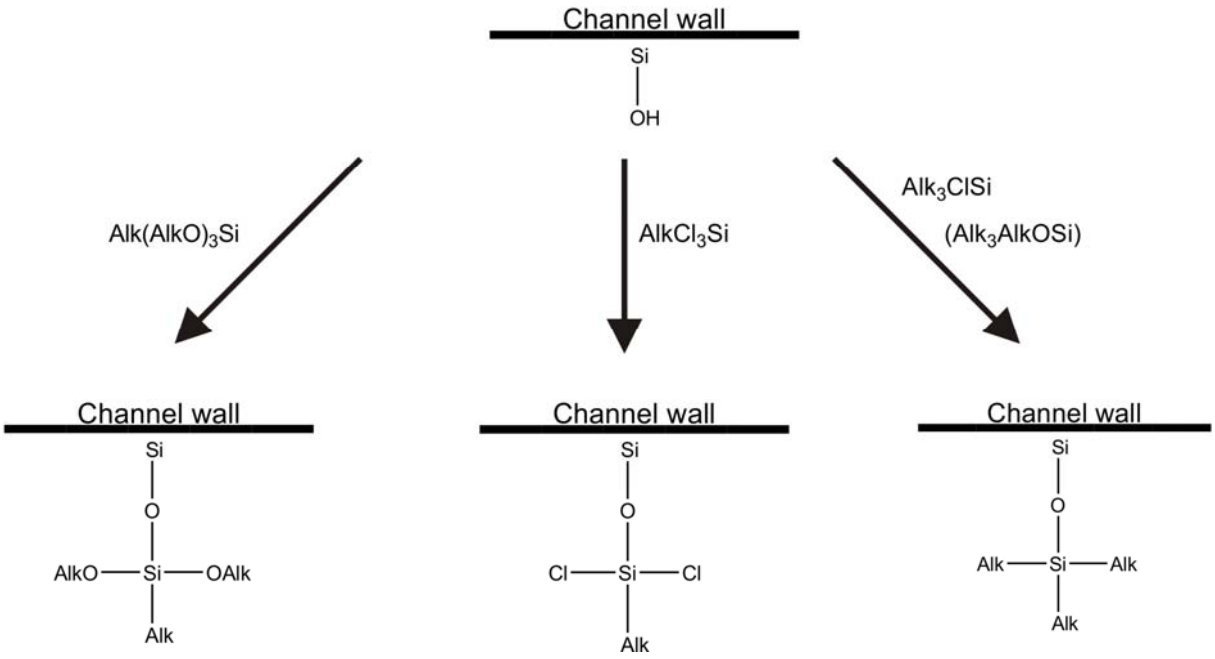

Figure 23 Silylation with chloro- and alkoxysilanes.

An excess of chlorosilanes was used to allow a complete conversion of the silanol groups. The density on the surface was calculated based on a silanol content of 3 nm^{-2} for MCM-41[141] and using a surface area of 1000 m^2/g leading to an amount of 5 mmol/g.

All samples show similar amounts of adsorbed NR (Table 7). The samples were loaded by dispersing a distinct amount of MCM-41 in a standard solution of ~11 mg/L NR in pentane, corresponding to ~7 μmol/g (MCM-41) for a standard synthesis (5.6.1) by assuming a complete uptake of NR. The resulting NR loading varies between 4.7 and 6.5 μmol/g (MCM-41), indicating more than 50 % adsorption. The corresponding luminescence spectra of the solid samples are given in Figure 24. Unmodified MCM-41 shows relatively weak luminescence intensity after NR adsorption. For silylated samples, a hypsochromic shift and an increased intensity is detected. While the appearance of NR in unmodified silicas is purple, it changes to a bright red-pink if included in silylated MCM-41. Grafting of alkoxysilanes by use of ODTMS (octadecyltrimethoxysilane) in amounts below the total amount of silanol groups instead shows no significant difference compared to unmodified NR loaded MCM-41 samples.

#	Surface modification	Amount of silane [mmol/g(MCM-41)]	Amount of NR [μmol/g(MCM-41)]
MN1	ODTMS	0.7	6.5
MN2	ODMCS	38	5.1
MN3	TMCS	79	6.4
MN4	without	--	4.7

Table 7 Loading and surface modification data of NR- MCM-41 samples.

[141] X. S. Zhao, G. Q. Lu, A. K. Whittaker, G. J. Millar, H. Y. Zhu, *J. Phys. Chem. B* **1997**, *101*, 6525; I. G. Shenderovich, G. Buntkowsky, A. Schreiber, E. Gedat, S. Sharif, J. Albrecht, N. S. Golubev, G. H. Findenegg, H.-H. Limbach, *J. Phys. Chem. B* **2003**, *107*, 11924.

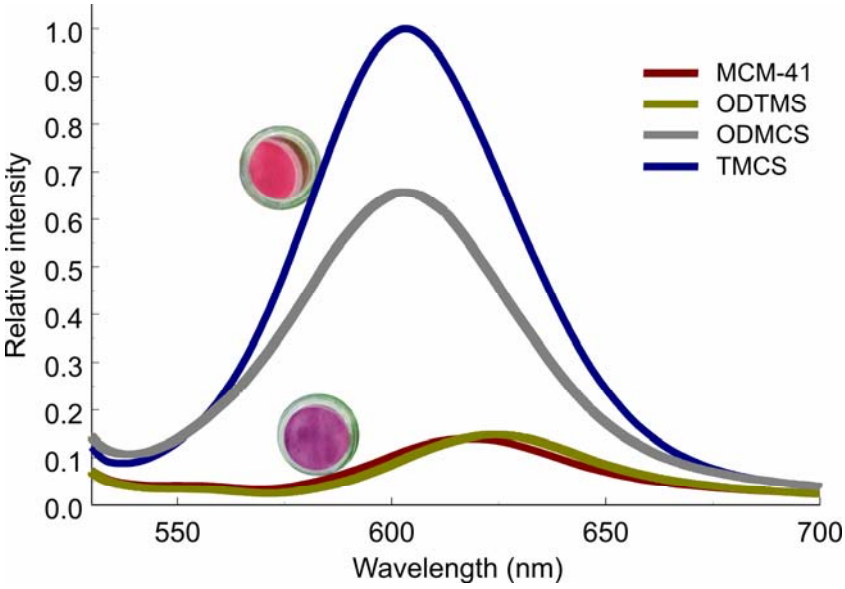

Figure 24 Luminescence spectra of adsorbed NR in unmodified, TMCS-, ODMCS- and ODTMS grafted MCM-41; Excitation was performed at 500 nm; Photographic images of samples MN3 and MN4 are shown next to the corresponding plots.

Slight intensity differences between the samples prepared with trimethylchlorosilane (TMCS) and octyldimethylchlorosilanes (ODMCS) are observed. Possible explanations are the different NR loadings as well as incomplete reaction of the silanol groups due to silylation with different alkylchlorosilanes.

3.4.3 Detection of surface polarity

A desirable feature is the creation of a detection range for different surface polarities. A silylated surface was used as a starting point, due to the intense luminescence of NR under these conditions. A modification with polar surface groups (aminopropyl) should then lead to a decrease of the luminescence. The synthetic approach includes the grafting of different amounts of amino groups (5.2.2) and subsequent silylation (5.2.7.1) to convert the remaining silanol groups. NR is finally adsorbed as described above (respectively 5.7.1). A scheme of the synthetic procedure is given in Figure 25.

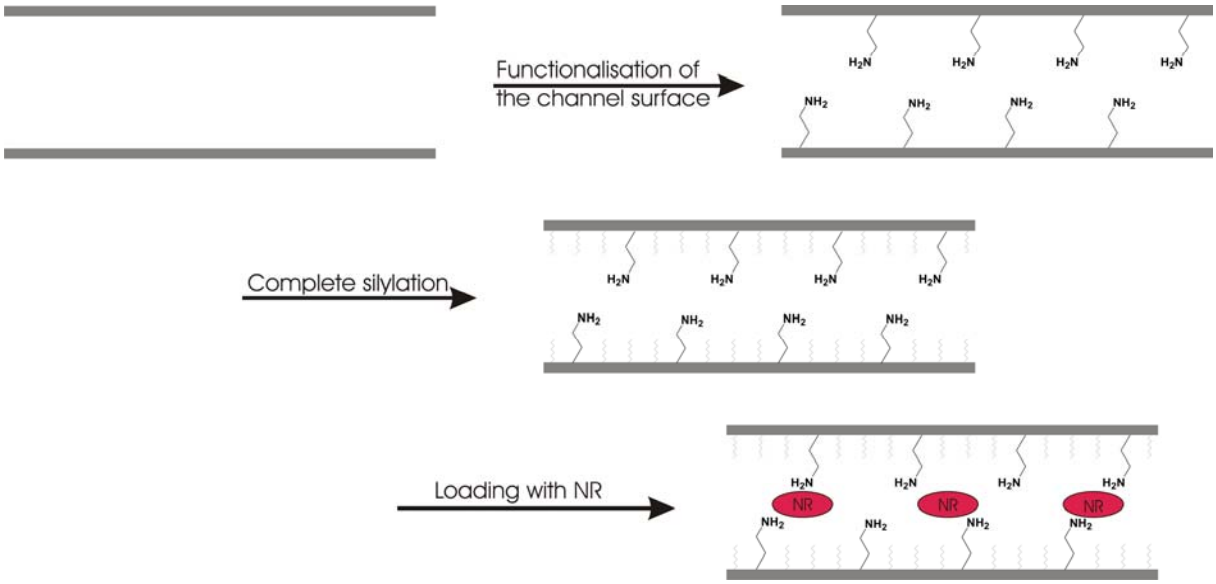

Figure 25 Surface modification and inclusion of NR.

The resulting NR loadings vary between 4 and 6.5 µmol/g (MCM-41) and are shown in Table 8. Slight variations occur, but show no trend in dependence of the amount of APTMS.

sample	APTMS content [µmol/g(MCM-41)]	NR loading [µmol/g(MCM-41)]
MN-3	0	6.4
MN-5	55	4.4
MN-6	110	4.0
MN-7	280	4.7
MN-8	1100	5.8

Table 8 Loadings of NR.

The pore size distribution and the corresponding C_{BET}-values confirm variations in the pore size and also in the surface properties upon functionalization. The pore size was calculated by the BJH method as well as by the DFT method utilizing the adsorption isotherm. For unmodified samples, DFT provides an excellent description of the pore size (3.9 nm). However, no adequate models exist for the treatment of organo-functionalized surfaces by DFT. This is possibly the reason for the equal pore sizes obtained for the modified samples (Table 9). Therefore, the variation of the pore size is more accurately verified by calculation with BJH. For highest amounts of APTMS, the smallest pore size of about 2.1 nm (BJH) is obtained. Reduction of the APTMS amount leads to an increase of the pore size. This is in

agreement with the size of the different silanes, since the aminopropyl group of APTMS is more bulky than the methyl groups of TMMS.

The largest differences in the C_{BET}-values are found for unmodified and silylated samples, corresponding to the expected polarity differences. For the different amounts of grafted APTMS, only a slight change of the C_{BET}-values is obtained (from 29 to 38).

Sample	APTMS content [µmol/g]	C_{BET}	Pore size[a] [nm]	Pore size[b] [nm]
MN-3	0	29	3.54	2.44
MN-5	55	30	3.54	2.37
MN-6	110	29	3.54	2.38
MN-7	280	31	3.54	2.37
MN-8	1100	38	3.18	2.12
MN-4	unmodified	94	3.93	2.78

Table 9 Pore size analysis data in function of APTMS modification.
[a] Average pore size calculated from the adsorption isotherm by the DFT method.
[b] Average pore size calculated from the adsorption isotherm by the BJH method.

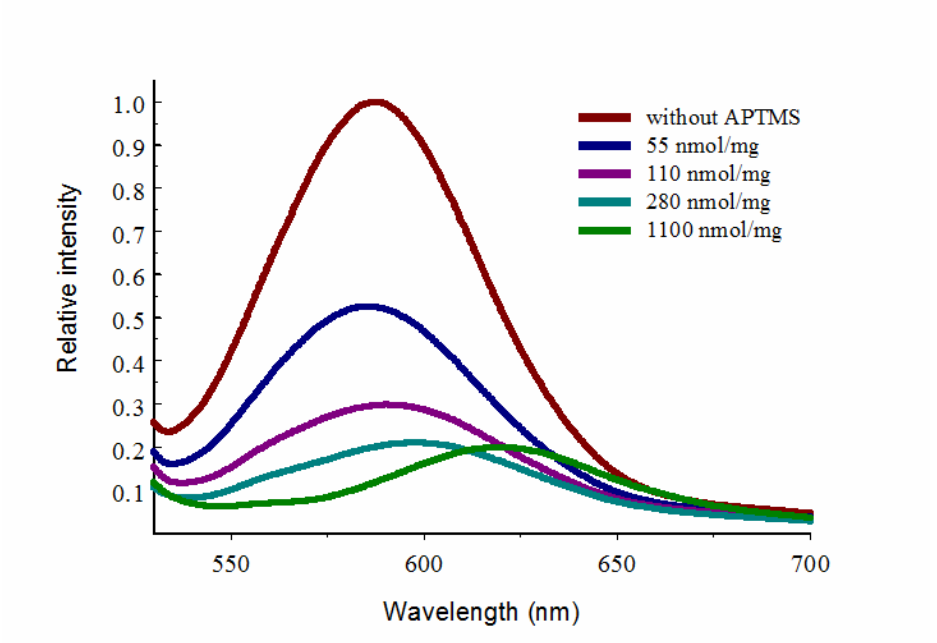

Figure 26 Luminescence spectra of NR-MCM-41 samples of different polarity; Excitation was performed at 500 nm.

The luminescence spectra of the solid samples are shown in Figure 26. Highest luminescence intensity is observed for samples without amino groups. An increase of the amino content

leads to a decrease of the intensity and also a slight shift for high APTMS concentrations. The results prove the applicability of NR as a detection agent for the polarity of the silica surface and confirm the C_{BET}-values. It is remarkable that despite of only slight differences in the C_{BET}-values for different amino contents, the NR luminescence seems to be particularly sensitive to the small differences in the surface properties in this polarity range.
However, aggregation of NR molecules in the channels, which would lead to a quenching of the luminescence, is a potential problem.

3.4.4 Covalent attachment

Direct coupling of a NR derivative to the surface of MCM-41 provides a possible solution for the aggregation problem. Besides co-condensation, a grafting approach is suitable for this task, avoiding extreme basicity, pressure and temperature, which are required for co-condensation. Various linkers are possible for the connection to the silica surface.
Relatively stable and frequently used bonding types for the connection are ester, amide or ether bonds. This requires modification of the silica surface and NR with amino-, carboxyl-, hydroxyl- or halogen groups. A retrosynthetic scheme of the pathways is shown in Figure 27. The surface functionalization is performed with amino-, halogen- or carboxyl groups, which can be attached to the surface via the respective silane. Carboxyl groups were generated via functionalization with TESPN (3-(Triethoxysilyl)propionitrile) and subsequent oxidation of the nitril groups with sulfuric acid via 5.2.5 and 5.2.6. As a NR derivative, a 2-hydroxy functionalized form was chosen. The retrosynthesis of HNR is shown in Figure 28. The synthesis is conducted by introduction of a 2-nitroso group to 3-diethylaminophenol (5.3.1.1) and subsequent reaction of 5-diethylamino-2-nitrosophenol (DNP) with an equimolar amount of 1,6-dihydroxy-naphthalene (5.3.1.2).

Three different linking types are outlined in Figure 27, where type I is coupled by a combination of an amide and an ester linker and requires more synthetic effort due to an additional synthesis step (Figure 27, bottom). The product was synthesized by a reaction of HNR with adipic acid (5.3.1.3) and subsequent coupling with the amino functionalized silica via reaction 5.4.2.2 resulting in a yield of about 15 %. The surface bound amino group is generated by reaction with APDIPES (3-Aminopropyldiisopropylethoxysilane) (5.2.2).

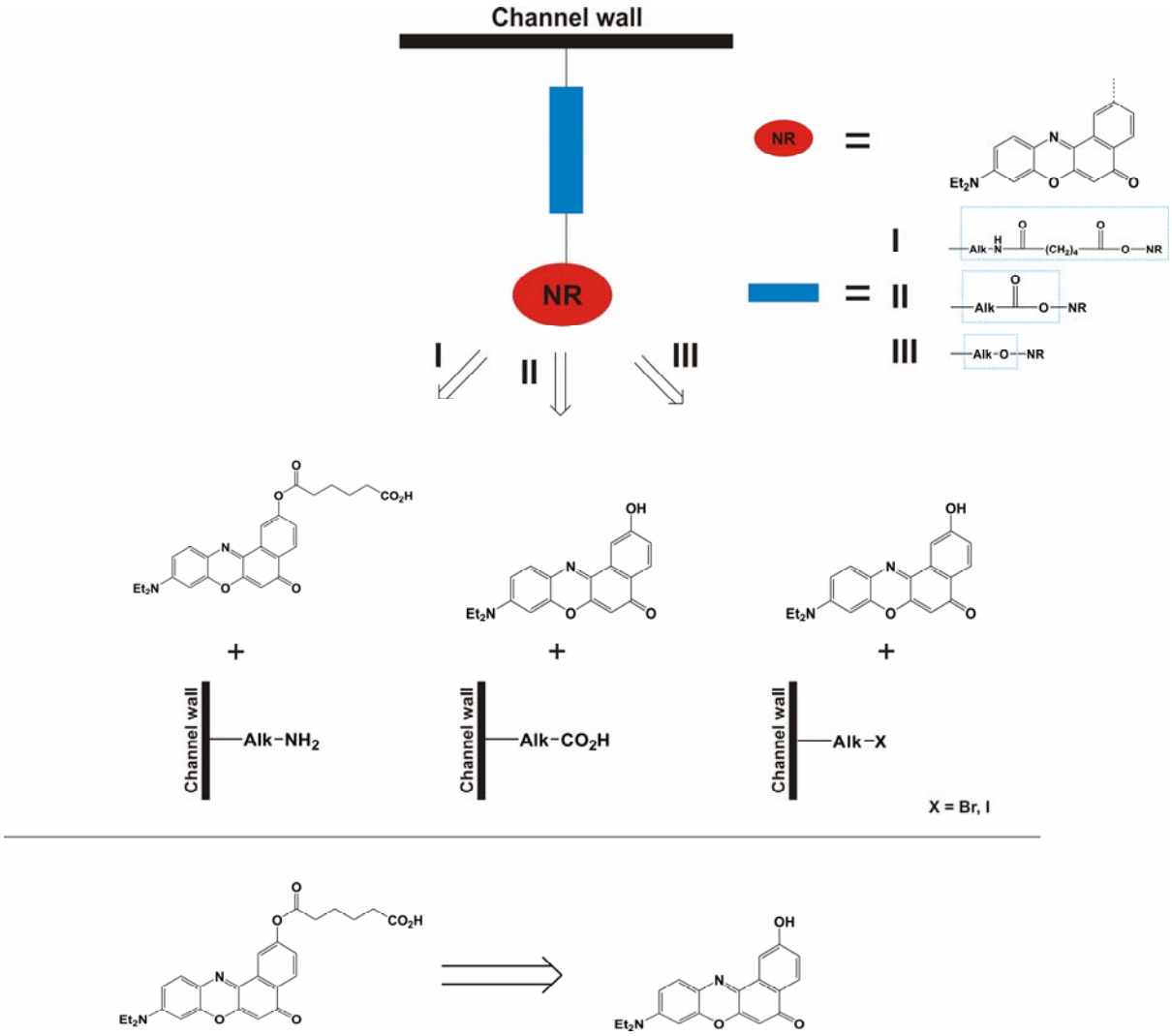

Figure 27 Retrosynthetic scheme of different NR functionalization pathways.

Synthesis route II gave deeply coloured samples. Coupling was accomplished by introduction of carboxylic groups to the surface. This required grafting of TESPN and subsequent oxidation with sulfuric acid according to 5.2.5 and 5.2.6. Afterwards the coupling was achieved by reaction with HNR under addition of DCC in dichloromethane (5.4.2.3). Partial discoloration of these samples was observed by extraction under reflux with ethanol over 24 h, indicating lack of stability of surface anchoring. Additionally, the samples showed very low fluorescence intensity, although a high content of NR was found (about 140 µmol/g). This is most likely due to self-quenching by close proximity of the NR moieties.

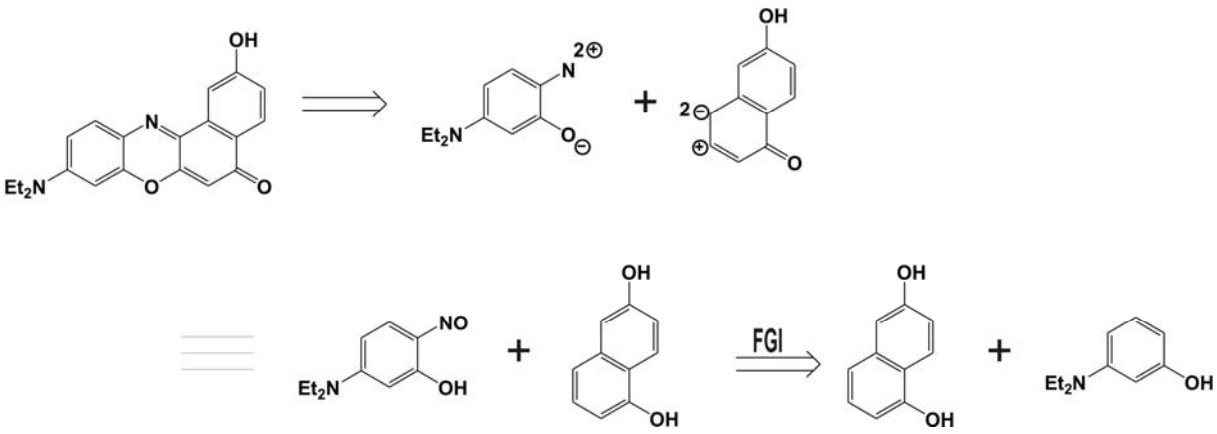

Figure 28 Retrosynthesis of 2-hydroxy nile red (HNR).

Products synthesized by type III showed good stability without decomposition after Soxhlet extraction with ethanol for at least 16 h. Furthermore, type III offers a synthesis with a comparatively small synthetic effort and was therefore chosen for further studies. HNR is used without modification for this pathway. The silica surface is modified with a halogen, by use of BPTCS, BPTMS or IPTMS (5.2.3). Subsequent coupling with HNR via an ether bond by a nucleophilic substitution under addition of potassium carbonate was accomplished by synthesis 5.4.2. Blank tests with non-modified silica were conducted to exclude possible reactions or physisorption of HNR and showed only minor coloration of the samples. Decrease of the initial reaction temperature of 100 °C to RT resulted in a negligible coloration and amount of retained HNR. It is supposed that as a side reaction, silanol groups react with HNR. A decrease of the reaction temperature to RT is therefore reasonable. Generally the yields for this synthesis are between 1-10 % (relative to HNR) depending on the synthesis method. Assuming a complete grafting of the halogen silanes, an excess amount of bromo and iodo groups is present.

Compared to bromine, iodine is known as the better leaving group for nucleophilic substitutions. Grafting with IPTMS should therefore improve the reaction with HNR. The measurement of the luminescence of iodoproyl and bromopropyl samples converted with HNR indeed showed a slightly increased intensity for iodopropyl functionalized silica (MNR3 and MNR5). More explicit differences can be observed by comparing the luminescence of HNR functionalized silica samples with initial amounts of 100 µmol/g and 500 µmol/g of BPTCS and IPTMS (Figure 29). The amounts of RT grafted HNR are rather low and are only slightly above or below the detection limit for analysis by 5.7.1.1. The corresponding data with the amount of surface-bound NR is shown in Table 10.

Sample	Synthesis	Grafted silane	Amount [µmol/g]	HNR grafting [µmol/g]
MNR1	5.4.2.1.1	BPTCS	500	2.9
MNR2	5.4.2.1.2	BPTCS	100	a
MNR3	5.4.2.1.2	BPTCS	500	a
MNR4	5.4.2.1.2	IPTMS	100	a
MNR5	5.4.2.1.2	IPTMS	500	1.9

Table 10 Comparison of HNR grafted samples synthesized with different silane precursors; a) Below the detection limit.

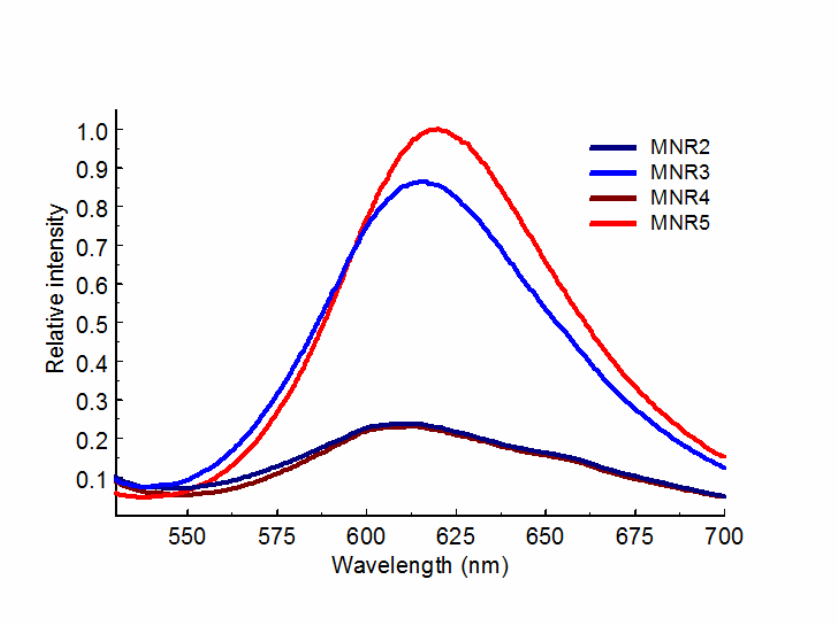

Figure 29 Luminescence spectra of HNR grafted samples synthesized by 100 and 500 µmol/g of BPTCS and IPTMS; Excitation was performed at 500 nm.

Similar to physisorbed MCM-41, a silylation of MNR1 with TMMS (5.2.7.4) resulted in an increase of the luminescence intensity and also a slight hypsochromic shift as is shown in Figure 30. As is discussed below, the hypsochromic shift can become more pronounced under drastic silylation conditions.

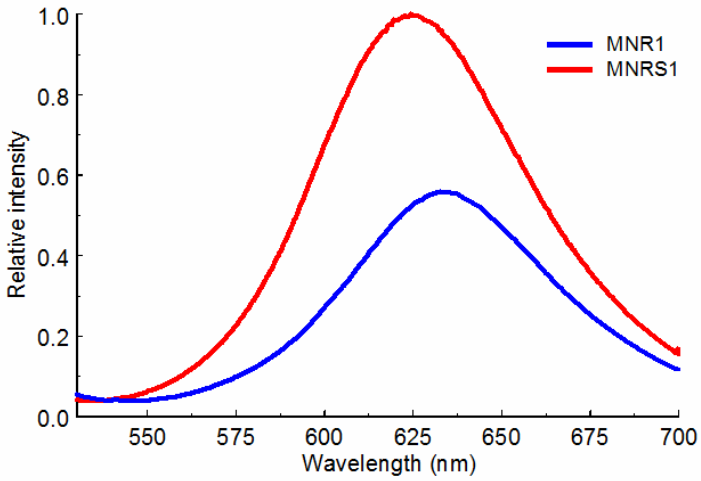

Figure 30 Luminescence spectra of silylated and non-silylated NR grafted MCM-41; Excitation was performed at 500 nm.

A comparison of the luminescence spectra of NR samples grafted via ether bond with physisorbed NR in unmodified (polar) and silylated (unpolar) MCM-41 is shown in Figure 31. Emission maxima between 619 nm and 625 nm were obtained for HNR coupled silica. Adsorbed NR gave a lower emission maximum (610 nm) for inclusion in silylated and a higher emission maximum (634 nm) for inclusion in unmodified MCM-41.

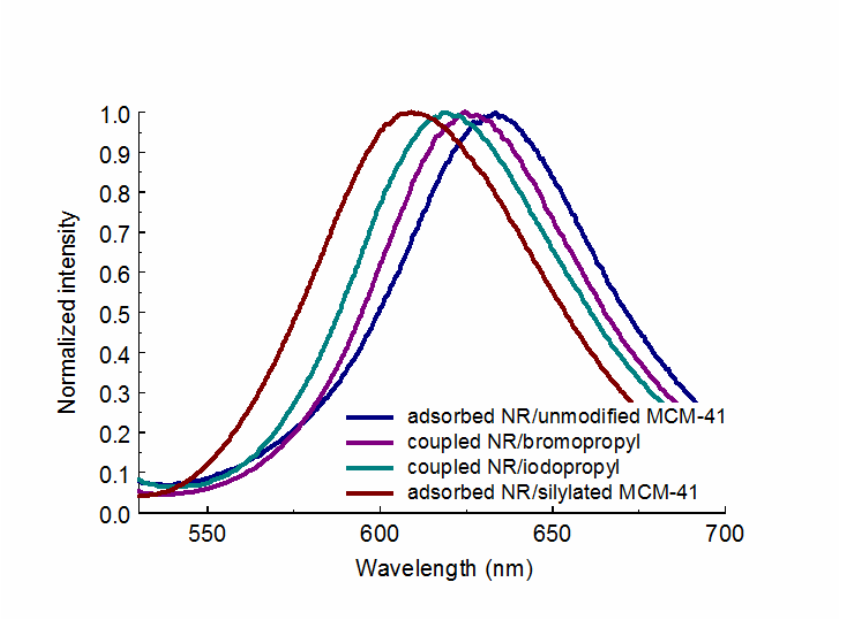

Figure 31 Luminescence spectra of physisorbed and grafted NR; Excitation was performed at 500 nm.

3.4.5 Co-condensation of nile red

Functionalization of the surface by co-condensation offers some advantages over grafting (see also 2.3). Uniform distribution of the organic group with a high degree of site isolation can be accomplished by co-condensation. Introduction of NR was achieved under acidic conditions by utilizing the standard synthesis procedure of SBA-15 (5.1.2). In order to obtain a reactive silane species, HNR was coupled with IPTMS in a premodification step, similar to the grafting of HNR, by taking equimolar amounts of IPTMS and HNR under addition of potassium carbonate.

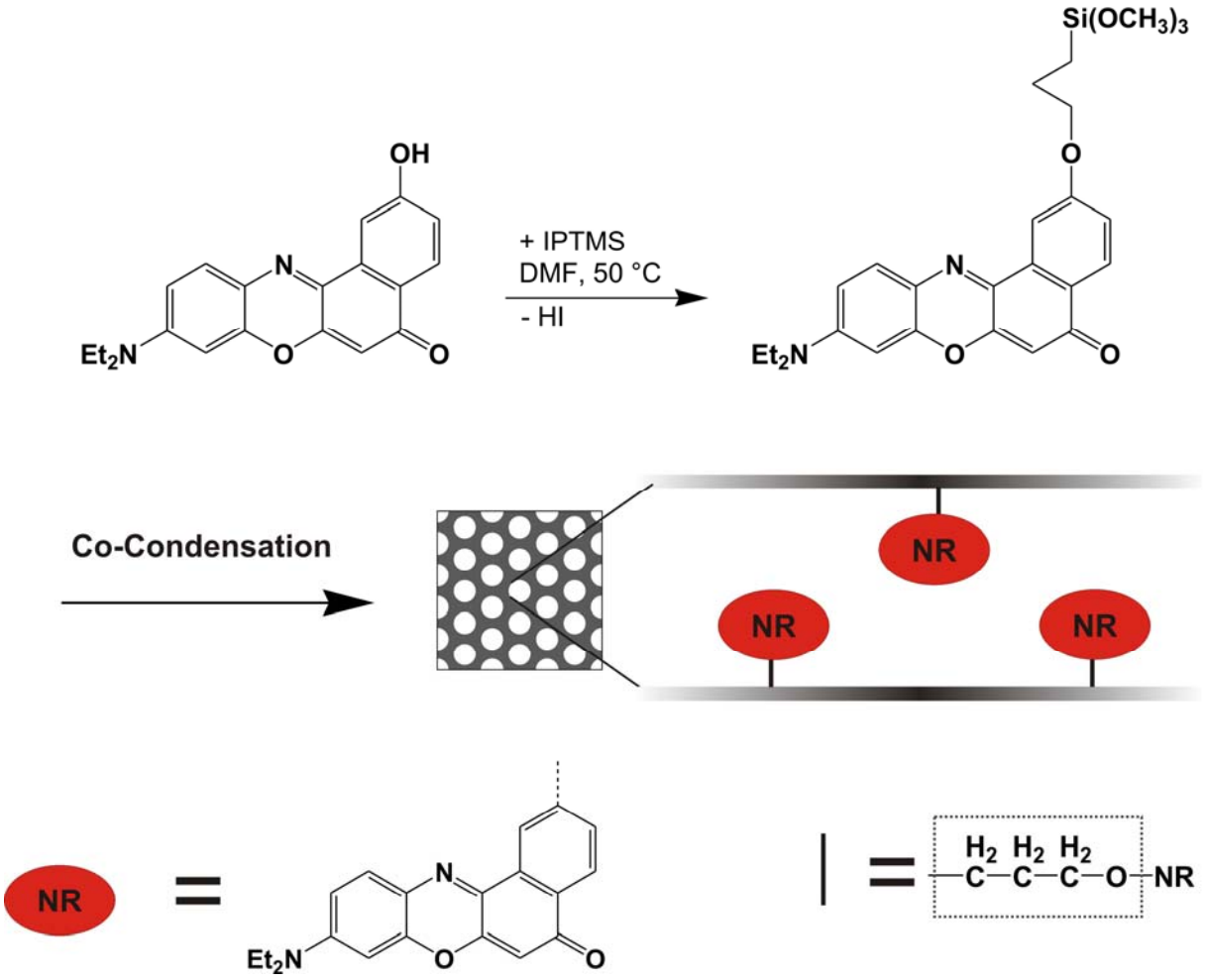

Figure 32 Scheme for the co-condensation with HNR.

The volume of DMF was reduced to 1 mL in order to use the mixture in situ for co-condensation. Reaction conditions are described in 5.5.3. A scheme for the preparation of the HNR co-condensed material is given in Figure 32. The template was removed by Soxhlet extraction with ethanol. It should be noted that ethanol can react with silanol groups under

these conditions.[142] Therefore, variations in emission spectra of co-condensed silica samples, which occur for different batches, could be connected to this extraction procedure, since a partial surface modification with ethyl groups will affect the surface polarity.

Different surface polarities were produced by silylation with TMMS under addition of triethylamine or pyridine at RT or under reflux, respectively (5.2.7.4/5.2.7.6). Relatively mild conditions had to be used, since the more reactive TMCS also attacks the grafted NR. The luminescence spectra of the corresponding samples show a distinct shift of the emission maxima. C_{BET}-values confirmed the different surface properties (Table 11).

Sample	Synthesis	C_{BET}	d_{BJH}[a] [nm]	λ_{Em}[b] [nm]	S_{BET}[c] [m²/g]	V_{tot}[d] [cm³/g]	S_{micro}[e] [m²/g]
CC-SNR1	Co-condensed	150 (96)[f]	7.8	634	988	1.40	150
CC-SNRMS2	Co-condensed, silylation	34	7.4	594	531	0.79	0
MNR1	Gafted	89	2.8	633	867	0.67	0
MNRS1	Grafted, silylation	42	2.5	625	765	0.58	0

Table 11 Nitrogen adsorption and luminescence data of co-condensed SBA and grafted MCM-41 HNR modified silica.

[a] Average pore size calculated from the adsorption isotherm by the BJH method.

[b] Emission maxima for excitation performed at 500 nm.

[c] Total BET surface area.

[d] Total pore volume (calculated at $p/p_0 = 0.95$).

[e] Micropore surface area calculated by t-plot method after de Boer.

[f] see text for explanation.

Luminescence spectra of silylated and non-silylated samples of co-condensed HNR and grafted HNR for SBA-15 and MCM-41 silica materials are shown in Figure 33. Non-silylated materials feature bands in the same range at 630 to 635 nm. Silylated materials exhibit a hypsochromic shift, with the co-condensed material showing luminescence at shorter wavelength. In addition, the intensity increases for the silylated products. These results are in agreement with the C_{BET}-values. Since the shift of NR luminescence is especially pronounced

[142] C. C. Ballard, E. C. Broge, R. K. Iler, D. S. St. John, J. R. McWhorter, *J. Phys. Chem.* **1961**, *65*, 20; T. Kimura, K. Kuroda, Y. Sugahara, K. Kuroda, *J. Porous Mater.* **1998,** *5,* 127.

in the range between C_{BET}-values of 30 and 40, the relatively large wavelength shift between sample CC-SNRMS2 and MNRS1 is corresponding to this fact. The different polarities of the silylated samples is probably due to the different silylation reactions for co-condensed (5.2.7.6) and grafted material (5.2.7.4) which results in an incomplete silylation for the latter. This is also confirmed by the relative reduction of the surface areas and pore volumes, which is less pronounced for the postsynthetically modified samples (MNR1+MNRS1). The C_{BET}-value for CC-SNR1 is exceptionally high (C_{BET} = 150). A more reasonable value of C_{BET} = 96 with better correlation coefficient (r = 0.999993) vs. (r = 0.999714) is used instead, which is obtained by excluding the isotherm points between a relative pressure of 0.24 and 0.3. An explanation for the unusual C_{BET}-value can be given by the calculation of the micropore volume after de Boer,[143] resulting in 0.046 cm³/g for CC-SNR-1, which affects the applicability of the BET equation for monolayer formation. Interestingly, the micropore volume disappears for the silylated material (CC-SNRMS2), indicating a closure of the micropores by grafting with MTMS.

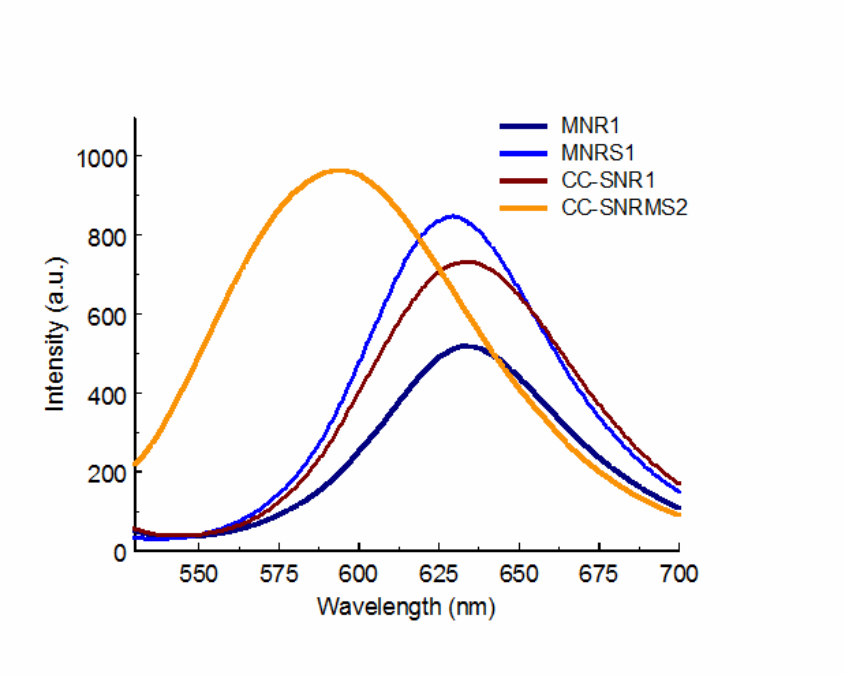

Figure 33 Luminescence spectra of silylated non-silylated samples prepared by co-condensation and grafting; Excitation was performed at 500 nm.

Another method to adjust the surface properties is by the direct addition of silanes with organic groups to the co-condensation mixture. Depending on the organic group, the NR luminescence should vary. In order to achieve vicinity between NR and organic group, a

[143] J. H. de Boer, B. G. Linsen, T. Van der Plaas, G. J. Zondervan, *J. Catal.* **1965**, *4*, 649.

precondensation for 3 h at 50 °C under addition of approximately two equivalents of water was performed. The mixture of both silanes was subsequently added to the co-condensation mixture. In order to prove this concept, co-condensation of aminopropyl- and methyl groups by use of the corresponding silanes APTMS and MTMS was conducted. Emission maxima and C_{BET}-values of the resulting samples are summarized in Table 12. The luminescence spectra are shown in Figure 34. Only negligible hypsochromic shifts are observed. Interestingly, the modification with APTMS seems to have a more pronounced effect on the emission maximum than the addition of MTMS. A possible explanation would be based on the larger size of the aminopropyl group compared to the methyl group. The methyl group is more likely to be fully incorporated in the silica structure, therefore becoming inaccessible. However, it has to be pointed out that the differences in wavelength are relatively small and irregularities between two different batches can result in shifts of up to about 10 nm. Additionally, microporosity was found for the samples CC-SNR1 and CC-SMNR3. The C_{BET}-values therefore have to be judged carefully. Nevertheless, the observed trend in the emission spectra is in agreement with the calculated C_{BET}-values.

sample	C_{BET}	Pore size$_{(BJH)}$ [nm]	λ_{Em} [nm]
CC-SNR1	96	7.8	634
CC-SMNR3	96	7.4	631
CC-SAPNR4	66	8.2	624

Table 12 Comparison of NR modified co-condensed samples with and without addition aminopropyl or methyl groups.

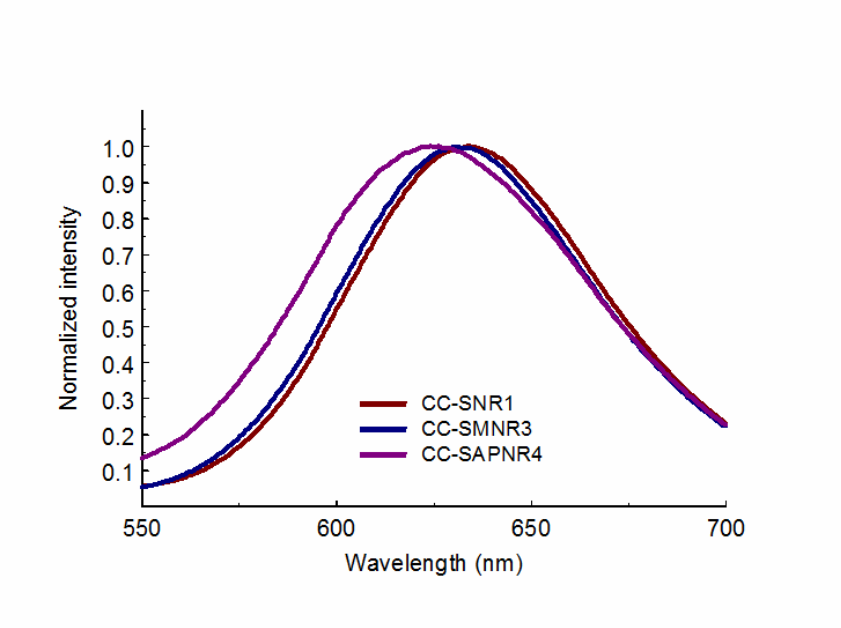

Figure 34 Normalized luminescence spectra of co-condensed NR samples; Excitation was performed at 500 nm.

Absorption and emission from NR not only depends on the surface properties, but also on the actual environment inside the channels. By using solvents with different polarities, the emission of surface-anchored NR can be influenced similar to NR in solution which shows distinct absorption and emission spectra in dependence of the solvent.[134]

Proof of the concept is obtained by measuring luminescence spectra of NR modified mesoporous silica dispersed in various solvents. The SBA-15 type silica was produced by co-condensation of a HNR and IPTMS modified sample (CC-SNR5). The emission maxima in different solvents are given in Table 13. The shift of the emission maximum corresponds to the reference values obtained in solution. However, only small shifts observed for CC-SNR5 in organic solvents indicate that the emission is affected by the silica surface. For water, a significant shift is observed and the emission intensity undergoes a pronounced decrease relative to the other solvents.

Solvent	Absorption of NR; λ_{max} [nm]	Absorption of HNR; λ_{max} [nm]	Emission of HNR; λ_{Em} [nm]	Emission of CC-SNR5; λ_{Em} [nm]
Toluene	522	525	568	638
Dichloromethane	535	538	602	640
1-Butanol	548	542	631	641
Water	593	--	--	665
Solid silica sample	--	--	--	~620

Table 13 Absorption maxima of HNR[144] and NR[134] and emission maxima of HNR[144] and CC-SNR5 in different solvents.

Conclusion

NR, featuring photophysical properties that are likely sensitive to solvent polarity, was successfully attached to mesoporous silica materials. Properties in terms of a hydrophilic/hydrophobic surface could be detected by either adsorption or covalent attachment. Especially for relatively hydrophobic surfaces, luminescence sensing is superior to values obtained through nitrogen adsorption (C_{BET}). A small array of silica particles with defined surface polarities was designed and differentiated by the emission of incorporated NR.

[144] K. Nagy, S. Göktürk, L. Biczók, *J. Phys. Chem. A* **2003**, *107*, 8784.

3.5 Coupling of organic dyes to iodopropyl functionalized SBA type silica

3.5.1 Coupling of NR

The different properties of the silica materials which were obtained by co-condensation with IPTMS were discussed in 3.2. The iodopropyl group provides an ideal starting point for further functionalization with NR. By postsynthetic treatment, different bifunctionalized samples were modified with HNR. The luminescence spectra show bands in the range of 621 to 644 nm (Figure 35). A higher content of IPTMS results in an emission at slightly longer wavelength and a significant increase of the amount of coupled HNR. The shift of the emission wavelength can therefore either be interpreted by partial self-absorption or by differences in the surface polarity due to the increased amount of iodopropyl and HNR moieties.

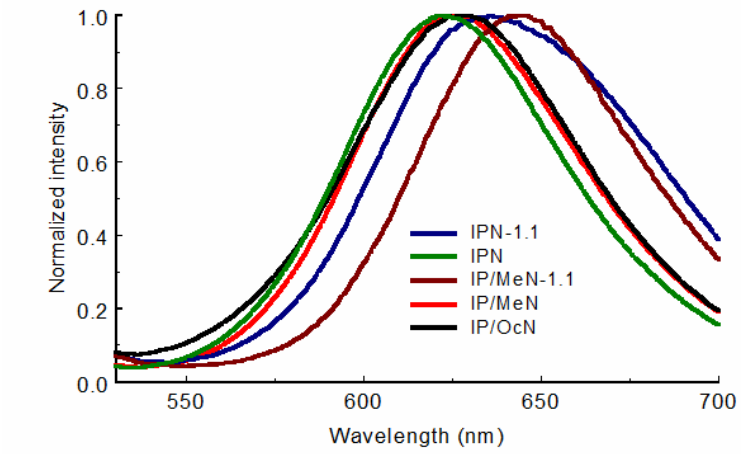

Figure 35 Luminescence spectra of HNR modified IPTMS co-condensed samples with different organic additives; Excitation was performed at 500 nm.

Subsequent silylation of the samples (5.2.7.6) resulted in a distinct hypsochromic shift of the emission wavelength, as shown in Figure 36. The corresponding data is given in Table 14. The C_{BET}-values exhibit rather large variation for the functionalized materials. It has to be considered that due to a broad PSD and the occurrence of microporosity, this specific silica material is less defined compared to MCM-41 or also HNR co-condensed material. Microporosity affects the applicability of the BET theory and more questionable results

concerning the reliability of the C_{BET}-values are obtained. Especially for non silylated material, the C_{BET}-values cover a range of 60 to 160 and are not corresponding to the emission maxima.

sample	Additives	n(IPTMS) [mmol]	C_{BET}	Pore size[a] [nm]	λ_{Em} [nm]
IPN-1.1	Ip	1.12	141	~7.2	635
IPN	Ip	0.15	92	9.9	621
IP/MeN-1.1	Ip/Me	1.12	63	~4.4	643.5
IP/MeN	Ip/Me	0.15	155	9.4	624
IP/OcN	Ip/Oc	0.15	109	-	629
IP/MSN	Ip/MS	0.15	56	6.7	607.5
IP/Me/MSN	Ip/Me/MS	0.15	63	7.9	603
IP/Oc/MSN	Ip/Oc/MS	0.15	52	-	600

Table 14 Nitrogen adsorption and luminescence data of IPTMS functionalized silica modified with HNR; Ip: IPTMS, Me: MTMS, Oc: OCTMS, MS: TMMS postsynthetically silylated silica. [a] Average pore size calculated from the adsorption isotherm by the BJH method.

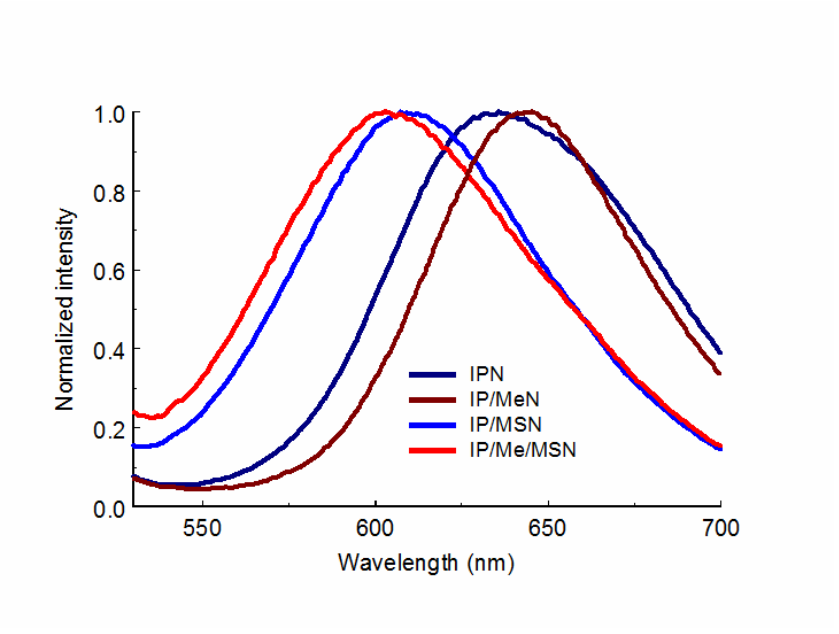

Figure 36 Luminescence spectra of unmodified and silylated HNR modified IPTMS samples; Excitation was performed at 500 nm.

3.5.2 Hybrid materials by functionalization with different fluorescent dyes

Mesoporous silicas containing two types of functional groups of complementary reactivity are of interest for further modification towards highly complex materials. This is exemplified by the directly synthesized mesoporous iodopropyl-aminopropyl-silica Ip/Ap. A narrow PSD is obtained when using 0.15 mmol of each IPTMS and APTMS (Figure 37).

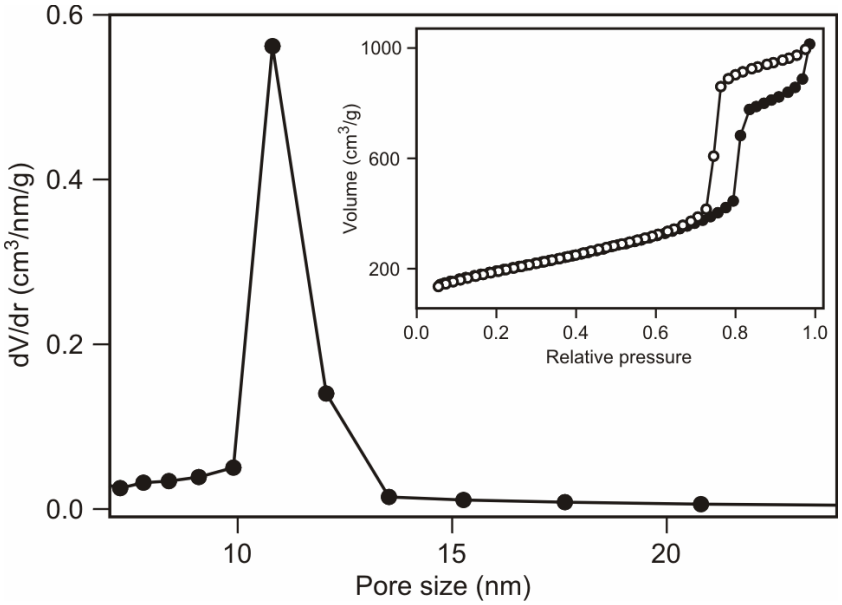

Figure 37 Pore size distribution of Ip/Ap. The corresponding nitrogen sorption isotherms are shown in the inset.

The iodopropyl and aminopropyl groups can be labeled selectively with HNR and fluorescein isothiocynate isomer I (FITC), respectively (Figure 38). No labeling was observed upon reaction of HNR with mesoporous aminopropyl-silica. Similarly, FITC did not bind to iodopropyl-silica. However, the consecutive reaction of Ip/Ap with HNR and FITC yields a material containing both fluorescent labels. Analysis by UV-Vis spectroscopy revealed a nile red content of 5 µmol/g and a fluorescein content of 14 µmol/g.

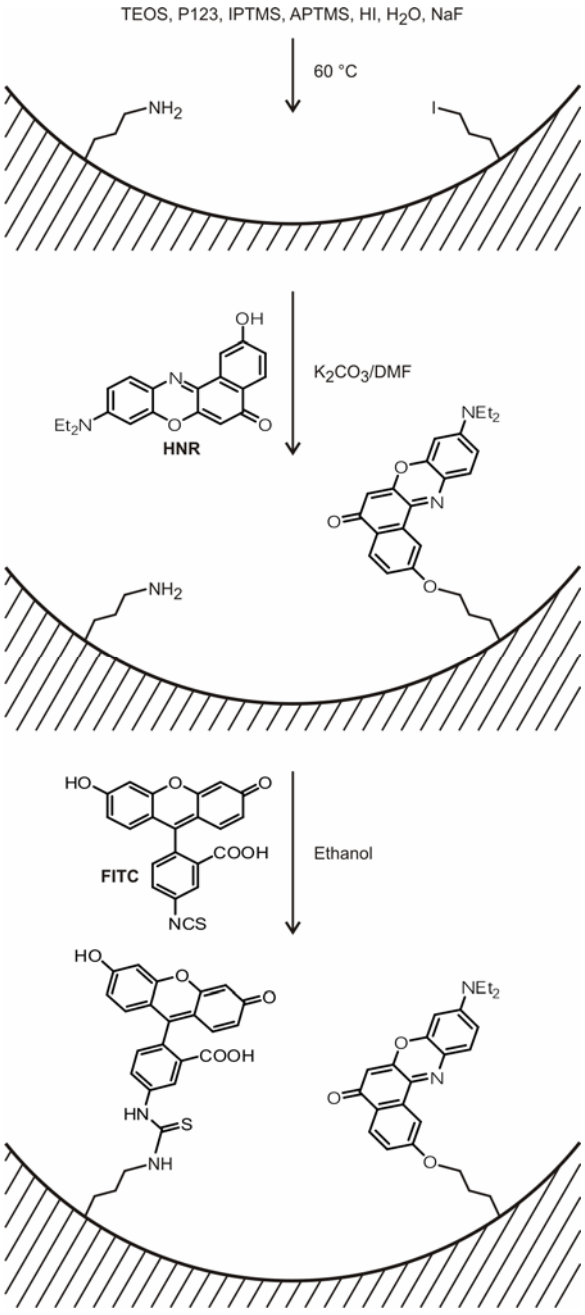

Figure 38 Labeling of iodopropyl-aminopropyl-functionalized mesoporous silica with 2-hydroxy substituted nile red (HNR) and fluorescein isothiocyanate (FITC).

The absorption spectrum of the powdered sample measured in an index-matching solvent (ethyl benzoate, Figure 39, bottom panel) features three maxima at 462, 488, and 537 nm, as well as a shoulder around 430 nm, corresponding well to the maxima found in the spectra of the materials containing only one of the labels (Figure 39, top panel). The occurrence of two maxima (and a short wavelength shoulder) in the absorption spectrum of coupled FITC indicates the presence of fluorescein moieties in different protonation states (dianion, monoanion, neutral).[145]

The photoluminescence spectrum of the FITC/HNR labeled sample (Figure 39, bottom panel) shows a comparatively weak luminescence of the coupled FITC. This can be attributed to the considerable overlap between the emission band of the FITC labels and the absorption band of the HNR labels, leading to radiative energy transfer. Assuming a homogeneous distribution of the fluorescent labels on the surface of Ip/Ap, a density of roughly 0.016 nm^{-2} is obtained, corresponding to one label per 60 nm^2. Additionally taking into account the fact that most of the surface of the material is concave, leading for example to situations where labels occupy sites on opposing channel walls, non-radiative energy transfer might contribute to the low luminescence intensity of the coupled FITC labels.

[145] M. M. Martin, L. Lindqvist, *J. Lumin.* **1975**, *10*, 381.

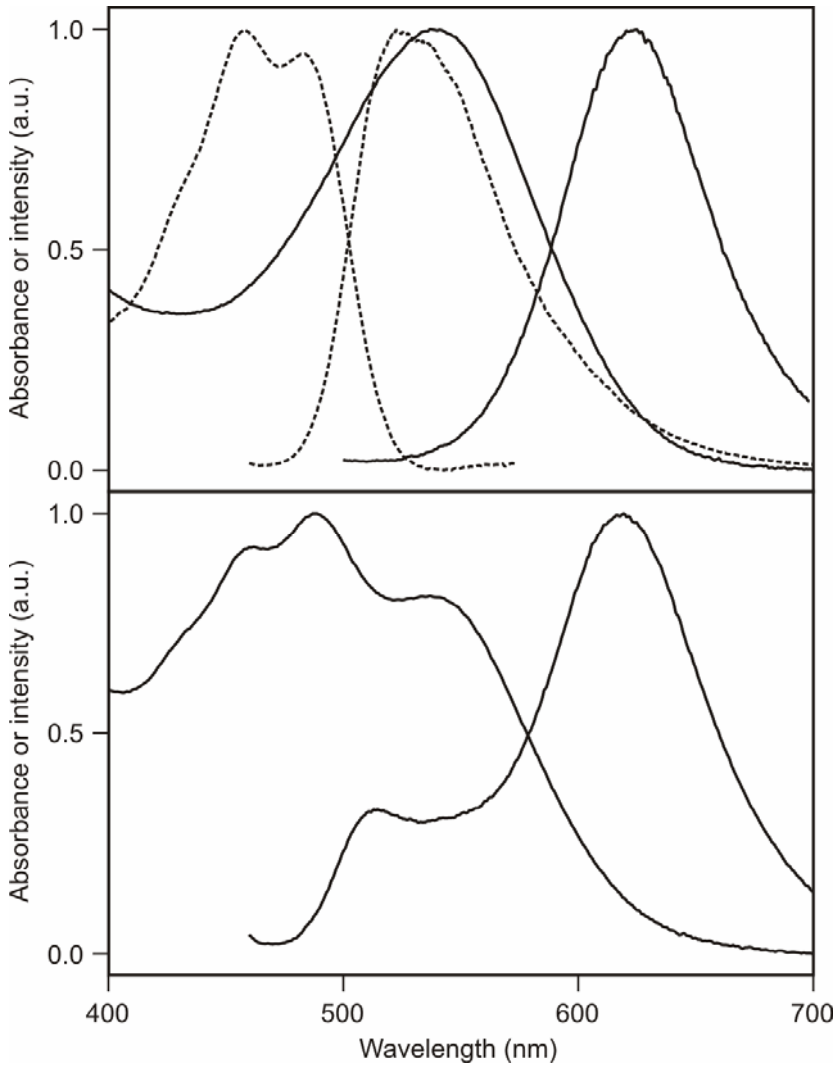

Figure 39 Absorption and photoluminescence spectra of Ip/Ap after either FITC labeling (dashed curves, top panel, excitation at 450 nm) or HNR labeling (solid curves, top panel, excitation at 490 nm). The bottom panel shows the absorption and photoluminescence spectra (excitation at 450 nm) of an Ip/Ap sample after consecutive labeling with HNR and FITC as schematically shown in Figure 38.

Conclusion

The labeling of bifunctionalized SBA-15 with HNR was performed. Only slight differences of the emission maxima by different alkyl functionalization were detected. Co-condensation of a second functional group for the labeling with a further luminescent dye resulted in a FITC/HNR labeled silica sample, thus proving the applicability of bifunctionalized SBA-15 for independent grafting of at least two target moieties.

3.6 Adsorption of TICT molecules

Phenomena of dual fluorescence or emission bands with large Stokes shifts are often found for donor-acceptor substituted benzenes. The origin of this particular property has been explained by different concepts (twisted intramolecular charge-transfer (TICT)[146], Pseudo-Jahn-Teller ICT (PICT),[147] rehybridised ICT (RICT)[148]).[149] The TICT model explains the appearance of dual fluorescence based on a rotational relaxation in the electronically excited state. Consequently, the fluorescence can result from a primarily excited "locally excited" state (LE) with relatively small Stokes shift and also from a TICT state which originates from a highly polar excited-state conformer. An emission from the TICT state, which is promoted in polar solvents, leads to a large Stokes shift. A fine tuning of the photophysical properties by use of the solvent polarity or viscosity was frequently investigated.[150,151] Some research has focused on the combination of TICT molecules with mesoporous materials, as for example 4-(dicyanomethylene)-2-methyl-6-(p-dimethylaminostyryl)-4*H*-pyran adsorbed in MCM-41[152] as well as dimethylaminobenzonitrile (DMABN) or p-N,N-dimethylamino-benzoic acid adsorbed on porous silica.[153,154,155] Herein, the use of TICT molecules as sensors for the surface properties of mesoporous silica materials is investigated, employing MCM-41 with different surface characteristics. DMABN as the prototype TICT compound[156] and 4,4`-diaminodiphenyl sulfone (DAPS)[151] (Figure 40) were utilized.

---

[146] K. Rotkiewicz, K. H. Grellmann, Z. R. Grabowski, *Chem. Phys. Lett.* **1973**, *19*, 315; W. Rettig, *Angew. Chem. Int. Ed. Engl.* **1986**, *25*, 971; E. Lippert, W. Rettig, V. Bonacic-Koutecký, F. Heisel, J. A. Miehé, *Adv. Chem. Phys.* **1987**, *68*, 1.

[147] U. Leinhos, W. Kühnle, K. A. Zachariasse, *J. Phys. Chem.* **1991**, *95*, 2013; W. Schuddeboom, S. A. Jonker, J. H. Wartman, U. Leinhos, W. Kühnle, K. A. Zachariasse, *J. Phys. Chem.* **1992**, *96*, 10809; K. A. Zachariasse, T. von der Haar, A. Hebecker, U. Leinhos, W. Kühnle, *Pure Appl. Chem.* **1993**, *65*, 1745; T. von der Haar, A. Hebecker, Y. V. Iíichev, Y. B. Jiang, W. Kühnle, K. A. Zachariasse, *Recl. Trav. Chim. Pays-Bas.* **1995**, *114*, 430; K. A. Zachariasse, M. Grobys, T. von der Haar, A. Hebecker, Y. V. Iíichev, Y. B. Jiang, O. Morawski, W. Kühnle, *J. Photochem. Photobiol. A* **1996**, *102* 59; Y. V. Iíichev, W. Kühnle, K. A. Zachariasse, *J. Phys. Chem. A*, **1998**, *102*, 5670.

[148] A. Sobolewski, W. Domcke, *Chem. Phys. Lett.* **1996**, *259*, 119; A. Sobolewski, W. Domcke, *Chem. Phys. Lett.* **1996**, *250*, 428; A. Sobolewski, W. Sudholt, W. Domcke, *J. Phys. Chem. A* **1998**, *102*, 2716.

[149] P. R. Bangal, S. Panja, S. Chakravorti, *J. Photochem. Photobiol. A: Chem.* **2001**, *139*, 5.

[150] J. M. Hicks, T. M. Vandersall, E. V. Sitzmann, K. B. Eisenthal, *Chem. Phys. Lett.* **1987**, *135*, 413; J. M. Hicks, M. T. Vandersall, Z. Babarogic, K. B. Eisenthal, *Chem. Phys. Lett.* **1985**, *116*, 18; J. D. Simon, S.-G. Su, *J. Phys. Chem.* **1990**, *94*, 3657.

[151] D. S. Bulgarevich, O. Kajimoto, K. Hara, *J. Phys. Chem.* **1995**, *99*. 13356.

[152] H. Guo, X. Zhang, M. Aydin, W. Xu, H.-R. Zhu, D. L. Akins, *J. Mol. Struct.* **2004**, *689*, 153.

[153] R. Günther, D. Oelkrug, W. Rettig, *J. Phys. Chem.* **1993**, *97*, 8512.

[154] K. Yanghee, C. Hyung Woo, Y. Minjoong, S. Nam Woong, K. Dongho, *Chem. Phys. Lett.* **1997**, *264*, 673.

[155] A. Levy, D. Avnir, M. Ottolenghi, *Chem. Phys. Lett.* **1985**, *121*, 233.

[156] C. Cornelissen-Gude, W. Rettig, *J. Phys. Chem. A* **1998**, *102*, 7754; E. Lippert, W. Lüder, H. Boos, *Adv. Mol. Spectrosc. Proc. Int. Meet. 4th 1959*, **1962**, 443; E. Lippert, W. Lüder, H. Boos, in *Advances in Molecular Spectroscopy,* edited by A. Mangini, Pergamon Press, Oxford, **1962**, p. 443.

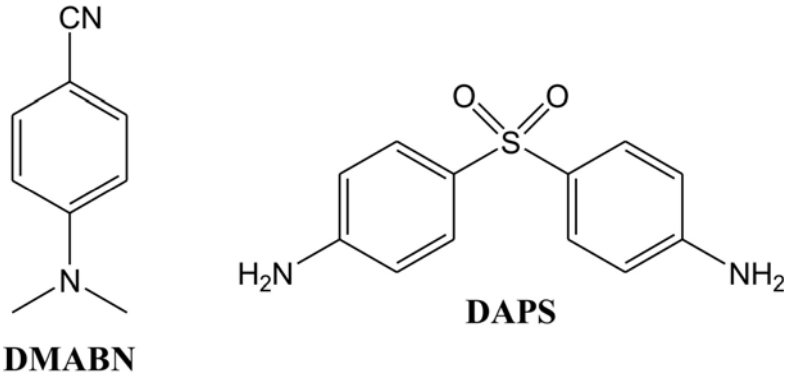

Figure 40 Structures of dimethylaminobenzonitrile (DMABN) and 4,4`-diaminodiphenyl sulfone (DAPS).

Adsorption of the organic dyes in MCM-41 (5.1.1) was achieved by dispersing the mesoporous silica in a solution of the dyes for a period of 1 h. DMABN was dissolved in pentane and DAPS in chloroform.

#	Pore size[a] [nm]	Pore size[b] [nm]	S_{BET}[c] [m²/g]	C_{BET}
M1	2.8	3.9	974	108
MMS1 (silylated)	2.4	3.5	596	30

Table 15 Nitrogen adsorption data;
[a] Average pore diameter calculated from the adsorption isotherm by the BJH method;
[b] Average pore diameter calculated from the adsorption isotherm by the DFT method;
[c] Total BET surface area.

Different silica surface properties were created by highly reactive silylation conditions with TMCS (5.2.7.1). Adsorption was carried out as for unmodified MCM-41. Table 15 summarizes the differences in pore size and surface properties calculated from the nitrogen adsorption data. After silylation, the pore size is reduced and the surface properties have changed as indicated by the decrease of the C_{BET}-value (108 vs. 30).

The emission spectra of the samples featured a large shift depending on the surface properties. Silylated MCM-41 with hydrophobic surface showed fluorescence from the LE state, whereas in hydrophilic, unmodified MCM-41 a large bathochromic shift is observed originating from an emission of the TICT state. The corresponding emission maxima are given in Table 16 and the emission spectra in Figure 41 and Figure 42.

Sample	Fluorescent molecule	λ_{Em} [nm]
M1	DMABN	434
MMS1 (silylated)	DMABN	344
M1	DAPS	395
MMS1 (silylated)	DAPS	330

Table 16 Fluorescence data.

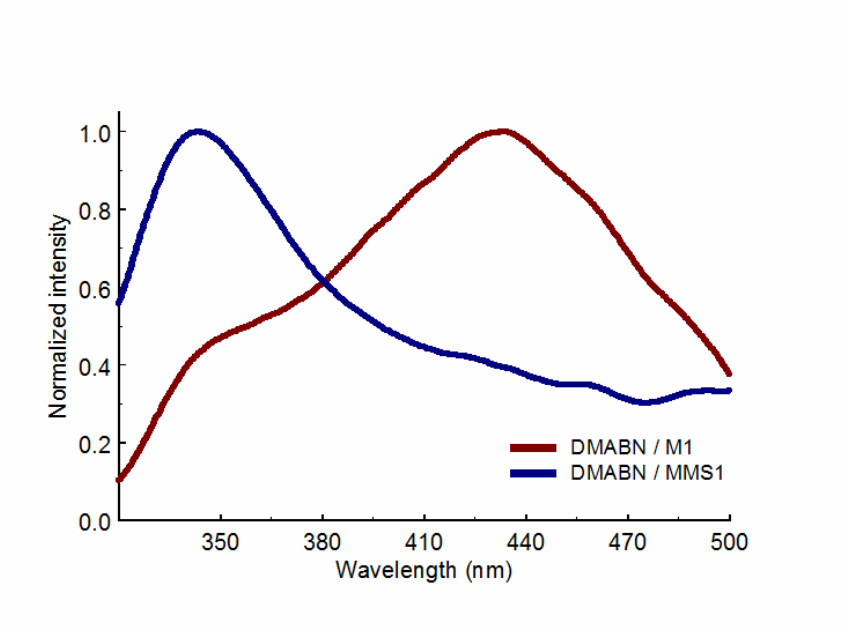

Figure 41 Emission spectra of DMABN adsorbed in unmodified and silylated MCM-41. Excitation was performed at 280 nm.

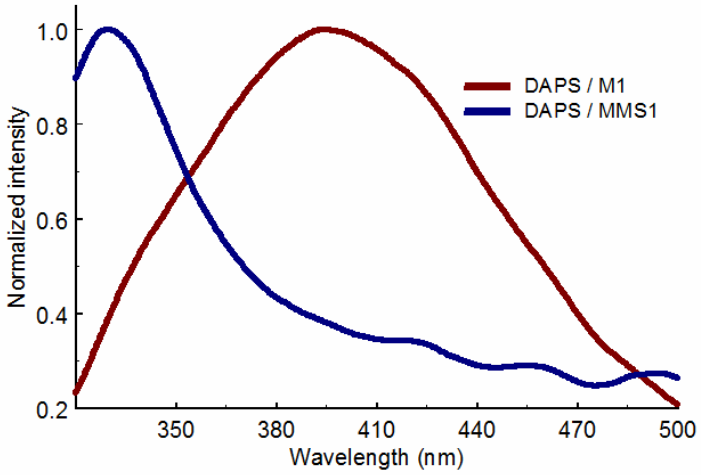

Figure 42 Emission spectra of DAPS adsorbed in unmodified and silylated MCM-41. Excitation was performed at 280 nm.

Conclusion

The principle of TICT molecules showing dual fluorescence with large red shifts in polar solvents was successfully applied to mesoporous silica materials. By utilizing the different emission properties of the TICT molecules in dependence of the polarity of the environment, a detection of the different surface properties was achieved. Fine tuning of this method, e. g. for the detection of intermediate polarities, is expected to provide further insights concerning the use of these TICT molecules as sensors for surface properties of mesoporous materials.

3.7 Functionalization with spiropyran

3.7.1 Introduction

Because of their photochromic properties, spiropyrans have been intensely investigated. Based on the changing properties of a material irradiated with light, many applications were suggested as for example logic gates,[157] switchable energy transfer systems[158] and smart membranes.[159] Besides grafting to thin films[160] or encapsulation in zeolites,[161] some efforts of incorporation in MCM-41 were also done to investigate the photochromic properties and to enable applications as sensors.[162] Spiropyran (SP) can switch between a closed form and an open merocyanine (MC) form. The predominant structure is strictly dependent on the polarity of the solvent. For MC, two isomeric structures, namely zwitterionic and quinoidal, are likely (Figure 43). Since the aromaticity of the closed form is reduced by the formation of the cycle, the open form contributes significantly to the structure, especially in polar environment where the more polar MC form is stabilized.

In nonpolar solvents kept in the dark, the closed form, which can be converted by UV irradiation to MC, is predominant. Under visible irradiation, a reversion to the closed form occurs. The switching between these two isomers is very sensitive to the environment. The closed form is predominant in unpolar and the open form in polar conditions. Tagaya et al. found that, for a reversible switching of SP´s in a silica matrix, a coexistence of polar and nonpolar regions was essential.[163] The stability of the respective form depends on the acidity and on the polarity of the environment in which the molecules are incorporated either by adsorption or covalent bonding.

Different diastereoisomers of the merocyanine form are possible due to trans and cis isomerization at the conjugated bond between the indoline and the chromene parts, whereas the TTC (trans-trans-cis) form is the most dominant in solution.[164]

---

[157] F. M. Raymo, S. Giordani, *J. Am. Chem. Soc.* **2001**, *123*, 4651.
[158] M. Tomasulo, S. L. Kaanumal, S. Sortino, F. M. Raymo, *J. Org. Chem.* **2007**, *72*, 595.
[159] N. Arpan, L. Hongwei, B. Georges, *Angew. Chem. Int. Ed.* **2006**, *45*, 4094; I. Vlassiouk, C.-D. Park, S. A. Vail, D. Gust, S. Smirnov, *Nano Lett.* **2006**, *6*, 1013.
[160] J. M. Galvin, G. B. Schuster, *Supramol. Sci.* **1998**, *5*, 89.
[161] C. Schomburg, M. Wark, Y. Rohlfing, G. Schulz-Ekloff, D. Wöhrle, *J. Mater. Chem.* **2001**, *11*, 2014.
[162] I. Casades, M. Àlvaro, H. Garcia, M. N. Pillai, *Photochem. Photobiol. Sci.* **2002**, *1*, 219.
[163] H. Tagaya, T. Nagaoka, T. Kuwahara, M. Karasu, J.-I. Kadokawa, K. Chiba, *Microporous Mesoporous Mater.* **1998**, *21*, 395.
[164] J. Hobley, U. Pfeifer-Fukumua, M. Bletz, T. Asahi, H. Masuhara, H. Fukumura, *J. Phys. Chem. A* **2002**, *106*, 2265.

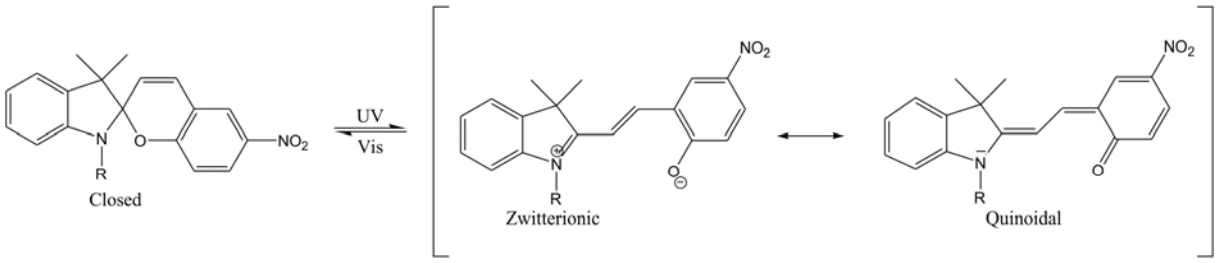

Figure 43 Isomeric structures of spiropyran.

3.7.2 Grafting

In order to generate a covalent bond between the photoactive moiety and the channel wall, the well known 6-nitro BIPS (3′,3′-dimethyl-6-nitrospiro[2*H*-1-]-benzopyran-2,2-indoline) derivative of the common SP with an adequate linking group was synthesized. A 3-carboxypropyl group at the 1-position was therefore introduced to generate SPCOOH (1′-(3-Carboxypropyl)-3′,3′-dimethyl-6-nitrospiro-[2*H*-1]-benzopyran-2,2′-indoline).[165 166] The silica was premodified by grafting with APTMS to enable the coupling via an amide bond under addition of EDC. A scheme of the functionalization is shown in Figure 44.

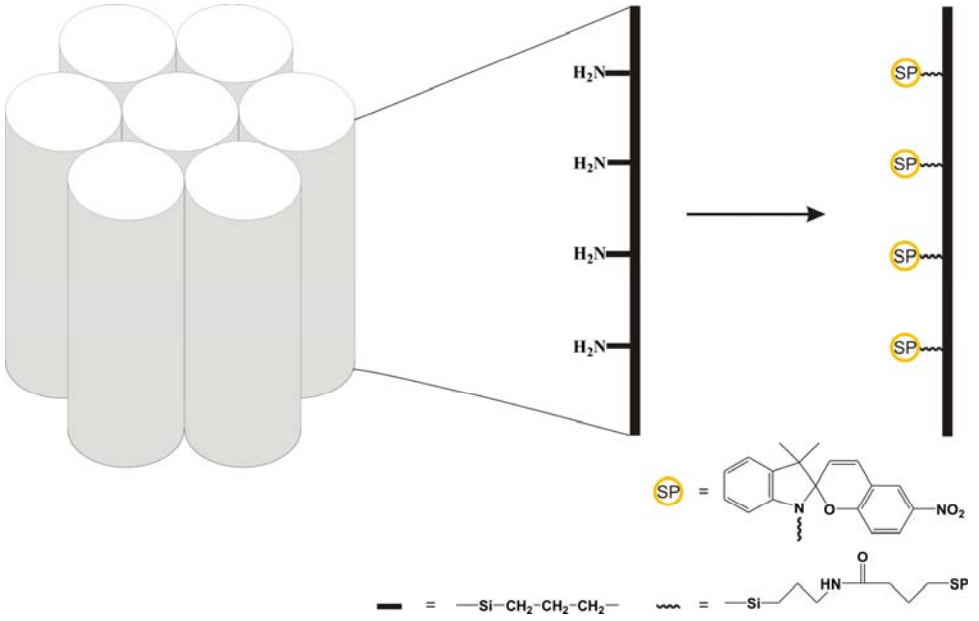

Figure 44 Scheme of spiropyran grafting.

[165] A. A. Garcia, S. Cherian, J. Park, D. Gust, F. Jahnke, R. Rosario, *J. Phys. Chem. A* **2000**, *26*, 6103.
[166] R. Rosario, D. Gust, M. Hayes, F. Jahnke, J. Springer, A. A. Garcia, *Langmuir* **2002**, *18*, 8062.

The amount of grafted SP was estimated by dissolving a quantified amount of the modified sample in an aqueous solution of NaOH. Acidic and basic conditions favour a hydrolysis to Fischer´s base and the 4-nitro-salicylaldehyde by addition of water and in a subsequent retro-aldol reaction (Figure 45).[167] By measuring the corresponding absorption spectrum of the decomposition products, the amount of SP could be determined. ($\varepsilon = 10747\ M^{-1}cm^{-1}$; $\lambda_{max} = 389$ nm).

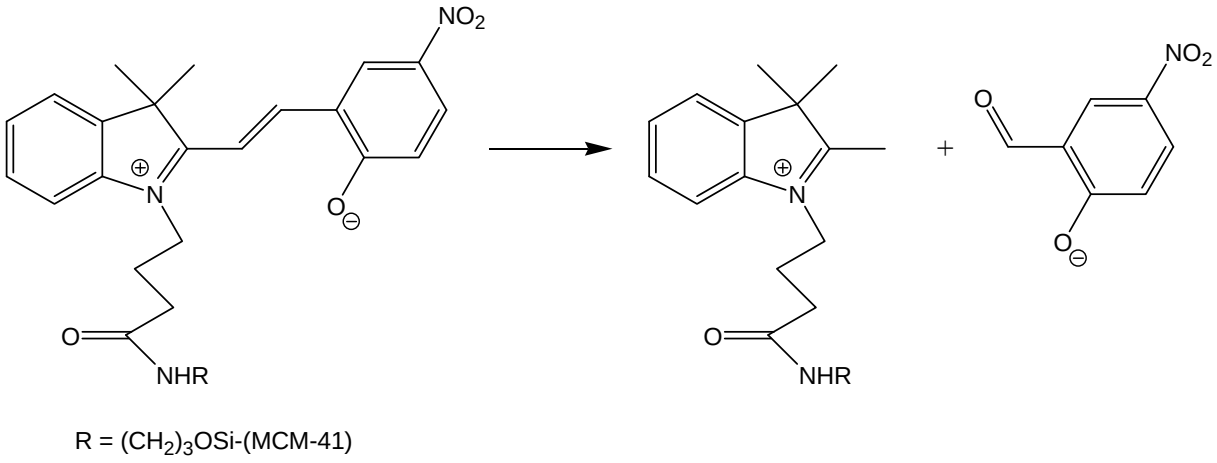

Figure 45 Hydrolysis of grafted SP to Fischer´s base and 4-nitro-salicylaldehyde.

Table 17 shows the experimental (SP_{ex}) as well as the theoretical (SP_{theo}) amounts of SP (assuming quantitative coupling). Furthermore, the applied amount of APTMS with respect to MCM-41 is given.

For the samples SP1-5 the amount of SP is controlled by the grafted amino groups. (SP5 shows an overestimated yield of SP due to the detection limits of the absorption at low concentrations). While for low amino contents a high yield of SP could be detected, it decreases significantly for higher contents. The highest loading was found for SP1 with 290 μmol/g (MCM-41) (26%), which could not be increased significantly for larger amounts of amino groups.

[167] T. Staffhorst, D. Hilvert, *Chem. Commun.* **2009**, 287.

Sample	APTMS [µmol/g(MCM-41)]	SP_{theo} [µmol/g(MCM-41)]	SP_{ex} [µmol/g(MCM-41)]	Yield [%]
SP1	1133	1294	290	26
SP2	567	603	212	35
SP3	133	345	65	49
SP4	57	777	31	54
SP5	6	766	11	---
SP6	567	105	56	53
SP7	567	158	85	54
SP8	567	309	131	42
SP9	567	785	233	30
SP10	567	718	276	38

Table 17 Yield of SP coupling by postsynthetic modification.

Similar results were obtained by varying the SP content for samples SP6-10. For high concentrations, the yield decreases to 38-30 % and a maximal amount of 276 µmol/g (MCM-41). A high density of grafted APTMS, leading to sterical hindrance, is a likely reason for this behaviour.[168]

3.7.3 Co-condensation

Apart from the postsynthetic route, an in situ synthesis was investigated. Co-condensation of SP in mesoporous silica of SBA-15 type was already investigated by Burns et al. utilizing the phenolic part by using 6-iodospiropyran as covalent binding site.[169] In contrast, the covalent bonding to the silica structure was created via the nitrogen of the indoline part of SP. Therefore, SPCOOH was coupled with APTES and afterwards used in situ in a typical MCM-41 co-condensation reaction by aging in aqueous ammonia for 48 h (5.5.1). The advantage of this method is a more uniform distribution of the functional groups. However, incorporation in the channel walls can occur, leading to a situation where some of the SP units might not be able to switch “freely” at the channel surface. The achieved loadings are

[168] H. Ritter, D. Brühwiler, *J. Phys. Chem. C.* **2009**, *113*, 10667.
[169] C. T. Burns, S. Y. Choi, M. L. Dietz, M. A. Firestone, *Separ. Sci. Technol.* **2008**, *43*, 2503.

given in Table 18. APTES and SP were used in 1:1.5 molar ratios in order to ensure a complete coupling. Amounts of SP_{theo} were calculated by assuming a complete reaction with APTES. SP amounts between 33 and 2074 μmol/g (MCM-41) were applied. Yields of co-condensed SP (CCSP) were between 13 and 30 %. For the highest loading of about 260 μmol/g (MCM-41), a yield of only 13 % could be achieved and further increase was not possible. This is in agreement with the results for grafted SP where the maximum loading is 290 μmol/g (MCM-41), although higher grafting yields were achieved (SP1).

Sample	APTES [μmol/g(MCM-41)]	SP_{theo} [μmol/g(MCM-41)]	SP_{ex} [μmol/g(MCM-41)]	Yield [%]
CCSP1	35	35	8	21
CCSP2	56	56	16	30
CCSP3	116	116	24	21
CCSP4	239	239	82	34
CCSP5	793	793	164	21
CCSP6	2072	2072	263	13

Table 18 Yield of co-condensed SP.

The switching behaviour is different for samples prepared by the postsynthetic and the co-condensation approach. For the postsynthetic material, switching between MC and SP could be achieved up to 250 μmol/g (MCM-41), whereas the limit for the co-condensed material is reached at about 24 μmol/g (MCM-41) (CCSP3).

3.7.4 Pore size analysis

Nitrogen adsorption isotherms of the co-condensed and grafted samples were measured and analyzed. Data is shown in Table 19 (grafting) and Table 20 (co-condensation). The PSD´s depicted in Figure 46 show a sharp maximum for the grafted samples SP3-SP4. Only slight deviations from the standard sample of unmodified MCM-41 are obtained. However, for higher SP loadings, the PSD broadens and decreases significantly. By increasing the SP amount, the pore size is reduced successively from about 2.8 nm for unmodified MCM-41 to about 2.4 nm. Especially for SP1 and SP2, a distinct pore size is no longer observed and a broad PSD between 2.2 and 2.6 nm is obtained instead. Similarly, the primary pore volume

decreases significantly from about 0.63 to 0.41 cm³/g. The surface area and the C_{BET}-values decrease from more than 800 to about 650 m²/g and from over 80 to 50, respectively. In terms of pore structure quality, a distinct difference between samples SP3 and SP2 with SP loadings of 65 and 212 μmol/g (MCM-41) can be observed. In this range, the defined structure of MCM-41 is degraded, concluding that a maximum of SP, while retaining a distinct pore size, can only be achieved for values below approximately 200 μmol/g (MCM-41).

Sample	V_P [cm³/g][a]	Pore size [nm][b]	S_{BET} [m²/g][c]	C_{BET}
SP1	0.41	2.38	643.0	48.1
SP2	0.44	2.65	651.2	51.4
SP3	0.61	2.71	800.7	69.2
SP4	0.64	2.77	814.4	81.5
SP5	0.63	2.71	817.8	65.9
SP6	0.46	2.59	698.2	53.2
SP7	0.47	2.59	658.3	58.6
SP8	0.49	2.65	698.2	53.1
SP9	0.45	2.38-2.71	622.7	63.5

Table 19 Structural data obtained by nitrogen adsorption for postsynthetically modified MCM-41.

[a] Primary pore volume (calculated at $p/p_0 = 0.4$ from the desorption isotherm).

[b] Average pore size calculated from the adsorption isotherm by the BJH method.

[c] Total BET surface area.

Sample	V_P [cm³/g][a]	Pore size [nm][b]	S_{BET} [m²/g][c]	C_{BET}
CCSP1	0.58	2.48	802.4	48.2
CCSP2	0.50	2.26	783.6	37.8
CCSP3	0.51	2.22	769.8	36.5
CCSP4	0.66	2.32	1061.4	21.1
CCSP5	0.49	2.27	782.4	36.9
CCSP6	0.37	2.06	640.6	34.1

Table 20 Structural data obtained by nitrogen adsorption for co-condensed silica.

[a] Primary pore volume (calculated at $p/p_0 = 0.4$ from the desorption isotherm).

[b] Average pore size calculated from the adsorption isotherm by the BJH method.

[c] Total BET surface area.

The co-condensed samples show similar behaviour, as illustrated in Figure 46. Pore size as well as pore volume are decreasing significantly from about 2.5 to about 2.1 nm and 0.58 to 0.37 cm³/g, respectively, for increasing SP loadings and only broad PSD´s were obtained. The surface areas and the C_{BET}-values are showing no definite trend in any direction.

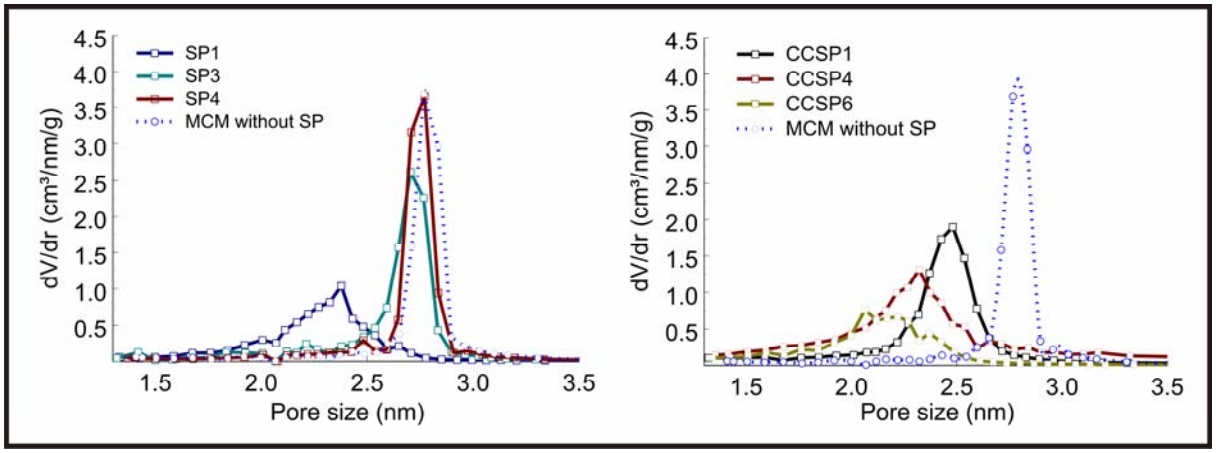

Figure 46 Pore size distribution of grafted (left) and co-condensed (right) samples. Average pore size was calculated from the adsorption isotherm by the BJH method.

A comparison of both synthesis methods by examination of the nitrogen adsorption data shows a generally more defined PSD for grafted SP samples. The pore size reduction is not as pronounced as for the co-condensed samples. The C_{BET}-values are generally smaller for co-condensed samples, which indicates different surface properties. For higher loadings, the C_{BET}-values of the grafted samples approach the co-condensed samples.

3.7.5 Photochemical properties

The change between the two SP isomers could be followed either by absorption or luminescence spectroscopy. In acidic media, the protonated form of the MC (HMC) occurs. This form was found after adsorption of SP in MCM-41,[170] which makes it worthy of consideration in the case of coupled SP. Figure 47 shows a scheme of the different compounds in dependence of illumination and acidity. A mechanism of the conversion was proposed by Woijtyk et al.[171] by supposing an interconversion to the two protonated forms HSP and HMC of spiropyran. According to this theory, a conversion between HSP and HMC must always involve SP as an intermediate. Unfortunately, the HSP form could not be

[170] I. Casades, M. Álvaro, H. García, M. N. Pillai, *Photochem. Photobiol. Sci*. **2002**, *1*, 219.

identified in UV/Vis spectra by Woijtyk et al. In the following, the focus will be held on the other three forms. Absorption in the range of 300 – 700 nm and properties of the three species of the common N-methylated 6-NO_2-BIPS are as follows:

SP:

The absorption can be interpreted as a combination of the two independent absorption spectra of the trimethylindole ring and the phenolic chromophores which act as independent units. There is no conjugation between these two moieties. Absorption bands appear in the UV; highest at about 340 nm in acetone[171]. Phosphorescence was detected at 515 nm in TCE.[172]

MC:

The MC form exhibits an absorption band at about 560 nm in acetone. This band is often used for the detection of spiroyprans. However, there are also bands in the range of 300 to 400 nm, which are more difficult to interpret since they are overlapping with the SP bands. The fluorescence spectrum exhibits a maximum at 652 nm in acetone.[173]

HMC:

This form which occurs in acidic environment exhibits an absorption band at about 405 nm in acetone.[171]

[171] J. T. C. Wojtyk, A. Wasey, N.-N. Xiao, P. M. Kazmaier, S. Hoz, C. Yu, R. P. Lemieux, E. Buncel, *J. Phys. Chem. A* **2007**, *111*, 2511.
[172] A. K. Holm, O. F. Mohammed, M. Rini, E. Mukhtar, E. T. J. Nibbering, H. Fidder, *J. Phys. Chem. A* **2005**, *109*, 8962.
[173] R. Rosario, D. Gust, M. Hayes, J. Sprinter, A. A. Garcia, *Langmuir* **2003**, *19*, 8801.

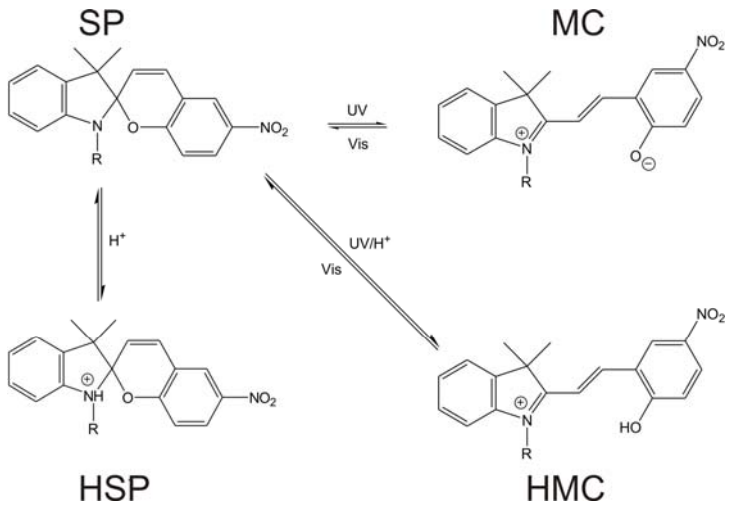

Figure 47 Different forms of SP under UV/Vis irradiation and in acidic environment.

Absorption

Absorption spectra for the different isomers of SPCOOH are shown in Figure 48. In $CHCl_3$ and under addition of triethylamine, the absorption band of MC is observed at about 572 nm and 579 nm, respectively. The addition of trifluoroacetic acid (TFA) in contrast favours the HMC form which shows an absorption band at 420 nm. After Vis irradiation, neither the MC nor the HMC absorption band is detected. Bands of all three forms are present in the range of 300 to 400 nm, for which reason they will not be used for further validation.

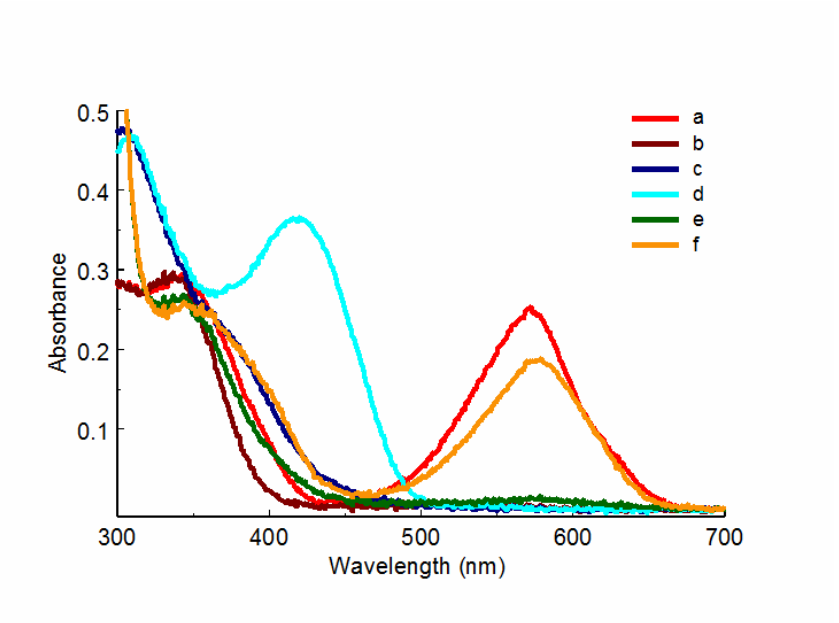

Figure 48 Absorption spectra of 6-NO_2-BIPS in $CHCl_3$ for SP, MC and HMC under UV (366nm) (a), under Vis (b), with addition of 100 µL TFA under Vis (c) and UV (366 nm) (d); addition of 500 µL triethylamine under Vis (e) and UV (366 nm) (f).

Similar UV/Vis spectra were recorded for 6-NO_2-BIPS grafted to the modified silica samples. However, the switching ability of the SP is drastically reduced, which is probably due to the fixation and interaction with the surface. Since none of the samples appeared completely colorless under Vis irradiation, it is assumed that either the equilibrium could never be changed completely to SP or that the formation of HMC or hydrogen bonding to the silanol groups are affecting the spectra.

Absorption spectra of the coupled 6-NO_2-BIPS were generally measured as a suspension in $CHCl_3$ or DMF. Figure 49 shows examples of a common UV/Vis measurement. The absorption of MC was detected at 530 nm in $CHCl_3$ and 560 nm in DMF.

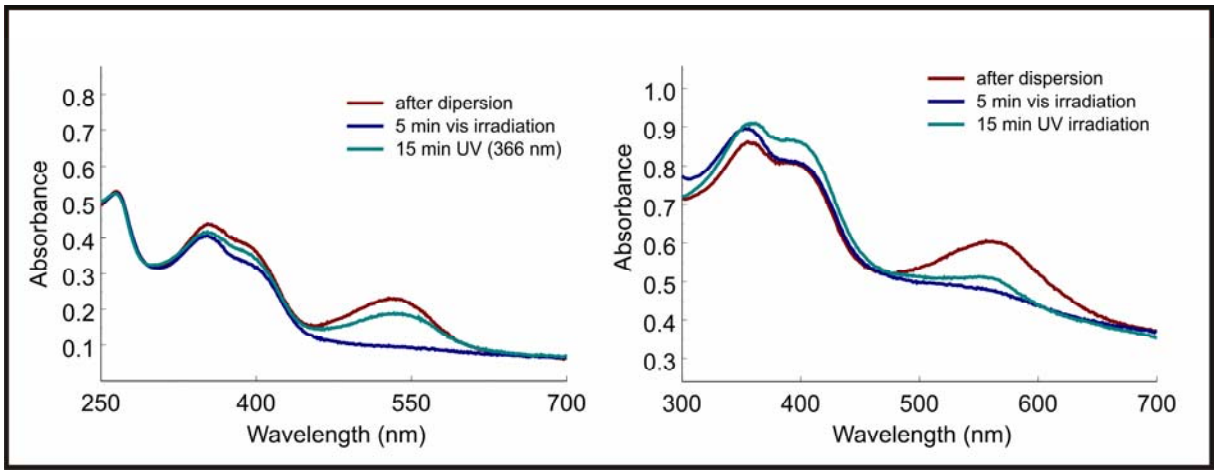

Figure 49 Absorption spectra of dispersions of 6-NO_2-BIPS coupled to MCM-41 in $CHCl_3$ (left) and DMF (right); Dependence on UV (366 nm) and Vis irradiation.

Emission

Emission spectra of the samples were taken in different solvents as suspensions and also as solid samples. $CHCl_3$ and EtOH showed relatively good suspension stabilities and will therefore be mostly referred to. If not indicated otherwise, a sample with a loading of 65 µmol /g (MCM-41) was used for the following experiments as a model compound for grafted SPCOOH.

The MC emission of the coupled SPCOOH is detected at about 600 nm. A comparison with the emission spectra of the educts was done and is depicted in Figure 50. The three educts and the grafted material were dissolved or dispersed in $CHCl_3$. While the indoline only shows

a weak luminescence at about 440 nm, the methylester (SPCOOMe) exhibits the emission of MC at 650 nm. The carboxylic acid (SPCOOH) instead shows a rather broad emission signal between SPCOOMe and the emission of the grafted material at 600 nm. For SPCOOH and SPCOOMe, a hypsochromic shift is found for solvents of increased polarity and due to hydrogen bonding capability [173] Compared with $CHCl_3$ an environment of higher polarity and the possibility of hydrogen bonding is existent in the mesoporous silica channels, leading to a shift to shorter wavelength.

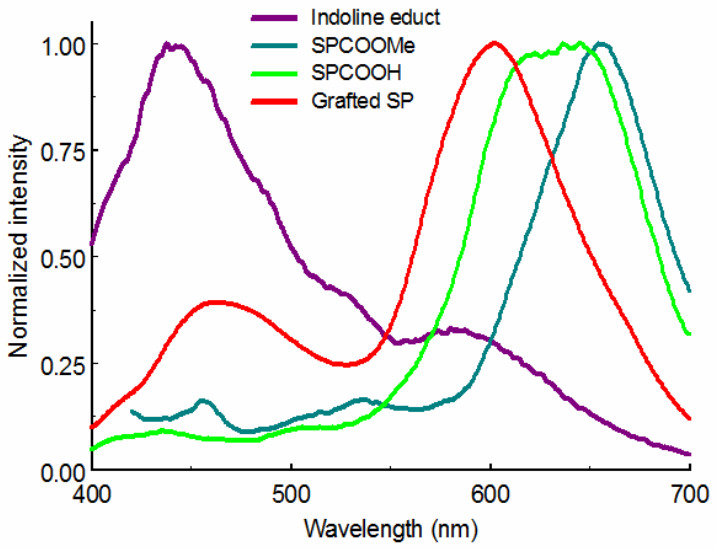

Figure 50 Emission spectra of coupled SPCOOH and the educts SPCOOH, SPCOOMe and indoline derivative in $CHCl_3$ (λ_{ex} = 340 nm).

Since the silica material is known to be acidic depending on the synthetic pathway and surface modifications, the formation of HMC also has to be considered. Therefore, emission spectra of SP were also investigated upon addition of TFA, since HMC is formed under these conditions. Figure 51 (left) shows emission and excitation spectra for SPCOOH with and without 20 µl of TFA in 3 ml of $CHCl_3$. Emission occurs at 620-640 (MC) and 600 nm (HMC) while the excitation is shifting from about 570 (MC) and 390 (MC) to 450 nm (HMC). It should be noted that addition of acid has to be done carefully to avoid decomposition by hydrolysis (see above), which would lead to an irreversible decrease of the MC emission at about 600 nm and a slight increase of the relatively weak emission of the indoline derivative at about 440 nm. No significant decomposition was observed for addition of up to about 2 Vol % TFA and measuring within 12 h.

Figure 51 (right) compares the excitation spectra of MC and HMC and the corresponding emission spectra of the grafted sample. The excitation of coupled SPCOOH shows the same signal at 390 nm as for the MC form of the educt, but the second signal at 570 nm is shifted to a broad signal at about 480 - 530 nm.

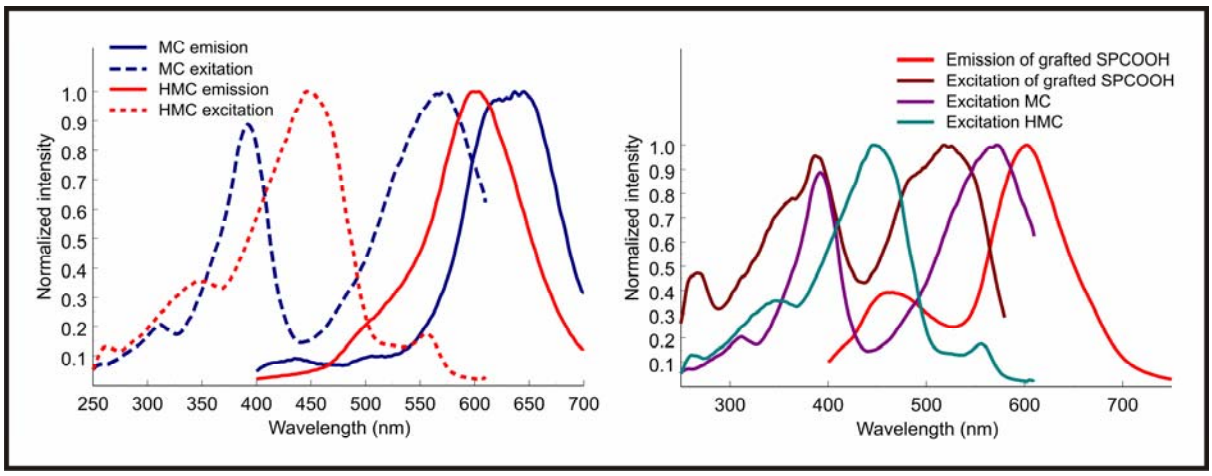

Figure 51 Excitation and emission spectra of MC (λ_{Em} = 630 nm, λ_{Ex} = 340 nm) and HMC (λ_{Em} = 630, λ_{Ex} = 340 nm) of SPCOOH (left) and of MC (λ_{Em} = 630 nm), HMC (λ_{Em} = 630 nm) and grafted SPCOOH (λ_{Em} = 600 nm, λ_{Ex} = 340 nm) (right) in $CHCl_3$ and $CHCl_3$/TFA (0.7 Vol %).

Only a slight shift of the emission in dependence of the solvent could be observed by varying between ethanol, $CHCl_3$, DMF and cyclohexane (Figure 52 left). Emission maxima were found at 602 nm for $CHCl_3$ and cyclohexane and 615 nm for ethanol and DMF.

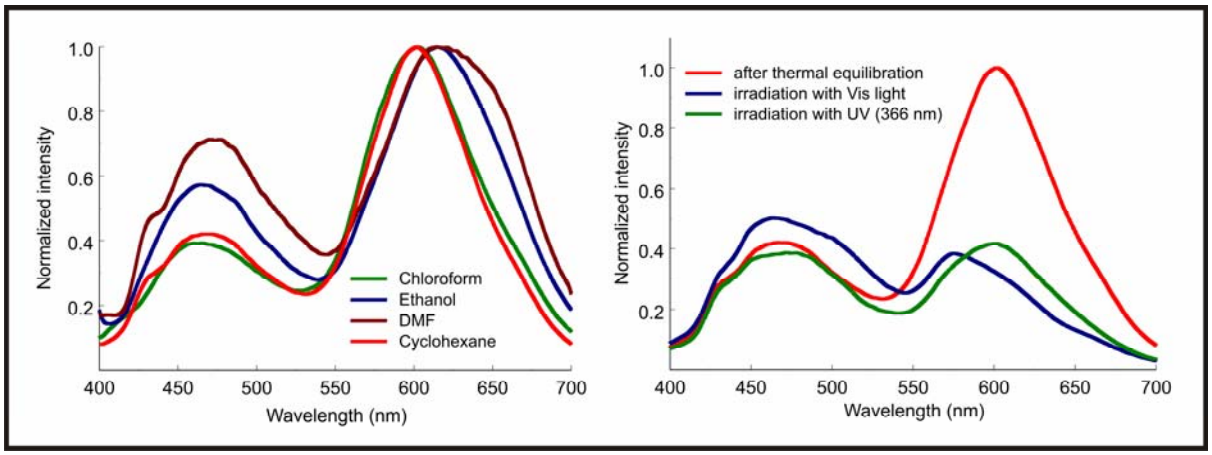

Figure 52 Emission spectra of 6-NO_2-BIPS modified silica in different solvents (left) and under Vis and UV (366 nm) irradiation in cyclohexane (right) (λ_{ex} = 380 nm).

Analysis of the coupled SPCOOH shows a distinct variation of the MC signal at 600 nm under irradiation with UV and Vis light (Figure 52 (right)). The initial emission after thermal equilibration of the dry sample at about 600 nm is reduced drastically by Vis irradiation. However, irradiation with UV light at 366 nm fails to reach the initial level and only a slight increase of the intensity is obtained. Switching of the free educt is much more efficient (Figure 53). In contrast to the switching behaviour of solid samples (see also below) the solvent apparently reduces the switching ability in a dramatic fashion.

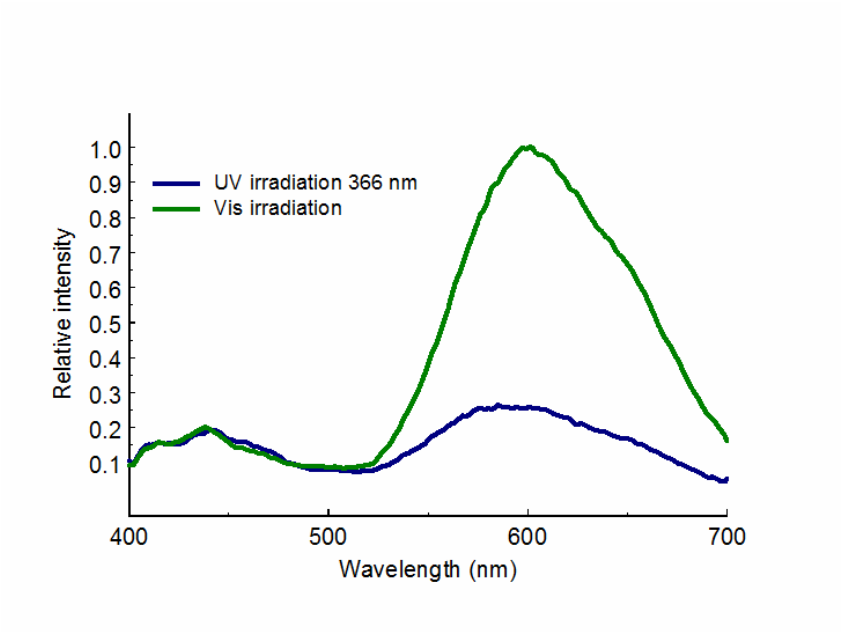

Figure 53 SPCOOH under Vis and UV (366 nm) irradiation in $CHCl_3$ (λ_{ex} = 380 nm).

3.7.6 Emission of solid sample

In addition to measurements of suspensions, also powdered samples were investigated. In this case switching could be repeated without a significant loss of intensity. Figure 54 depicts a solid sample with a 6-NO_2-BIPS loading of about 65 µmol/g (MCM-41) after irradiation with UV (366 nm) and Vis light. The initial emission is reduced after Vis irradiation and can be restored partially after irradiation at 366 nm. Compared to fluorescence measurements in solvents (Figure 52, right), the switching properties are improved. As seen in Figure 55, the change between SP and MC form can also be followed by eye, which could be exploited for the development of optical sensors.

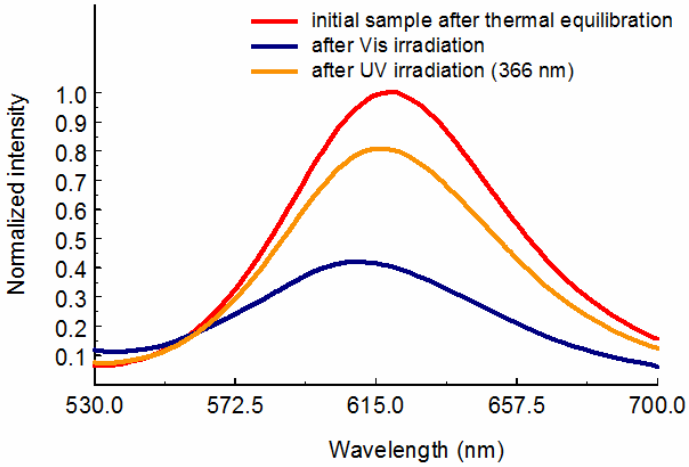

Figure 54 Solid sample emission spectra of 6-NO_2-BIPS modified silica after irradiation with Vis and UV (366 nm) light (λ_{ex} = 340 nm).

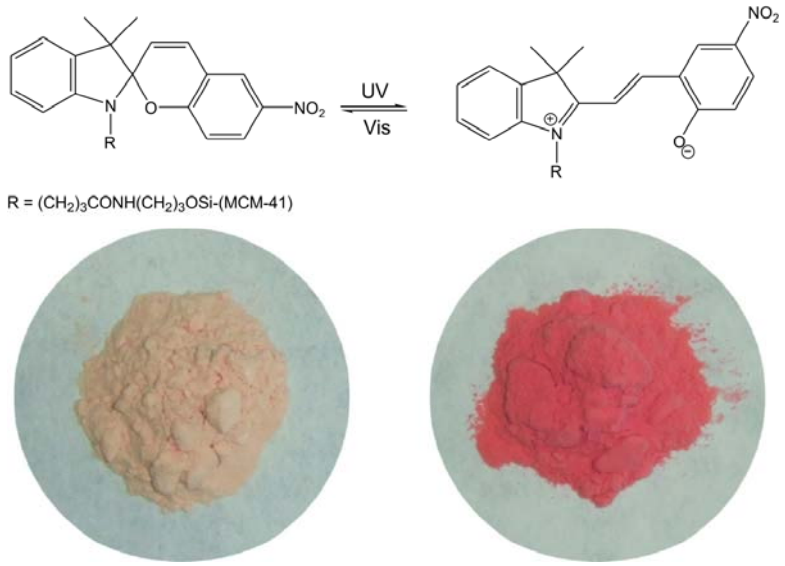

Figure 55 Scheme of MC and SP forms of 6-NO_2-BIPS modified silica (top) and corresponding photographic images of the samples (bottom).

For a typical SP3 type sample with a loading of about 65 µmol/g (MCM-41), changing between MC and SP was reversible (Figure 56). It can also be seen that the initial intensity can not be reached again, since SP is excited as well as MC upon UV irradiation. The irradiation was switched between λ_{ex} = 340 nm and λ_{ex} > 500 nm to obtain the MC and the SP form. For grafted samples, switching could be observed for low as well as for high loadings of about 250 µmol/g (MCM-41). This is in contrast to co-condensed samples which could only be switched up to 24 µmol/g (MCM-41). Framework incorporation of SP is a

possible explanation of the absence of efficient switching at higher loadings. This is supported by the broader PSD for higher loadings. Also partial decomposition for the co-condensed samples due to the basic synthesis conditions (see above) has to be considered in this context.

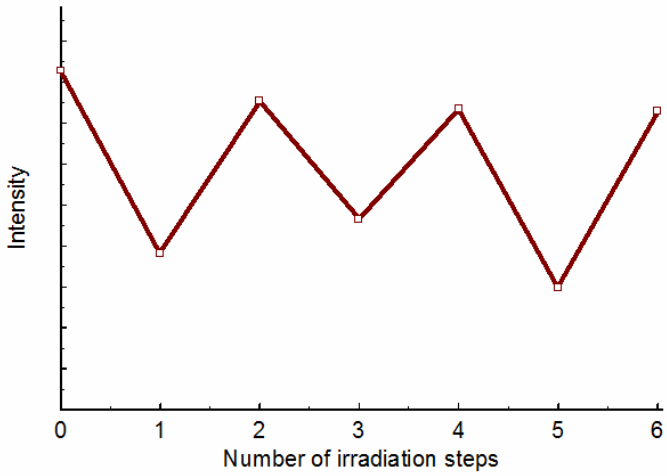

Figure 56 Changes in the emission at 620 nm (λ_{ex} = 340 nm) by switching between Vis and UV (340 nm) irradiation.

Conclusion

SP was attached to the surface of MCM-41 by postsynthetic as well as by co-condensation route. Differences in the PSD were evaluated by N_2-sorption measurements showing broader PSD of higher SP contents for both methods. Emission and absorption spectra of both samples were taken considering especially the SP, MC and HMC forms, which are likely present in this system.

Development of a silica synthesis route under slight acidic conditions could be helpful to prevent possible decomposition of SP.

The combination with luminescent systems as described in 3.3, 3.4, 3.5 and 3.8 should be investigated further in order to trigger a release by activation through irradiation. The different chemical properties of the isomers can be exploited for this purpose. In order to minimize an interfering effect of hydrogen bonding by surface silanol groups, capping by silylation should also be considered.

3.8 Adsorption of quantum dots

Due to their size-tunable properties, semiconductor quantum dots (QD´s) received much attention concerning potential applications in the field of optoelectronics,[174] solar cells,[175] light emitting devices,[176] or biosensing[177] and biolabeling.[178] QD´s offer a narrow, tunable symmetric emission spectrum.[177,179] A decrease of the QD size results in an increase of the separation between the energy levels. This change in the electronic structure can be followed by detection of the emission wavelength. A coating of QD´s with a passivation layer such as ZnS,[180] CdSe,[180] CdS[181] or ZnSe[182] increases the quantum efficiency. CdSe QD´s which are capped with ZnS feature increased quantum efficiency exceeding 50 % and additionally show decreased toxicity.[183] To avoid coagulation, which would affect the luminescence properties, the surface is typically coated with a hydrophobic organic group containing bulky (C8-C18) alkyl moieties (mostly tri-n-octylphosphine oxide (TOPO)).[184]

The combination of mesoporous materials and QD´s offers interesting possibilities in terms of organization and confinement. Research efforts have focused on the in-situ synthesis of QD´s in mesoporous silicas.[185] Inclusion in nanofibers of porous alumina and the doping in large pore size silica materials were studied as well.[186] The mesoporous material provides a stable and accessible surface with well defined PSD for the loading of QD´s. An additionally well defined morphology offers possibilities for the investigation of the properties of single QD´s inside the silica by means of optical microscopy based methods.

In order to prepare a material for optical studies, CdSe/ZnS QD´s with a hydrophobic coating (PlasmaChem GmbH, Berlin) were used. A silica material with well defined morphology and

---

[174] C. J. Murphy, *Anal. Chem.* **2002**, *74*, 520A.
[175] U. H. Wendy, P. Xiaogang, A. P. Alivisatos, *Adv. Mater.* **1999**, *11*, 923; N. C. Greenham, X. Peng, A. P. Alivisatos, *Phys. Rev. B* **1996**, *54*, 17628.
[176] S. Coe, W.–K. Woo, M. Bawendi, V. Bulovic, *Nature* **2002**, *420*, 800.
[177] W. C. W. Chan, D. J. Maxwell, X. H. Gao, R. E. Bailey, M. Y. Han, S. M. Nie, *Current Opinion in Biotechnology* **2002**, *13*, 40.
[178] A. P. Alivisatos, *Nat. Biotechnol.* **2004**, *22*, 47; A. P. Alivisatos, *Science* **1996**, *271*, 933.
[179] W. C. W. Chan, S. Nie, *Science* **1998**, *281*, 2016; M. Bruchez Jr., M. Moronne, P. Gin, S. Weiss, A. P. Alivisatos, *Science* **1998**, *281*, 2013.
[180] A. R. Kortan, R. Hull, R. L. Opila, M. G. Bawendi, M. L. Steigerwald, P. J. Carroll, L. E. Brus, *J. Am. Chem. Soc.* **2002**, *112*, 1327.
[181] X. Peng, M. C. Schlamp, A. V. Kadayanich, A. P. Alivisatos, *J. Am. Chem. Soc.* **1997**, *119*, 7019.
[182] C. F. Hoener, K. A. Allan, A. J. Bard, A. Campion, M. A. Fox, T. E. Mallouk, S. E. Weber, J. M. White, *J. Phys. Chem.* **2002**, *96*, 3812.
[183] M. A. Hines, P. Guyot-Sionnest, *J. Phys. Chem.* **1996**, *100*, 468.
[184] G. Kalyuzhny, R. W. Murray, *J. Phys. Chem. B* **2005**, *109*, 7012; M. Kuno, J. K. Lee, B. O. Dabbousi, F. V. Mikulec, M. G. Bawendi, *J. Chem. Phys.* **1997**, *106*, 9869.
[185] H. Parala, H. Winkler, M. Kolbe, A. Wohlfart, R. A. Fischer, R. Schmechel, H. v. Seggem, *Adv. Mater.* **2000**, *12*, 1050; H. Winkler, A. Birkner, V. Hagen, I. Wolf, R. Schmechel, H. v. Seggem, R. A. Fischer, *Adv. Mater.* **1999**, *11*, 1444.
[186] X. Gao, S. Nie, *J. Phys. Chem. B* **2003**, *107*, 11575.

large pores was employed as a host. Therefore, a SBA-15 type material with pore sizes between 20 and 24 nm (BJH method) was synthesised by adding mesitylene (TMB) as a swelling agent (5.1.3). The morphology of the particles was controlled by adjusting the amount of KCl and TMB in the synthesis to achieve spherical particles as described in the literature.[187] An adequate environment for the hydrophobic QD´s was prepared by grafting octadecyltrimethoxysilane (ODTMS) to the silica surface. Synthesis procedure 5.2.4.3 resulted in a sufficient amount of grafted moieties as was shown by IR spectroscopy (Figure 57), elemental analysis and N_2 sorption (Table 21) for different grafting procedures of 5.2.4.

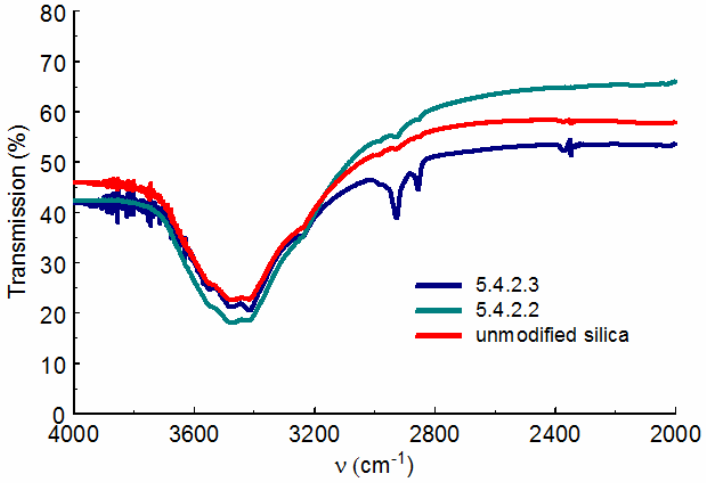

Figure 57 Comparison of IR spectra of unmodified silica and silica samples grafted by method 5.4.2.2, and 5.4.2.3.

#	Synthesis number	C-content[a]	H-content[a]	Pore size[b] [nm]	C_{BET}
L S-2		0.2	0.4	23.1	175
L S/Od-3	5.2.4.2	4.2	1.6	23.1	132
L S/Od-2	5.2.4.3	11.5	2.4	19.2	39

Table 21 Comparison of ODTMS grafting conditions;
[a] Weight percentage calculated from elemental analysis;
[b] Average pore diameter calculated from the adsorption isotherm by the BJH method.

[187] L. Wang, T. Qi, Y. Zhang, J. Chu, *Microporous Mesoporous Mater.* **2006**, *91*, 156.

The QD´s exhibit a size of 2 to 7 nm. The SBA-15 type silica features a pore size of about 18 nm to 19 nm (BJH method) after the functionalization (L S/Od-1/-2) and offers sufficient space for an inclusion of the QD´s. The corresponding nitrogen adsorption data is given in Table 22; Figure 58 depicts the pore size distribution of the silica materials. Grafting of ODTMS causes a reduction of the pore size of approximately 4 nm. The change to a hydrophobic surface is confirmed by the decrease of the C_{BET}-values to about 40.

#	Grafting	S_{BET}[a] [m²/g]	Pore volume [cm³/g]	Pore size[b] [nm]	Pore size[c] [nm]	C_{BET}[d]
L S-1	--	716	2.01	23.4	17.3(broad)	119
L S-2	--	743	1.91	23.1	17.3	175
L S/Od-1	ODTMS	481	1.67	18.2	16.1	41
L S/Od-2	ODTMS	373	1.35	19.2	15.0	39

Table 22 Nitrogen adsorption data;
[a] Total BET surface area;
[b] Average pore diameter calculated from the adsorption isotherm by the BJH method;
[c] Average pore diameter calculated from the adsorption isotherm by the DFT method;
[d] C-value by means of the BET method.

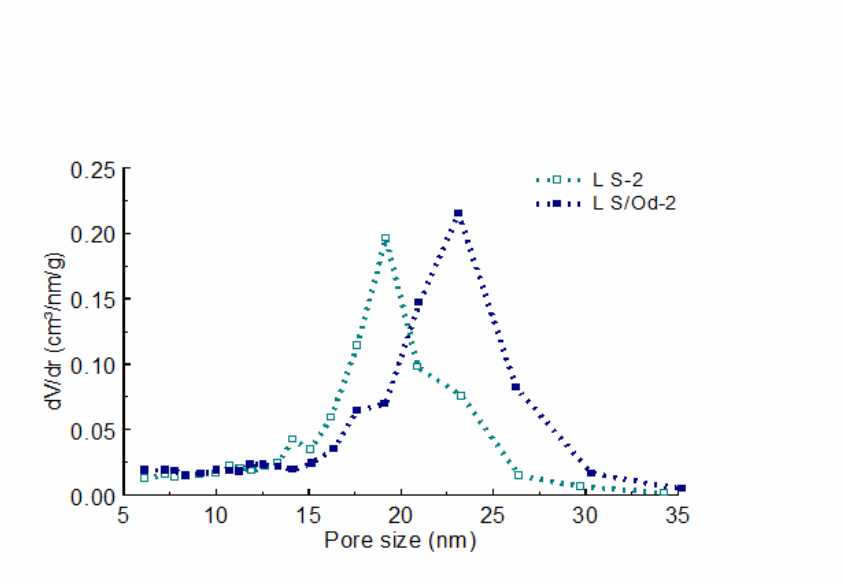

Figure 58 Comparison of the PSD calculated from the adsorption branch by the BJH method for unmodified and ODTMS modified large pore size SBA-15.

Incorporation of the QD´s is achieved by adsorption from a corresponding dispersion by procedure 5.6.5. Different amounts of QD´s were included by varying the concentration of the dispersions.

SEM images showed spherical particles of sizes between 1 and 5 μm (Figure 59). However, extensive treatment with 1-butanol during loading and washing seemed to cause a partial decomposition of the spherical particles.

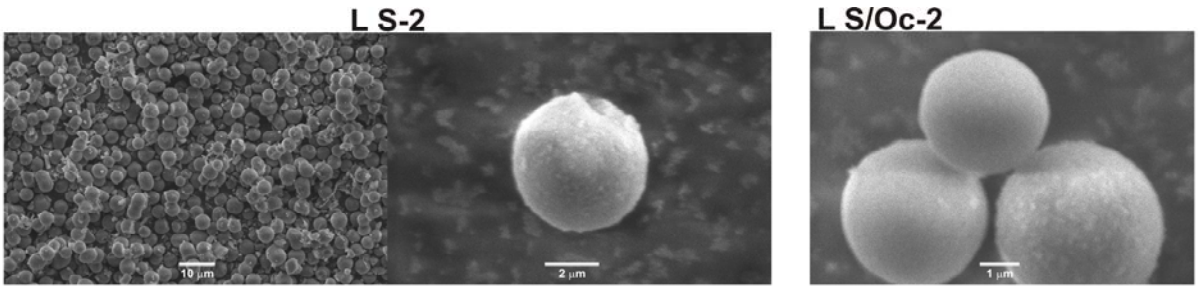

Figure 59 SEM images of large pore size SBA-15 before (left) and after (right) grafting of ODTMS.

The emission of single QD´s was investigated in order to gather information about concentration and organization inside the silica material. A confocal microscope setup as described in 5.8 was used for this purpose. Following confocal microscope measurements were performed at the University of Tübingen in the group of Prof. Dr. A. Meixner by Dipl. Phys. A. Chizhik.

Laser polarization conversion technique

The measurements of the QD´s transition dipole moment (TDM) orientation were performed using laser beam polarization conversion (LBPC) technique.[188] Figure 60 schematically shows an optical line for the conversion of the linearly polarized Gaussian beam into a doughnut mode laser beam. A key element of the system is a mode converter consisting of four λ/2 plates glued together as shown in a scheme (chapter 5.8). Passing the linearly polarized Gaussian beam through the mode converter creates an azimuthal polarization of the laser beam. A pinhole is used to remove higher spatial frequencies before the beam is expanded to fit in the objective back aperture. The collimated beam is reflected by a non-polarizing beam-splitter cube and focused onto the sample with the microscope objective.

[188] L. Novotny, M. R. Beversluis, K. S. Youngworth, T. G. Brown, *Phys. Rev. Lett.* **2001**, *86*, 5251; R. Dorn, S. Quabis, G. Leuchs, *Phys. Rev. Lett.* **2003**, *91*, 233901; A. V. Failla, H. Qian, H. Qian, A. Hartschuh, A. J. Meixner, *Nano Lett.* **2006**, *6*, 1374.

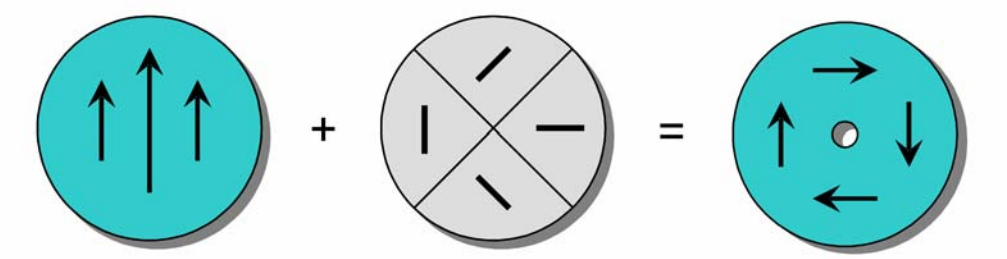

Figure 60 **C**onversion of linearly polarized- to azimuthally polarized laser beam by a polarization converter.

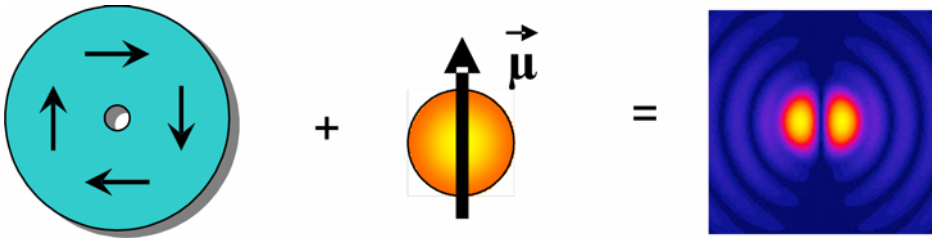

Figure 61 Calculated excitation from an azimuthally polarized laser beam irradiated on the TDM of a QD.

The excitation of a single QD included in a polymer matrix as well as in silica spheres by scanning it through the focal region of an azimuthally polarized laser beam with doughnut-shaped intensity profile gives rise to an image consisting of two nearby bright spots of elliptical shape resembling a “coffee bean”. This situation is displayed in Figure 61. The projection of the TDM on the substrate is oriented along the dark gap between the two halfs of the coffee bean. Out-of-plane orientations of the TDM lead to a weaker intensity of the coffee bean image, while TDM´s oriented exactly perpendicular to the surface cannot be seen at all. Weaker images are also obtained if the luminescence intensity of the QD is smaller.

The QD loaded silica spheres were spin coated in very low concentration on a quartz cover slide of 170 µm thickness. For this purpose, a single milligram quantity of the sample was dispersed in ethanol. A droplet (10 µL) of this highly diluted mixture was spin-coated on a quartz cover slide. To fix the spheres on the surface of the cover slide, a droplet (10 µL) of a solution of 1 % poly(methyl methacrylate) (PMMA) in toluene was spin coated on top of the spheres. In order to exclude the influence of possible impurities, a droplet of the polymer was spin-coated onto a quartz cover slide and spectroscopically verified.

For the preparation of the sample with single QD´s embedded in the polymer matrix, a small amount of the QD´s was dispersed in toluene and subsequently mixed with a solution of 1 % PMMA in toluene. One droplet (10 µL) of the final solution was spin-coated on the clean glass cover slide surface. (The polymer matrix was used to fix particles on the surface and to exclude rotation or movement of the particles.)

The typical emission spectrum of single CdSe/ZnS QD´s is presented in Figure 62. The maximum of the emission at 610 nm corresponds to the electron-hole recombination energy.

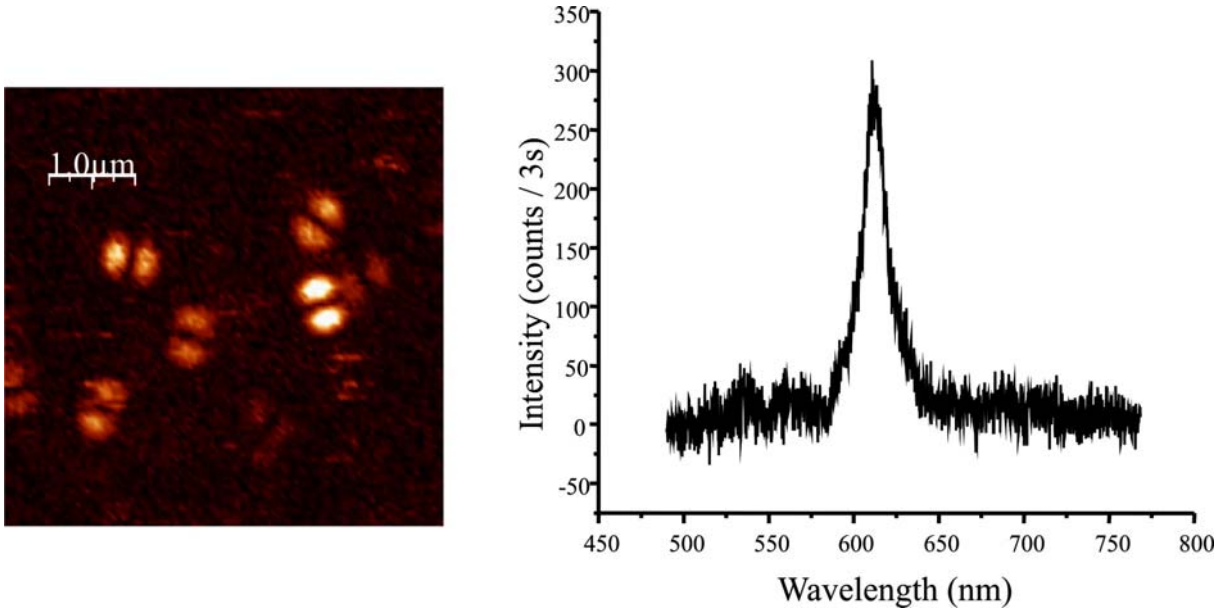

Figure 62 Fluorescence microscopy picture and emission spectrum of CdSe/ZnS QD´s embedded in PMMA matrix.

The fluorescence images and normalized emission spectra of two porous silica beads without QD´s are presented in Figure 63 (left). The emission spectrum has a broad shape with a maximum around 550 nm. The origin of this weak photoluminescence is assigned to oxygen related defect sites.[189] Different colors indicate spectra which were recorded one after another (from 1 to 4) from the same area of the silica bead. Fast bleaching of the emission was observed.

[189] M. E. Gimmon-Kinsel, K. Groothuis, K. J. Balkus Jr., *Microporous Mesoporous Mater.* **1998**, *20*, 67.

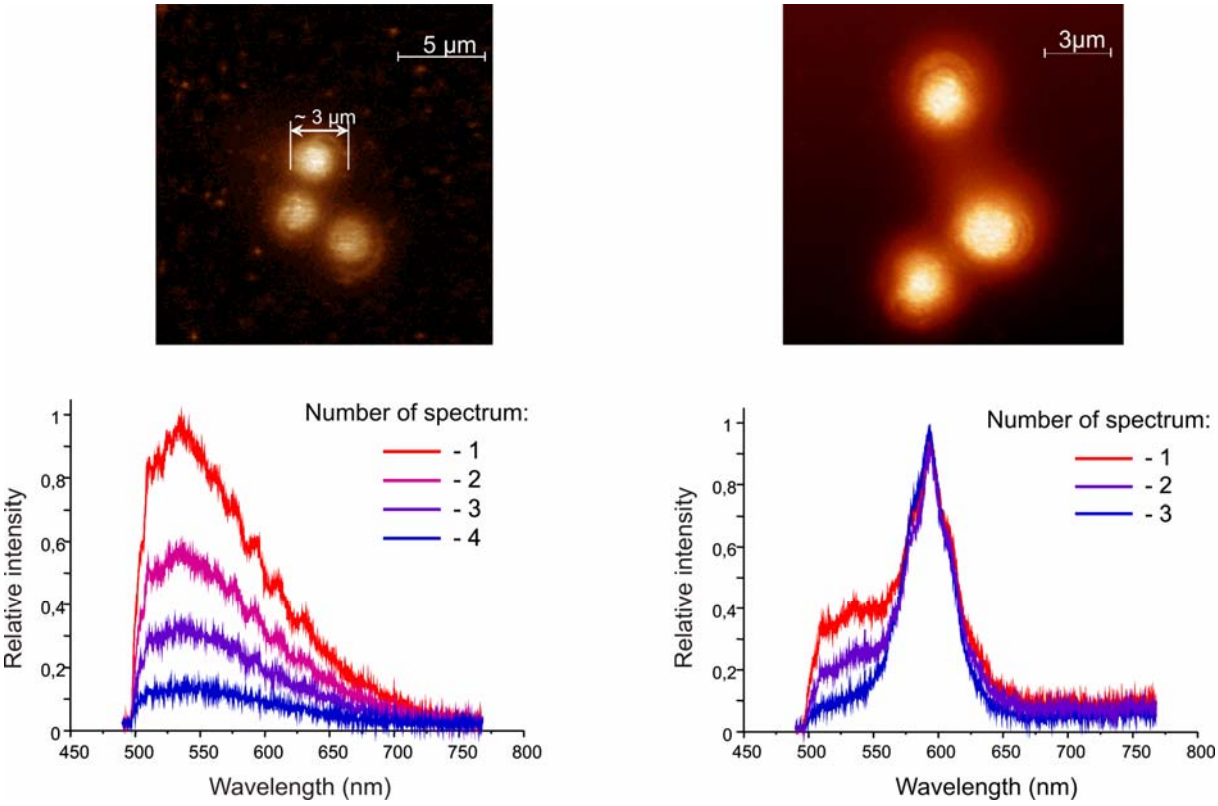

Figure 63 Fluorescence images and corresponding spectra of silica spheres without (left) and with (right) CdSe/ZnS QD´s.

Figure 63 (right) shows the fluorescence images and normalized emission spectra of three porous silica beads with high concentration of included QD´s in the channels. The emission spectra exhibit a shoulder and a maximum: with the shoulder at around 520 nm, corresponding to the emission of the porous silica and with the maximum at 610 nm, corresponding to the emission of included QD´s. A series of spectra which were taken one after another from the same area of the bead is shown. The band which corresponds to the emission of the QD´s exhibits almost no bleaching whereas the short wavelength band, which corresponds to the porous silica, features fast bleaching.

Figure 64 shows fluorescence images of single porous silica beads with different concentrations of the included QD´s. The left image displays two porous silica beads with relatively high concentration of QD´s. The middle and right images show porous silica beads with low concentration of the included QD´s. High concentration was achieved by adsorption from a dispersion with 2.7 mg/L and low concentration from 6.3 ng/L of QD´s. The excitation patterns of single QD´s in the channels were observed.

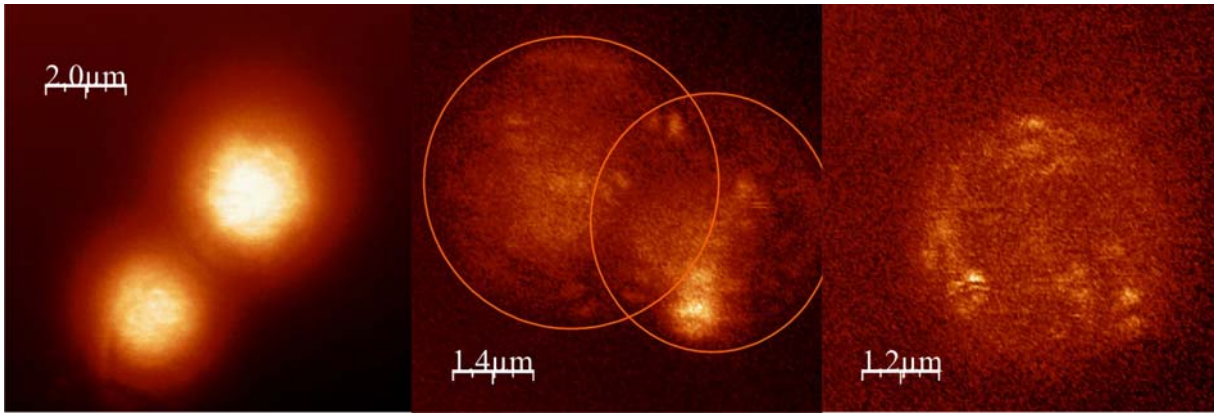

Figure 64 Fluorescence images of CdSe/ZnS QD´s in silica spheres adsorbed from dispersions of different concentration.

Due to the dimensions of the silica beads it is not possible to acquire the complete picture of the single QD´s distribution in a single scan. However, the spatial distribution of the QD´s in the channels can be reconstructed by stepwise z-scanning, thus collecting fluorescence images from different cross-sections of the silica bead. Figure 65 shows a series of fluorescence images acquired at five different levels, from the bottom to the central part of a silica bead with included QD´s in the channels. Figure 65 (1) gives the fluorescence image acquired with the laser beam focused on the boundary between the cover slide and the silica bead. The images shown in Figure 65 (2-5) correspond to the shift of the focal plane upwards by about 30 nm, 60 nm, 90 nm and 110 nm, respectively. Using this method, a complete picture of the distribution of QD´s throughout the whole silica bead can be acquired.

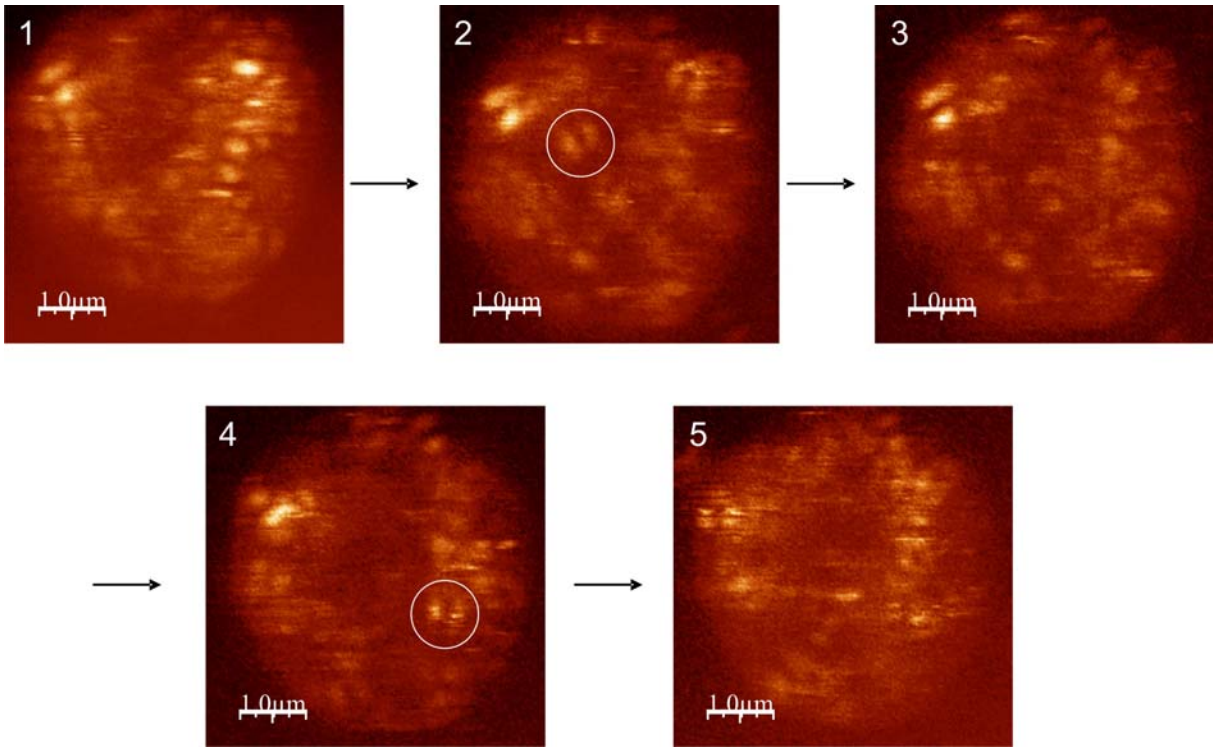

Figure 65 Fluorescence images at z = 0 nm (1), z = 30 nm (2), z = 60 nm (3), z = 90 nm (4), z = 110 nm (5) of a CdSe/ZnS QD loaded silica bead.

Conclusion

A loading of the porous silica with QD´s in different concentrations was accomplished as was shown by confocal microscopy measurements. Single QD´s could be detected by fluorescence imaging. However, measurement of the orientation of QD´s relative to the channel system requires introduction into a one dimensional (arrays of silica nanochannels[190]) silica material. First experiments with hexagonal fibers were problematic due to their relatively small pore size (2.9 nm). A successful approach would require small (less than 3 nm) QD´s coated with short alkyl groups or monodirectional silica channels with larger pore sizes.

[190] Y. Kievsky, I. Sokolov. IEEE *Trans. Nanotechnol.* **2005**, *4*, 490.

Chapter 4

Conclusion/ Outlook

The focus of this thesis is on the functionalization of mesoporous silica with luminescent molecules and quantum dots, with emphasis on stimuli-responsive systems and concepts that provide information on the host material itself. The host materials were prepared based on SBA-15 and MCM-41 type syntheses using typical structure directing agents P123 and CTAB. The modification of the channel surfaces with various alkoxysilanes was studied in detail. Functional organic groups were attached to introduce fluorescent molecules.

The functionalization with iodopropyl groups via an adjusted one pot synthesis was investigated. The resulting silica structure and its formation in function of the addition of alkylmethoxysilanes were studied in detail. It was shown that the addition of trimethoxymethylsilane had a positive influence on the pore structure of the resulting silica material in terms of a narrow pore size distribution. The synthesis of a bifunctional material was demonstrated by co-condensation with IPTMS and APTMS, yielding iodopropyl and aminopropyl groups on the surface. Complementary reactivity and accessibility of the functional groups was shown by coupling with two different fluorescent labels, namely fluorescein and nile red. The co-condensation method for functionalization with iodopropyl groups was successfully extended and proved to be suitable for the synthesis of multifunctionalized mesoporous materials.

The pore surface attachment of fluorescent organic molecules was shown to allow conclusions concerning the channel surface characteristics and on the other hand enables the system to detect incorporated molecules or the actual environment (detection of gas or solvent composition). Under this aspect, organic fluorescent molecules nile red, DMABN and DAPS were adsorbed or covalently attached to mesoporous silica. Furthermore, the inclusion of resorufin as well as luminescent nanoparticles of CdSe/ZnS was investigated. The studies provided insight into the reversible physisorption of these species, as well as into the luminescence properties in confined systems.

As an example for TICT molecules, which are known to be sensitive towards solvent polarity, DMABN and DAPS were incorporated into MCM-41. Differences in the surface properties were detected by changes in the fluorescence of the TICT molecules and further verified by evaluation of the nitrogen adsorption isotherms (C_{BET}-values). Concepts for sensing either the mesoporous silica surface properties or adsorbed molecules of different polarity seem therefore generally feasible. However, covalent attachment of the molecules, which would

exclude the possibility of aggregation, should be pursued. This additionally would allow the detection of solvent polarity without leaching of the TICT molecules.

The attachment of nile red was investigated under the aspect of sensing, since it is already well known in labeling of biologic systems. Adsorption of NR in different MCM-41 samples was demonstrated and quantified. By analyzing the emission intensity and wavelength, a dependence on the actual surface modification was found. A series of slightly different surface polarities was created by varying the grafted amino content on the surface and subsequently differentiated by the corresponding emission spectra of adsorbed nile red. Covalent attachment was accomplished by three different linkers which were mainly evaluated concerning the stability of the nile red bond to MCM-41. A co-condensed SBA-15 type material of nile red was prepared and compared to a material obtained by a postsynthetic route. Applicability for sensing of solvent polarities was demonstrated by detection of emission spectra of suspensions which showed wavelength shifts in dependence of the actual solvent polarity similar to the corresponding solution systems. For the design of hydrophobic "pockets" on the hydrophilic silica material, only weak detection by covalently introduced nile red could be observed. However, if a more efficient formation of the pocket in the liquid crystal templating process could be achieved, detection by nile red seems to be very likely. This would clear the way for defined pore structures providing an optimized environment for target molecules attached to the surface. A more detailed categorization of the emission spectra by grafting of nile red to differently modified surfaces is expected to yield promising results concerning the analysis of mesoporous silica surfaces.

Inclusion of coated (CdSe/ZnS) quantum dots in mesoporous silica has already attracted considerable attention. In this work, confocal microscope images of (CdSe/ZnS) quantum dots were presented. General results concerning the amount of included quantum dots by adsorption from different solutions were obtained. However, investigations regarding the orientation of the quantum dots relative to the channel would require mesoporous silica particles with a channel system that is defined in relation to the particle morphology. Hexagonal fibers with oriented channels would feature the required properties. Adjusting the relative sizes of quantum dots and channels is challenging in these systems.

The release of Res^- from functionalized MCM-41 was monitored by its emission signal. This system can be used to model the release of drug molecules. The amount of grafted positive

groups was shown to be a relevant parameter. The system shows promising perspectives for a combination with a light sensitive molecule that allows triggering of the release by an external stimulus.

Attachment of photochromic molecules was investigated by focusing on the spiropyran system. A combination of the photochromic properties with the defined confinement of mesoporous silica allows a controlled access or release. Consequently, these systems are promising for smart devices. Spiropyran was covalently attached to mesoporous silica MCM-41 via postsynthetic (grafting) and by in situ (co-condensation) routes. The coupled amounts of spiropyran for both methods were compared and the resulting pore structures were investigated by N_2-sorption. The change between spiropyran and merocyanine forms was studied by fluorescence and absorption measurements, revealing a decreased activity for high loadings and for co-condensed materials. Emission spectra were studied in different solvents. Switching of grafted spiropyran was shown to be reversible by irradiation with UV and visible light.

Applications of these systems for controlled release are promising. However, an interfering effect of the silica structure influencing the switching behaviour has to be overcome or minimized. Furthermore, the change in the chemical properties by switching from spiropyran to the zwitterionic merocyanine form is expected to affect adsorption and release properties. One interesting example is the increased metal sorption capacity of the merocyanine form, which could be exploited for the inclusion of ionic compounds.

Chapter 5

Experimental

5.1 Synthesis of mesoporous silicas

5.1.1 Synthesis of MCM-41[191]

An amount of CTAB (2.20 g, 6 mmol) was dissolved under slight warming in a mixture of 52 mL of water and 24 mL of aqueous ammonia (28 %). After the solution had been cooled to RT, a volume of tetraethyl orthosilicate (TEOS) (10 mL, 45 mmol) was slowly added under vigorous stirring to the clear solution, and the resulting gel was stirred for 3 h at RT. The mixture was then transferred to a teflon-lined autoclave and heated at 110 °C for 48 h. The product was obtained by filtration, washed with copious amounts of water (at least 1 L), and dried at RT.

Template removal by:

I calcination

The template was removed by first heating the as-synthesized MCM-41 at 300 °C for 2 h and subsequent calcination in air at 550 °C for 16 h. Heating rates of approximately 2 °C/min were applied.

II extraction[192]

An amount of 1 g of as-synthesized MCM-41 was suspended in 150 mL of a solution of NH_4NO_3 in ethanol (2 g/L) and heated at 60 °C for 15 min. After filtration and washing with 50 mL of ethanol the procedure was repeated twice and the resulting mixture was filtered and subsequently dried at 80 °C for 24 h.

5.1.2 Synthesis of SBA-15[193]

P123 (2.20 g, ~0.4 mmol) was dissolved in a solution of 31 mL of 4 N hydrochloric acid and 49 mL of water (1.55 N hydrochloric acid) at RT until the solution was clear (ca. 2 h). Under

[191] D. Brühwiler, H. Frei, *J. Phys. Chem. B* **2003**, *107*, 8547.
[192] N. Lang, A. Tuel, *Chem. Mater.* **2004**, *16*, 1961.
[193] D. Zhao, Q. Huo, J. Feng, B. F. Chmelka, G. D. Stucky, *J. Am. Chem. Soc.* **1998**, *120*, 6024.

intense stirring, TEOS (5 mL, 22 mmol) was slowly added and the solution was stirred for 20 h at RT. The resulting white mixture was transferred to a teflon-lined autoclave and heated under static conditions at 100 °C for 24 h. Filtration of the product and extensive washing with at least 1 L of water resulted in the as-synthesized form of the SBA-15.

Template removal by:

I calcination

The template was removed by first heating the as-synthesized SBA-15 at 300 °C for 2 h and subsequent calcination in air at 550 °C for 16 h. Heating rates of approximately 2 °C/min were applied.

II extraction[194]

The template was removed by Soxhlet extraction with ethanol under reflux for 24 h. The product was subsequently dried at 80 °C.

5.1.3 Large pore SBA-15[195]

P123 (2.20 g, ~0.4 mmol) and potassium chloride (3.49 g, 47 mmol) were disolved in 50.5 mL of water and 29.5 mL of 4 N hydrochloric acid for one hour until the solution became clear. Afterwards, 1,3,5-trimethylbenzene (TMB) (1.98 mL, 14 mmol) was added and the mixture was stirred for 2 h at RT. Finally, TEOS (5.2 mL, 23 mmol) was added dropwise under vigorous stirring. The white mixture was stirred for 10 min, transferred to a teflon-lined autoclave and heated under static conditions at 35 °C for 24 h, followed by another period of 24 h at 100 °C. The resulting product was filtered, washed with copious amounts of water (at least 1 L) and dried at RT.
The template was removed by Soxhlet extraction with ethanol for 24 h. The product was subsequently dried at 80 °C.

[194] J. A. Melero, G. D. Stucky, R. v. Grieken, G. Morales, *J. Mater. Chem.* **2002**, *12*, 1664.
[195] L. Wang, T. Qi, Y. Zhang, J. Chu, *Microporous Mesoporous Mater.* **2006**, *91*, 156.

5.2 Functionalization of mesoporous silica

5.2.1 Propyltrimethylammonium chloride[196]

An amount of 0.5 g of predried (80 °C, 3 h) MCM-41 was suspended in 20 mL of chloroform and an appropriate amount of 3-trimethoxysilylpropyl(trimethyl)ammonium chloride (TMSTAC) (50 wt % in methanol) was added. The slurry was stirred for 1 h and triethylamine (molar ratio triethylamine/TMSTAC = 2) was added. The reaction was performed for 18 h. The functionalized MCM-41 was filtered and washed with 180 mL of dichloromethane. The product was dried overnight at 80 °C.

5.2.2 Aminopropyl

An amount of 1 g of predried (80 °C, 3 h) MCM-41 was dispersed in 30 mL of dry toluene and an appropriate amount of 3-aminopropyltrimethoxysilane (APTMS) was added. The slurry was stirred under reflux for 3 h. After cooling to RT, the mixture was filtered and washed with 100 mL of dichloromethane. The sample was dried at 80 °C overnight.
The same procedure was applied for the reaction with other 3-aminopropylsilanes such as 3-aminopropyldiisopropylethoxysilane (APDIPES).

5.2.3 Bromopropyl

Bromopropyltrimethoxysilane (BPTMS):

For a standard reaction, 1 g of predried (80 °C, 3 h) MCM-41 was suspended in 20 mL of dry toluene and an appropriate amount of BPTMS was added. The reaction mixture was stirred for 6 h under reflux. The mixture was cooled to RT, filtered, washed with 100 mL of ethanol, and dried at 80 °C overnight.

The same reaction conditions were used for the reaction with 3-iodopropyltrimethoxysilane (IPTMS).

[196] I. Rodriguez, S. Iborra, A. Corma, F. Rey, J. L. Jorda, *Chem. Commun.* **1999**, 593.

Bromopropyltrichlorosilane (BPTCS):

A suspension of 1 g of predried (80 °C, 3 h) MCM-41 in 20 mL of dry toluene was prepared and an appropriate amount of BPTCS was added. The slurry was stirred for 6 h at 50 °C. After cooling to RT, the mixture was filtered, washed with 100 mL of ethanol, and dried at 80 °C overnight.

Variation of the synthesis conditions:

Synthesis number	Silane	$T_{Reaction}$ [°C]	Amount of silane [µmol/g]	$t_{Reaction}$ [h]
5.2.3.1	IPTMS	90	100 and 500	6
5.2.3.2	BPTMS	90	100 and 500	6
5.2.3.3	BPTCS	50	100 and 500	6
5.2.3.4	BPTCS	90	100 and 500	6

Table 23 Reaction conditions for halogenoalkyl grafting.

5.2.4 Octadecyl

An amount of 0.5 g of the mesoporous silica (predried at 80 °C, 3 h) was dispersed in 20 mL of dry toluene and an appropriate amount of octadecyltrimethoxysilane (ODTMS) and triethylamine (0.1 mL, 1 mmol) was added. The slurry was stirred under reflux for 24 h. After filtration, the product was washed with 100 mL of ethanol and dried at 60 °C overnight.

Variation of the synthesis conditions:

Synthesis number	$t_{Reaction}$ [h]	Amount of triethylamine [mL/g (silica)]
5.2.4.1	3	--
5.2.4.2	24	--
5.2.4.3	24	0.2

Table 24 Reaction conditions for octadecyl grafting.

5.2.5 Propionitrile

An amount of 1 g of predried (80 °C, 3 h) MCM-41 was suspended in 30 mL of dry toluene and an appropriate amount of triethoxysilylpropionitrile (TESPN) was added. The mixture was heated under reflux for 3 h. After cooling to RT, it was filtered, washed with 100 mL of ethanol, and dried at 80 °C overnight.

5.2.6 Carboxyl

An amount of 0.5 g of TESPN modified mesoporous silica (after 5.2.5.), which was predried for 3 h at 80 °C, was suspended in 27 mL of 50 wt% H_2SO_4 and heated under reflux for 3 h. After cooling to RT, the mixture was filtered, washed with 100 mL of water and 100 mL of ethanol. The product was dried at 80 °C overnight.

5.2.7 Silylation

An amount of 0.5 g of predried (80 °C, 3 h) mesoporous silica was dispersed in 25 mL of dry toluene. Trimethylchlorosilane (TMCS) (5 mL, 36 mmol) and pyridine (5 mL, 62 mmol) were added and the dispersion was heated under reflux for 24 h. After cooling to RT, the mixture was filtered and washed with 100 mL of dichloromethane and 100 mL of ethanol. The product was dried at 80 °C overnight.

The same reaction procedure with specific variations (Table 25) was applied for octyldimethylchlorosilane (ODMCS), phenyldimethylchlorosilane (PDMS) and trimethylmethoxysilane (TMMS).

Variation of the synthesis conditions:

Synthesis number	Silane	Amount of silane [mL/g]	$T_{Reaction}$ [°C]	Added amine, Volume [mL/g]
5.2.7.1	TMCS	10	Reflux	Pyridine, 10
5.2.7.2	ODMCS	10	Reflux	Pyridine, 10
5.2.7.3	PDMCS	10	Reflux	Pyridine, 10
5.2.7.4	TMMS	10	RT	Triethylamine, 10
5.2.7.5	TMMS	10	Reflux	Triethylamine, 10
5.2.7.6	TMMS	10	Reflux	Pyridine, 5

Table 25 Reaction conditions for alkyl- and phenyl grafting.

5.3 Synthesis of organic dyes

5.3.1 Synthesis of nile red

5.3.1.1. 5-Diethylamino-2-nitrosophenol (DNP)[197]

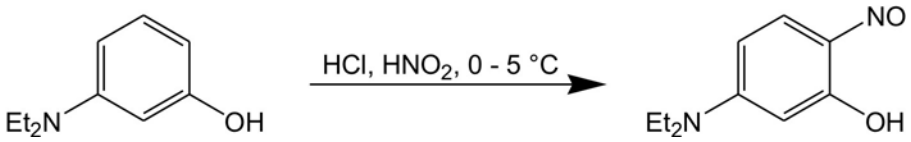

3-Diethylaminophenol (3.36 g, 20 mmol) was dissolved in 8 mL of 32 % aqueous HCl and 20 g of ice. Under stirring, a solution of $NaNO_2$ (1.68 g, 24 mmol) in 6 mL of water was added dropwise (during 1 h) to the above solution and the temperature was kept between 0 and 5 °C. The resulting brown slurry was stirred for 2 h. Following filtration and washing with 10 mL of 4 M aqueous HCl, the product was dried under vacuum and recrystallized with 150 mL of ethanol. A suspension was formed after addition of 20 mL of diethylether which was cooled to 0 °C and kept overnight for further crystallization. The precipitate was filtered, washed with a few milliliters of ethanol and dried under vacuum yielding a yellow product (DNP hydrochloride) (3.33 g, 14 mmol, 71 %). The DNP hydrochloride can be converted to the free compound by diluting in 100 mL of 0.1 M aqueous $NaHCO_3$, followed by an extraction with 100 mL and two times 50 mL of dichloromethane, with subsequent drying of the organic phase over Na_2SO_4.

^{13}C NMR (400 MHz, [$^2H_6$]DMSO) δ 169.6, 158.0, 150.1(C), 135.4, 116.3, 96.0(CH), 46.5, 14.9(NCH_2CH_3).

^{1}H NMR (400 MHz, [$^2H_6$]DMSO) δ 7.32(1H, d, J = 10 Hz), 6.90-6.87(1H, m), 5.74(1H, d, J = 3 Hz), 3.60-3.58(4H, m), 1.20(6H, t, J = 7.2 Hz).

IR (KBr)/cm^{-1}: 2980, 2937, 1629, 1514.

$C_{10}H_{14}N_2O_2$ (194.23g/mol): calcd. C: 61.8 N: 14.4 H: 7.3; found C: 61.9 N: 14.5 H: 7.4.

[197] Autorenkollektiv, Organikum, Wiley-VCH Verlag GmbH, Weinheim, **2001**, 392.

5.3.1.2. 9-Diethylamino-2-hydroxy-5*H*-benzo[*a*]phenoxazin-5-one (HNR)[198]

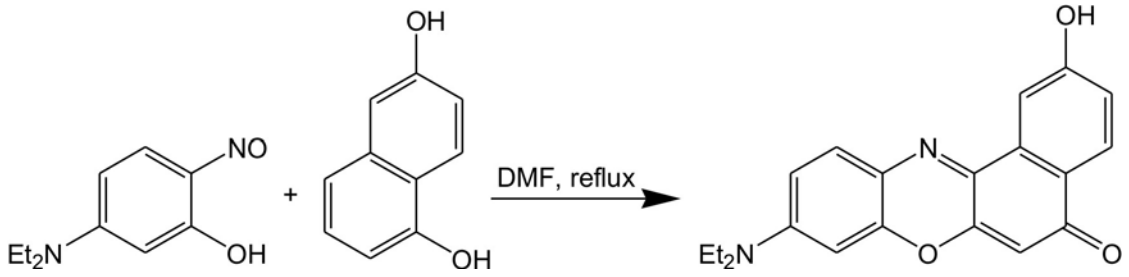

DNP hydrochloride (1.28 g, 5.5 mmol) and 1,6-dihydroxynaphthalene (0.90 g, 5.6 mmol) were dissolved in dry DMF and heated for 4 h under reflux. The solvent was removed under reduced pressure to yield a dark blue-green solid. Subsequent purification by column chromatography (ethyl acetate/isopropanol 4:1) resulted in a dark brown solid (0.66 g, 2.0 mmol, 36 %).

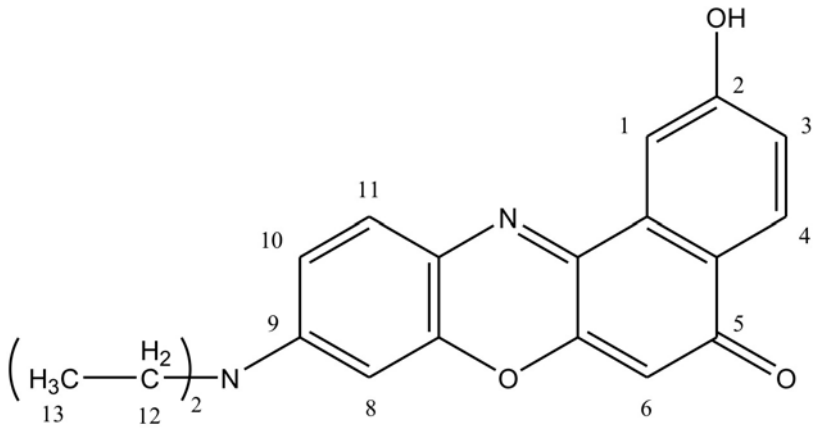

^{13}C NMR (500 MHz, [$^2H_6$]DMSO) δ 182.5(CO), 161.5, 152.5, 151.6, 147.3, 139.6, 134.6(C), 131.7, 128.3(CH), 124.8(C), 119.3, 110.8, 109.0, 105.0, 97.0(CH), 45.3, 13.3(NCH_2CH_3).
^{1}H NMR (500 MHz, [$^2H_6$]DMSO) δ 10.41(1H, s, OH), 7.98(1H, d, J = 8.5 Hz, 4-H), 7.89(1H, d, J = 2 Hz, 1-H), 7.59(1H, d, J = 9.5 Hz, 11-H), 7.10 (1H, dd, J = 8.5 Hz and 2.5 Hz, 3-H), 6.82(1H, dd, J = 9 Hz and 2.5 Hz, 10-H), 6.64(1H, s, J = 2.5 Hz, 8-H), 6.15(1H, s, 6-H), 3.52(4H, q, J = 7 Hz, 12-H), 1.18(6H, t, J = 7 Hz, 13-H).

[198] M. S. J. Briggs, I. Bruce, J. N. Miller, C. J. Moody, A. C. Simmonds, E. Swann, *J. Chem. Soc., Perkin Trans. 1* **1997**, 1051.

5.3.1.3. 9-Diethylamino-5-oxo-5*H*-benzo[*a*]phenoxazin-2-yl-(5-carboxy)-pentanoate[198]

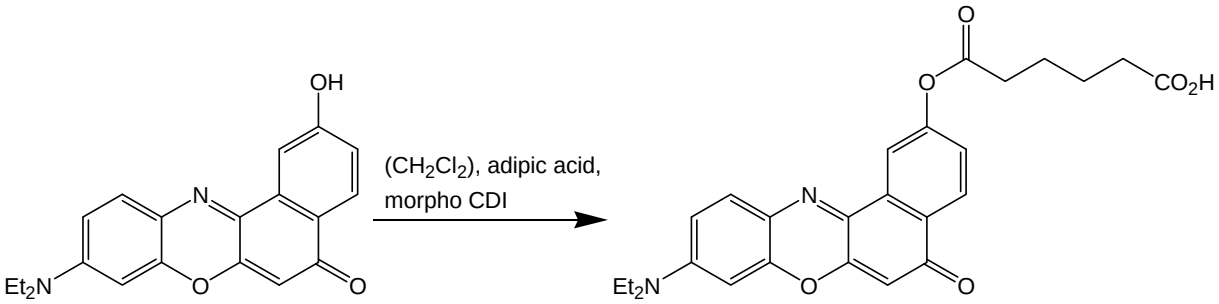

HNR (97 mg, 0.29 mmol), 1-cyclohexyl-3-(2-morpholinoethyl)carbodiimide, metho-*p*-toluenesulfonate (morpho CDI) (191 mg, 0.45 mmol) and adipic acid (51 mg, 0.35 mmol) were added to 30 mL of dichloromethane. A catalytic quantity of 4-dimethylaminopyridine (~5 mg) was added and the mixture was stirred under nitrogen for 20 h. The crude mixture was washed three times with 20 mL of water, dried with Na_2SO_4 and concentrated. The raw material was purified by column chromatography (ethyl acetate) to yield a dark red product.

^{13}C NMR (500 MHz, $CDCl_3$) δ 182.8, 171.4(-CO), 153.1, 152.3, 150.9, 146.8, 138.9, 133.7(C), 131.2(-CH), 129.4(C), 127.6(-CH), 124.8(C), 123.5, 116.3, 109.8, 105.4, 96.0(-CH), 45.1(-CH_2CH_3), 34.0, 29.7, 24.3, 22.7(-CH_2), 12.6(-CH_2CH_3).
^{1}H NMR (500 MHz, $CDCl_3$) δ 8.32-8.31(2H, 1-H and 4-H), 7.42(1H, d, J = 10 Hz, 11-H), 7.39(1H, dd, J = 9 Hz and 3 Hz, 3-H), 6.59(1H, dd, J = 9 Hz and 3 Hz, 10-H), 6.41(1H, d, J = 3 Hz, 8-H), 6.29(1H, s, 6-H), 3.47(4H, q, J = 7 Hz, 12-H), 2.74(2H, m, $COCH_2$), 2.01(2H, m, $COCH_2$), 1.23(6, m, 13-H).

5.3.2 Synthesis of spiropyran

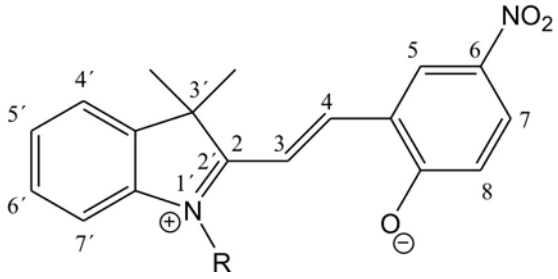

5.3.2.1. 1-(3-Carbomethoxypropyl)-3,3-dimethyl-2-methyleneindoline[199]

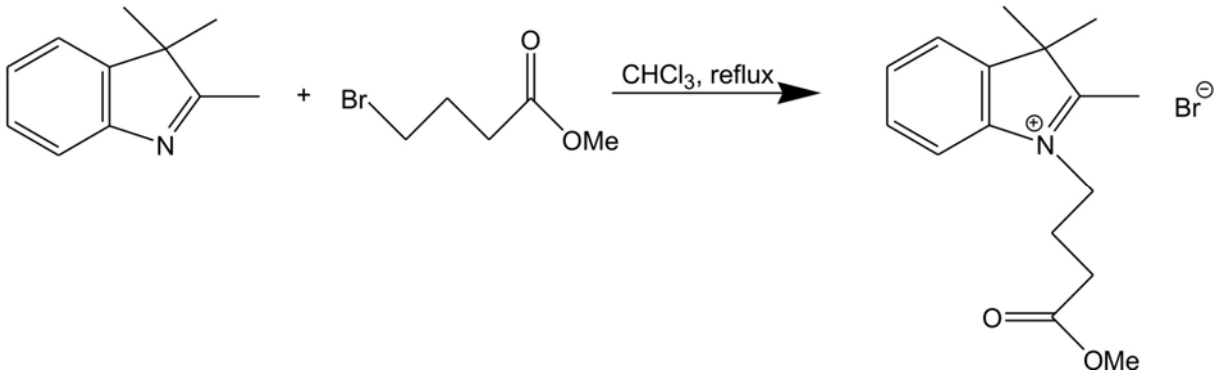

2,3,3-Trimethylindolenine (4.39 g, 28 mmol) was dissolved in 10 mL of chloroform and methyl-4-brombutyrate (5.04 g, 28 mmol) was added dropwise. The solution was heated under reflux for 20 h. The solvent was removed under vacuum and the residue was washed with 150 mL of diethyl ether and recrystallized from a mixture of diethyl ether and methanol (1:3) to yield the product (2.92 mg, 11 mmol, 40 %).

^{13}C NMR (500 MHz, $CDCl_3$) 196.3(-CO), 173.2, 141.5, 141.1(C), 130.1, 129.7, 123.0, 115.7 (-CH), 58.5(C), 54.6, 52.0, 48.6(-CH_2), 30.2, 23.1, 22.8, 18.4(-CH_3).

^{1}H NMR (500 MHz, $CDCl_3$) δ 7.99–7.54(4H, m, Ar-H), 4.93(2H, t, J = 8Hz, -C*H*$_2$CH$_2$CH$_2$COOCH$_3$), 3.66(3H, s, -COOCH$_3$), 3.20(3H, s, 2-CH$_3$), 2.76(2H, t, J = 6 Hz, -CH$_2$CH$_2$C*H*$_2$COOCH$_3$), 2.28(2H, m, -CH$_2$C*H*$_2$CH$_2$COOCH$_3$), 1.64(6H, s, 3-CH$_3$).

[199] A. A. Garcia, S. Cherian, J. Park, D. Gust, F. Jahnke, R. Rosario, *J. Phys. Chem. A* **2000** *26*, 6103.

5.3.2.2. 1´-(3-Carbomethoxypropyl)-3´,3´-dimethyl-6-nitrospiro[2*H*-1]benzopyran-2,2´-indoline (SPCOOMe)[200]

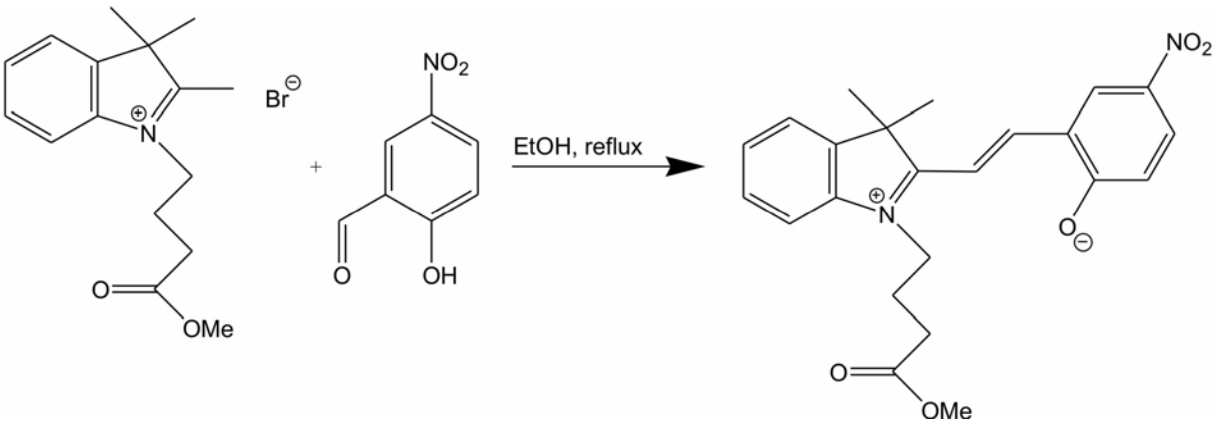

5-Nitrosalicylaldehyde (1.78 g, 11 mmol) was dissolved in 32 mL of ethanol and a solution of the quaternary salt of 1-(3-carbomethoxypropyl)-3,3-dimethyl-2-methyleneindoline (3.63 g, 14 mmol) in 80 mL of ethanol was added dropwise over 80 min. The mixture was heated under reflux for 6 h, subsequently cooled to RT and afterwards further to 0 °C in an ice bath. The mixture was filtered and washed with ethanol. The resulting solid was dissolved in 75 mL of dichloromethane and washed three times with 15 mL of 10 % aqueous sodium carbonate. The product was dried with sodium sulphate and the solvent was removed under vacuum. The raw product was recrystallized in 30 mL of ethanol to yield a yellow-green solid (2.07 g, 5 mmol, 48 %).

^{13}C NMR (500 MHz, [$^2H_6$]DMSO) δ 173.5(CO), 159.5, 147.0, 140.9, 135.9(C), 128.2, 127.8, 125.9, 122.7, 121.8, 121.7, 119.6(CH), 118.4(C), 115.5, 106.9(CH), 106.7(C), 58.4(CH_3), 52.6(C), 51.6, 31.4, 25.9(CH_2), 18.4(CH_3).
^{1}H NMR (500 MHz, [$^2H_6$]DMSO) δ 8.01(2H, m, H-5 and H-7), 7.19(1H, t, J = 7 Hz, H-6`), 7.09(1H, d, J = 7 Hz, H-4`), 6.90(2H, m, H-4 and H-5`), 6.74(1H, d, J = 9 Hz, H-8), 6.64(1H, d, J = 8 Hz, H-7`), 5.87(1H, d, J = 10 Hz, H-3), 3.62(3H, s, $COOCH_3$), 3.21(2H, m, N-C$H_2$$CH_2CH_2$), 2.37(2H, m, N-$CH_2CH_2CH_2$), 1.99(2H, m, N-$CH_2CH_2CH_2$), 1.26(3H, s, 3`-$CH_3$), 1.17(3H, s, 3`-$CH_3$).

[200] R. Rosario, D. Gust, M. Hayes, F. Jahnke, J. Springer, A. A. Garcia, *Langmuir* **2002**, *18*, 8062.

5.3.2.3. 1´-(3-Carboxypropyl)-3´,3´-dimethyl-6-nitrospiro-[2*H*-1]-benzopyran-2,2´-indoline (SPCOOH)[200]

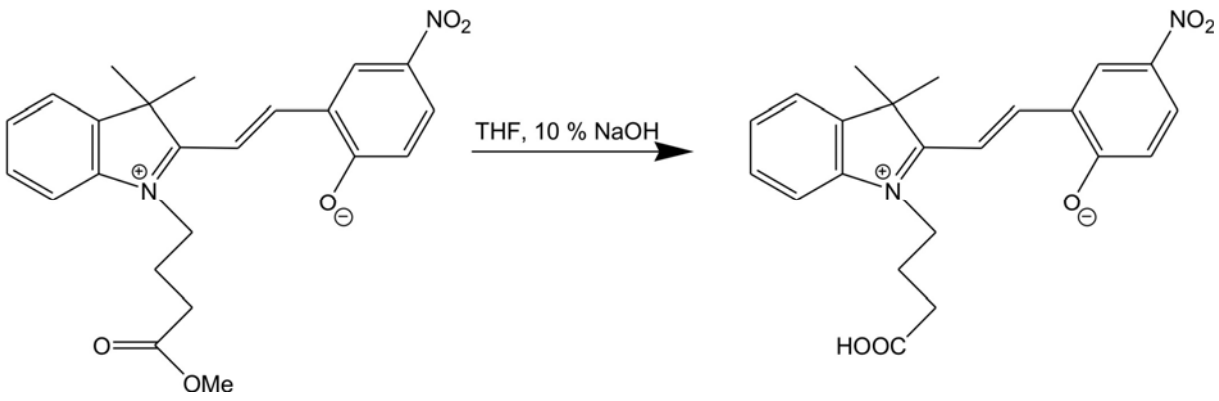

1-(3-Carbomethoxypropyl)-3,3-dimethyl-2-methyleneindoline (360 mg, 0.88 mmol) was dissolved in 13 mL of THF and 3 mL of 10 % aqueous sodium hydroxide was added. The mixture was stirred at RT for 26 h and was subsequently quenched with 6 mL of 10 % aqueous citric acid. The product was extracted two times with 20 mL and once with 10 mL of chloroform and the combined organic phases were dried with sodium sulphate. Removing of the solvent under vacuum yields a red product (350 mg, 0.88 mmol, ~100%).

^{1}H NMR (500 MHz, [$^{2}H_6$]DMSO) δ 8.00(2H, m, H-5 and H-7), 7.17(1H, m, H-6´), 7.08(1H, d, J = 7 Hz, H-4´), 6.89(2H, m, H-4 and H-5´), 6.73(1H, d, J = 9 Hz, H-8´), 6.62(1H, d, J = 8 Hz, H-7´), 5.86(1H, d, J = 10 Hz), 3.23(2H, m, N-C*H*$_2$CH$_2$CH$_2$), 2.39,(2H, m, N-CH$_2$CH$_2$C*H*$_2$), 1.99(2H, m, N-CH$_2$C*H*$_2$CH$_2$), 1.26(3H, s, 3`-CH$_3$), 1.16(3H, s, 3`-CH$_3$).

5.4 Grafting of fluorescent dyes to the silica surface

5.4.1 Coupling with spiropyran[200]

An amount of typically 250 mg of predried (3 h, 80 °C) amino functionalized mesoporous silica was dispersed in 25 mL of ethanol and SPCOOH (15 mg, 38 μmol) was added. The suspension was flushed with nitrogen for 5 min and 1-ethyl-3-(3-(dimethylamino)propyl)-carbodiimide (EDC) hydrochloride (40 mg, 0.2 mmol) was added. After stirring at RT for 4 h, the product was filtered, washed with 100 mL of ethanol and dried at 80 °C overnight.

5.4.2 Grafting of nile red by different linking groups

5.4.2.1. Ether bond

An amount of typically 250 mg of predried (3 h, 80 °C) halogenopropyl modified mesoporous sample was dispersed in 5 mL of dry DMF. HNR (20 mg, 60 μmol) and potassium carbonate (40 mg, 0.4 mmol) were added and the slurry was stirred for 4 h at 100 °C (5.4.2.1.1) or for 24 h at RT (5.4.2.1.2). The mixture was filtered and washed with 100 mL 0.1 N hydrochloric acid. The product was dispersed in 20 mL of water and centrifuged. The process was repeated three times until the water showed a pH ≥ 6. The sample was subsequently washed with 100 mL of ethanol and than extracted with ethanol in a Soxhlet (or washed with 100 mL of dichloromethane). The product was dried at 80 °C overnight.
The procedure is based on ref. 201.

5.4.2.2. Amide bond

An amount of 0.5 g of predried (3 h, 80 °C) 3-aminopropyl functionalized MCM-41 and DNR (3.2 mg, 7 μmol) were dispersed in 25 mL of ethanol and the solution was flushed with nitrogen for 5 min. EDC (74 mg, 0.5 mmol) was added and the suspension was stirred for 4 h at RT. The product was filtered, washed with 100 mL of ethanol and dried subsequently at 80 °C.

[201] A. B. Descalzo, M. D. Marcos, C. Monte, R. Martínez-Máñez, K. Rurack, *J. Mater. Chem.* **2007**, *17*, 4716.

5.4.2.3. Ester bond

HNR (30 mg, 89 μmol) was added to a dispersion of 200 mg functionalized MCM-41 (5.2.6) in 20 mL of dichloromethane. The mixture was stirred under nitrogen and dicyclohexylcarbodiimide (DCC) (40 mg, 193 μmol) and 4-(dimethylamino)pyridine (DMAP) (10 mg, 82 μmol) were added. The dispersion was stirred at RT for 18 h and was subsequently filtered. The product was washed with 100 mL of ethanol, 100 mL of dichloromethane and again with 100 mL of ethanol and dried at 80 °C overnight.
The stability was evaluated by Soxhlet extraction with ethanol for at least 16 h.

5.4.3 Coupling of fluorescein isothiocyanate[202]

About 80 mg of 3-aminopropyl functionalized mesoporous silica was dispersed in 25 mL of absolute ethanol containing an at least 1.5-fold excess of fluorescein isothiocyanate isomer I (FITC). The amount of FITC was calculated assuming quantitative grafting of the respective aminopropylsilane (about 8 mg of FITC for a batch prepared with a theoretical aminopropylsilane loading of 100 μmol per gram of MCM-41). After the suspension had been stirred in the dark at RT for 24 h, the colored product was recovered by filtration. Prolongation of the FITC coupling time did not lead to further fluorescein binding, indicating that complete labeling of the amino groups was obtained after 24 h. To ensure removal of unreacted FITC, the product was washed with 50 mL of ethanol, and finally dried at 80 °C.

[202] H. Salmio, D. Brühwiler, *J. Phys. Chem. C* **2007**, *111*, 923.

5.5 Co-Condensation

5.5.1 Spiropyran co-condensed in MCM-41

5.5.1.1. Coupling of spiropyran with APTES

A specific amount of SPCOOH (1.5 eq.) was dissolved in 5-8 mL of ethanol. APTES (1 eq.) was added dropwise to the purple solution under constant stirring and subsequently EDC (1 eq.) was added. The mixture was stirred for 2 to 4 h at RT. After reducing to about 2 mL, TEOS (5 ml, 22 mmol) was added by constant stirring and the mixture was used directly in 5.5.1.2.

5.5.1.2. Co-condensation

CTAB (1.10 g, 3.0 mmol) was dissolved in a mixture of 26 mL of water and 12 mL of aqueous ammonia (25 %) under slight warming. After cooling to RT, the mixture of APTES coupled spiropyran and TEOS (5.5.1.1) was added slowly. The slurry was stirred for 3 h at RT and aged for 48 h. Finally, the product was recovered by filtration, washed with copious amounts of water (at least 1 L) and dried at RT overnight.

5.5.1.3. Extraction

An amount of 1 g of the as-synthesized co-condensed MCM-41 was suspended in 150 mL of an ethanolic solution of NH_4NO_3 (2 g/L) and heated at 60 °C for 15 min. The silica was filtered off and washed with 50 mL of ethanol. The product was finally dried at 80 °C overnight.

5.5.2 SBA with iodopropyl groups

P123 (2 g, ~0.3 mmol) was dissolved in 80 mL of water and 580 µl of hydroiodic acid (55-58 %) (pH ~ 1.5) in a period of about 2 h. The template solution was poured into a 250 mL flask loaded with TEOS (4.75 mL, 21 mmol), 3-iodopropyltrimethoxysilane (IPTMS) (29.6 µL, 0.15 mmol) and a specific amount of X-trimethoxysilane. The solution was stirred at RT for 1.5 h and heated at 60 °C. Sodium fluoride (~40 mg) was added to the clear solution to start the polycondensation. The mixture was stirred for 72 h at 60 °C and afterwards cooled to RT, filtered and washed with 200 mL of acetone. To remove possible residues of template, the product was extracted with hot ethanol in a Soxhlet for at least 24 h.
The amount of iodo groups was estimated by elemental analysis.

5.5.3 HNR co-condensed in SBA-15

HNR (17 mg, 50 µmol) was dissolved in 1 mL of DMF. IPTMS (10 µL, 50 µmol) and potassium carbonate (18 mg, 125 µmol) were added. The mixture was heated to 50 °C and stirred for 24 h under nitrogen. After cooling to RT, a volume of 2 mL of ethanol was added. After short stirring, TEOS (5 mL, 22 mmol) was added to the reaction mixture.
The template solution was prepared by dissolving P123 (2.2 g, 0.4 mmol) in 31 mL of 4 N HCl and 39 mL of water by stirring for about 2 h.
The solution of TEOS and coupled HNR (with IPTMS) was added dropwise to the template solution under vigorous stirring. The resulting dispersion was stirred for 20 h, transferred to a teflon-lined autoclave and heated under static conditions at 100 °C for 24 h. After cooling to RT, the product was recovered by filtration, washed with copious amounts of water (at least 1 L) and dried at RT overnight.
The template was removed by extraction with ethanol in a Soxhlet for 24 h.

5.6 Adsorption from solution/dispersion

5.6.1 Nile red

A standard solution of NR in pentane (11 mg/L) was prepared. A volume of 20 mL of the stock solution was added to 100 mg of predried (3 h, 80 °C) mesoporous silica. The mixture was stirred for 1 h. The product was recovered by filtration and dried at 80 °C overnight.

5.6.2 Resorufin

To a predried (3 h, 80 °C) quantity (typically 100 mg or 1 g) of TMSTAC modified MCM-41, a volume of 20 mL of a stock solution of resorufin sodium salt in 1-butanol (about 450 µmol/L) was added. After stirring for 1 h at RT, the mixture was filtered and the product was washed with 10 mL of ethanol. The solid was dispersed in 25 mL of ethanol for 30 min and subsequently filtered off, washed with 20 mL of ethanol and dried at 80 °C overnight.

5.6.3 Dimethylaminobenzonitrile (DMABN)

An amount of 100 mg of predried (3 h, 80 °C) MCM-41 was dispersed in a volume of 20 mL of a solution of 100 mg/L DMABN in pentane. The mixture was stirred for 1 h and subsequently filtered. The product was dried at 80 °C overnight.

5.6.4 4,4´-Diaminodiphenyl sulfone (DAPS)

An amount of 100 mg of predried (3 h, 80 °C) MCM-41 was dispersed in a volume of 20 mL of a solution of 300 mg/L DAPS in chloroform. The mixture was stirred for 1 h and subsequently filtered. The product was dried at 80 °C overnight.

5.6.5 CdSe/ZnS quantum dots

Under continuous stirring and ultrasonification (~5 min), a weighed quantity of typically about 1 mg of CdSe/ZnS QD´s (PlasmaChem GmbH, Berlin) was dispersed in 1 mL of chloroform. This stock solution was diluted to a specific concentration and a distinct amount of this dispersion was added to a mixture of 50 mg of ODTMS functionalized SBA in 5 mL of 1-butanol. The mixture was stirred for 24 h, the solvent was removed by centrifugation and the product was washed two times by dispersing in 5 mL of 1-butanol and removal of the solvent by centrifugation. The product was dried at 60 °C overnight.

5.7 Determination of dye contents

5.7.1 Dissolving in $NaOH_{(aq)}$

5.7.1.1. HNR modified silica

A weighed amount of 10 - 20 mg of the predried (12 h at 60 °C) NR coupled silica was dispersed in a volume of 20 mL of a solution of 0.1 N $NaOH_{(aq)}$ and EtOH (V% = 1:1). The slurry was stirred at RT for 1 h. Afterwards it was centrifuged to remove possible residues (especially for hydrophobic samples) and the amount of NR in the coloured and clear solution was determined by measuring the UV/Vis absorption spectrum (λ = 541 nm, ε = 22000 L mol^{-1} cm^{-1}).

5.7.1.2. Fluorescein isothiocyanate modified silica[202]

A weighed quantity of typically 15-30 mg of the predried (12 h at 60 °C) fluorescein isothiocyanate isomer I functionalized silica was dispersed in 25 mL of 0.2 N $NaOH_{(aq)}$ and stirred for 3 h at RT. After dissolution of the silica, the clear solution was diluted with water, and the fluorescein concentration was determined by measuring the UV/Vis absorption spectrum (λ = 490 nm, ε = 88000 L mol^{-1} cm^{-1}).

5.7.1.3. Resorufin loaded silica

A weighed amount of typically 10-20 mg of the predried (3 h, 80 °C) resorufin loaded silica was dispersed in 10 mL of 0.02 N $NaOH_{(aq)}$ and stirred for 4 h at RT. The solution was centrifuged to remove possible residues and the amount of Res^- in the clear solution was determined by measuring the UV/Vis absorption spectrum (λ = 571 nm, ε = 72000 L $mol^{-1}cm^{-1}$).

5.7.2 Extraction in ethanol

5.7.2.1. Resorufin loaded silica

A specific amount of about 20 mg of the predried (3 h, 80 °C) resorufin loaded silica was dispersed in a volume of 20 mL of an aqueous solution of 1 N sodium chloride. The dispersion was stirred for 1 h. After centrifugation, the absorption of the clear solution was determined. The absorption spectrum was measured by addition of aqueous sodium carbonate buffer (pH = 9.2) (volume fraction 1:1) (λ = 571 nm, ε = 68000 L $mol^{-1}cm^{-1}$).

5.7.2.2. Nile red loaded silica

A weighed quantity of typically 10-20 mg of predried (3 h, 80 °C) NR loaded silica was dispersed in 25 mL of absolute ethanol and stirred for 1 h. The dispersion was centrifuged and the NR amount was determined by the UV/Vis absorption spectrum of the supernatant solution. (λ = 540 nm, ε = 40000 L mol^{-1} cm^{-1}).

5.8 Instrumentation

Nitrogen sorption

Nitrogen sorption isotherms were collected at 77 K with a Quantachrome NOVA 2200. Samples were vacuum-degassed at 80 °C for 3 h. Mesopore size distributions were evaluated from the adsorption branches of the nitrogen isotherms by means of the BJH method or by NLDFT using a kernel for silica at 77 K based on a cylindrical pore model available from the NOVAWin2 software. The total surface area was calculated by the BET method. The total pore volume (V_{tot}) was determined from the amount of nitrogen adsorbed at a relative pressure of 0.98. Microporosity was examined by use of the *t*-plot method of de Boer[203] or by the α_s-plot method.

IR

IR spectra were recorded in a range of 4000 – 800 cm^{-1} with a Perkin Elmer BX FT-IR spectrometer. The samples were measured as potassium bromide discs.

Elemental analysis

Elemental (CHN) analysis of the mesoporous materials was performed with a LECO CHNS-932. The iodine content of the samples was analyzed according to the Schöniger method.[204,205]

UV/Vis

Absorption spectra in the range between 200 and 800 nm were acquired on a CARY 300 and CARY 50.

---

[203] J. H. de Boer, B. G. Linsen, T. Van der Plaas, G. J. Zondervan, *J. Catal.* **1965**, *4*, 649.
[204] W. Schöniger, *Microchim. Acta* **1955**, *43*, 123.
[205] Iodine contents were estimated at laboratory of organic chemistry at the ETH Zürich.

^{13}C-NMR and ^{1}H-NMR

NMR spectra were recorded using a DRX-500 and a GEMINI-Varian instrument.

SEM

Scanning electron microscopy images were acquired on a JEOL JSM-6060.

Luminescence

Photoluminescence spectra were recorded with a Perkin-Elmer LS50B spectrofluorometer equipped with a front surface accessory for the measurement of powdered samples.

Confocal microscopy[206]

Two slightly different confocal microscope setups were used. The common scheme is shown in Figure 66. The optical measurements were performed with a modified inverted confocal microscope (Zeiss Axiovert 135 TV) using a high-numerical aperture immersion oil objective (Zeiss Plan Neofluar, 100/NA = 1.3). The term inverted refers to the fact that the polymer film with the porous silica spheres was on the opposite side of the cover slide with respect to the objective. An ultra fast laser system (Picoquant, model LDH-P-C470) operating at $\lambda = 473$ nm (2.62 eV) and providing pulses at a repetition rate of 10 MHz with a width of 300 ps served as excitation source for the measurement of fluorescence spectra. In order to discriminate against the stray light from the laser, the setup was equipped with a long-wave pass filter having its 50 % transmission value at 510 nm. Fluorescence spectra were acquired with a spectrograph (Acton Research SpectraPro 300i) equipped with a CCD camera (Princeton Instruments, model LNCCD-1340/100-EB/1).

[206] Confocal microscopy was performed at the University of Tübingen in the group of Prof. Dr. A. Meixner by Dipl. Phys. A. Chizhik.

To investigate the orientation of the quantum dots TDM, a similar custom-built confocal microscope setup additionally equipped with a mode conversion optical line for generation of azimuthally polarized laser beams was used.[207] The porous silica spheres with included quantum dots were excited at $\lambda = 488$ nm (2.54 eV) in the diffraction limited laser focus of the NA = 1.25 immersion oil objective. The typical image size was 200 × 200 pixels distributed over 2 × 2 or 5 × 5 µm. For each pixel, the signal was integrated over 5 ms, resulting in a acquisition time of 200 s. Monodirectional scanning process doubles this time to the value of 400 s for one fluorescence image.

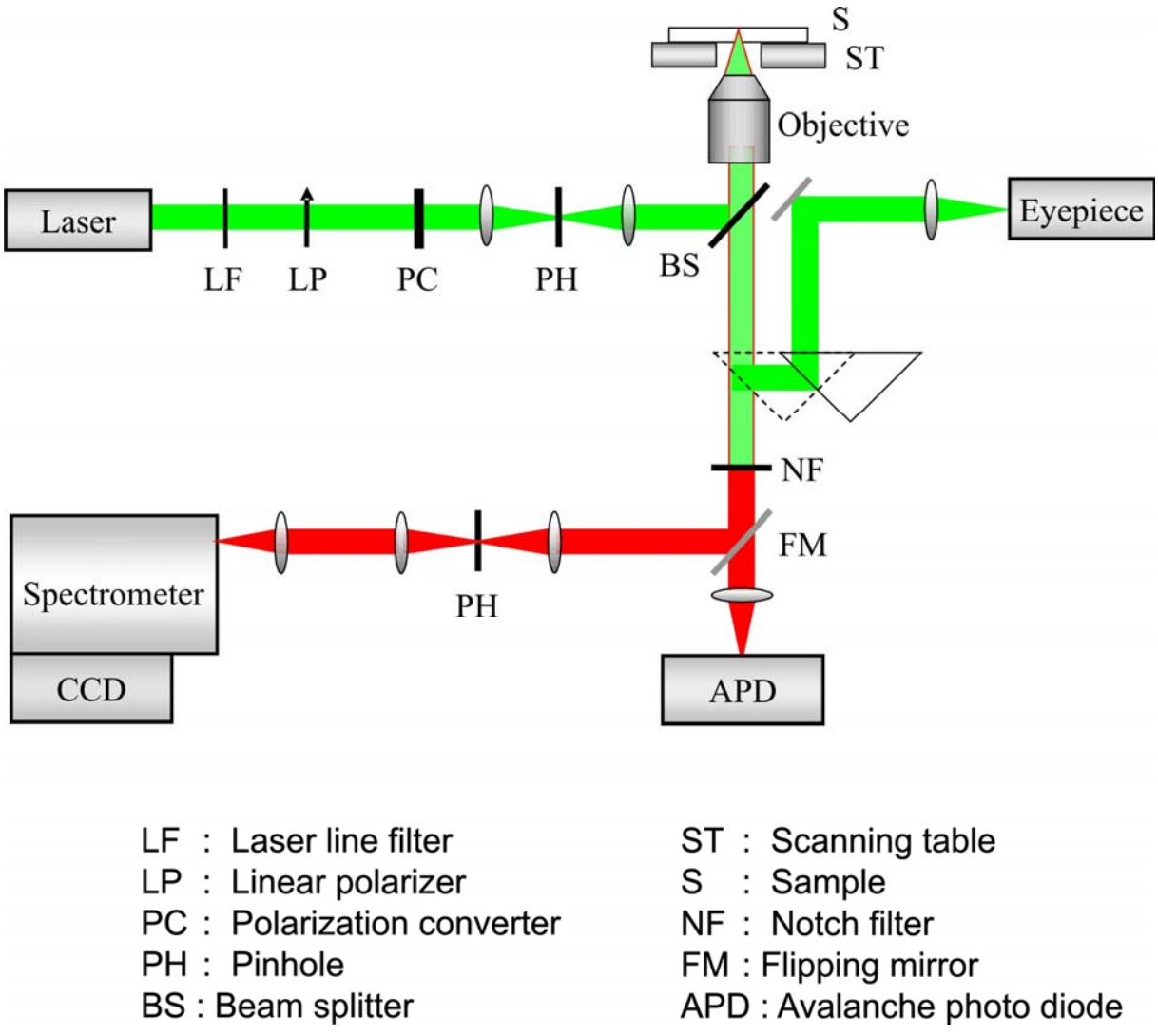

Figure 66 Experimental setup of the confocal microscope.

[207] L. Novotny, M. R. Beversluis, K. S. Youngworth, T. G. Brown, *Phys. Rev. Lett.* **2001**, *86*, 5251; R. Dorn, S. Quabis, G. Leuchs, *Phys. Rev. Lett.* **2003**, *91*, 233901; A. V. Failla, H. Qian, H. Qian, A. Hartschuh, A. J. Meixner, *Nano Lett.* **2006**, *6*, 1374.

Appendix

List of abbreviations

General:

BET	Brunauer, Emmett, Teller
BJH	Barrett, Joyner, Halenda
CNT	Carbon NanoTube
CSDA	Co-Structure Directing Agent
DDS	Drug Delivery System
DFT	Density Functional Theory
EISA	Evaporating Induced Self Assembly
FSM	Folded Sheet Material
HK	Horvath Kawazoe
HMC	protonated SpiroPyran
HSP	protonated MeroCyanine
LBPC	Laser Beam Polarization Conversion
LCT	Liquid Crystal Templating
LE	Locally Excited state
MC	MeroCyanine
MCM	Mobil Composition of Matter
NLDFT	Non Linear Density Functional Theory
PEO	PolyEthyleneOxide
PICT	Pseudo Intramolecular Charge Transfer
PMO	Periodic Mesoporous Organosilica
PSD	Pore Size Distribution
QD	Quantum Dot
RICT	Rehybridised Intramolecular Charge Transfer
RTMS	Alkyltrimethoxysilane
SBA	Santa Barbara Amorphous
SDA	Structure Directing Agent
SEM	Scanning Electron Microscopy
SF	Saito, Foley
SP	SpiroPyran
TDM	Transition Dipole Moment

TICT	Twisted Intramolecular Charge Transfer
TSE	Tensile Strength Effect
TTC	Trans-Trans-Cis-form
XRD	X-Ray Diffraction

Compounds:

APDIPES	3-Aminopropyldiisopropylethoxysilane
APTMS	3-Aminopropyltrimethoxysilane
APTES	3-Aminopropyltriethoxysilane
BPTCS	3-Bromopropyltrichlorosilane
BPTMS	3-Bromopropyltrimethoxysilane
CTAB	Hexadecyltrimethylammonium bromide
DAPS	4,4`-Diaminodiphenyl sulfone
DCC	Dicyclohexylcarbodiimide
DMABN	Dimethylaminobenzonitrile
DMAP	4-(Dimethylamino)pyridine
DMF	Dimethylformamide
DNP	Diethylamino-2-nitrosophenol hydrochloride
DNR	9-Diethylamino-5-oxo-5*H*-benzo[*a*]phenoxazin-2-yl-(5-carboxy)-pentanoate
DPDCS	Diphenyldichlorosilane
EDC	1-Ethyl-3-(3-(dimethylamino)propyl)carbodiimide
FITC	Fluorescein isothiocyanate isomer I
HNR	9-Diethylamino-2-hydrox-5*H*-benzo[*a*]phenoxazin-5-on
IBTMS	Isobutyltrimethoxysilane
iBu	Isobutyl
Ip	Iodopropyl
IPTMS	3-Iodopropyltrimethoxysilane
morpho CDI	1-Cyclohexyl-3-(2-morpholinoethyl)carbodiimide metho-*p*-toluenesulfonate
Me	Methyl
MTMS	Methyltrimethoxysilane
6-NO_2-BIPS	3´,3´-Dimethyl-6-nitrospiro[2*H*-1-]-benzopyran-2,2-indoline

NR	Nile red, 9-Diethylamino-2-hydroxy-5*H*-benzo[*a*]phenoxazine-2-one
Oc	Octyl
Od	Octadecyl
ODMCS	Octyldimethylchlorosilane
ODTMS	Octadecyltrimethoxysilane
OTMS	Octyltrimethoxysilane
P123	Poly(ethylene glycol)-block-poly(propylene glycol)-block-poly(ethylene glycol) ($EO_{20}PO_{70}EO_{20}$)
PDMCS	Phenyldimethylchlorosilane
Ph	Phenyl
PMMA	Poly(methyl methacrylate)
PTMS	Phenyltrimethoxysilane
Res^-	Resorufin anion
ResH	Resorufin
SPCOOH	1′-(3-Carboxypropyl)-3′,3′-dimethyl-6-nitrospiro-[2*H*-1]-benzopyran-2,2′-indoline
SPCOOMe	1′-(3-Carbomethoxypropyl)-3′,3′-dimethyl-6-nitrospiro[2*H*-1]benzo-pyran-2,2′-indoline
TEOS	Tetraethoxysilane, Tetraethyl orthosilicate
TES	Tetraethylsilane
TESPN	3-(Triethoxysilyl)propionitrile
TESPI	3-(Triethoxysilyl)propylisocyanate
TFA	Trifluoroacetic acid
THF	Tetrahydrofuran
TMB	Mesitylene, 1,3,5-Trimethylbenzene
TMCS	Trimethylchlorosilane
TMMS	Trimethylmethoxysilan
TMOS	Tetramethoxysilane
TMSTAC	Trimethoxysilylpropyl(trimethyl)ammonium chloride

Publications and conference contributions

Nanochannels for supramolecular organization of luminescent guests

D. Brühwiler, G. Calzaferri, T. Torres, J. H. Ramm, N. Gartmann, L.-Q. Dieu, I. López-Duarte, M. V. Martínez-Díaz, *J. Mater. Chem.* **2009**, *19*, 8040.

Functionalized silicate nanochannels: Towards applications in drug delivery and solar energy conversion

D. Brühwiler, H. Ritter, J. H. Ramm, L.-Q. Dieu, C. Bauer, I. Dolamic, N. Gartmann, *Chimia* **2009**, *63*, 8.

Direct synthesis and fluorescent imaging of bifunctionalized mesoporous iodopropyl-silica

J. H. Ramm, N. Gartmann, D. Brühwiler, submitted

Self organized patterns of zeolite crystals in polymer films

C. Bauer, L.-Q. Dieu, N. Zuber, N. Gartmann, I. Dolamic, J. H. Ramm, D. Brühwiler, submitted

---

Mesoporous hosts: Recent developments at UZH

Talk at the Marie-Curie RTN Nanomatch, Varenna (Italy) 4^{th} – 6^{th} March 2007

Optical sensing of nanochannel polarity

Talk at the Summer school of the Marie-Curie RTN Nanomatch, Jugowice (Poland) 16^{th} - 21^{st} September 2007.

Mesoporous nile red/silica hybrid materials

Talk at the Marie-Curie RTN Nanomatch, Zürich (Switzerland) 13^{th} – 15^{th} February 2008.

Tuning the properties of mesoporous silica

Talk at the Midterm Meeting of the Marie-Curie RTN Nanomatch, Eindhoven (The Netherlands) 16^{th} - 22^{nd} September 2008.

Functionalization of mesoporous silica

Talk at the Retreat of the CMSZH Graduate School for Chemical and Molecular Sciences Zürich, Grindelwald (Switzerland) 15th-18th January 2009.

Multifunctionalization of silca nanochannels with iodopropyl as anchoring group

Talk at the ESON´09 European Spring School on Supramolecular Organized Nanostructured Materials for Optoelectronic Applications, Peniscola (Spain) 20th April 2009.

Resorufin in the channels of MCM-41: In situ detection of release profiles

J. H. Ramm, D. Brühwiler

Poster at the Fall Meeting of the Swiss Chemical Society, Zürich 13.10.2006; Abstract: *Chimia*, **2006**, *60*, 402.

Optical sensing of nanochannel polarity

J. H. Ramm, D. Brühwiler

Poster at the Fall Meeting of the Swiss Chemical Society, Lausanne 12.9.2007; Abstract: *Chimia* **2007**, *61*, 509.

Postsynthetic Modification of Mesoporous Silica: Methods, Tools, and Perspectives

H. Ritter, J. H. Ramm, N. Gartmann, D. Brühwiler

Poster at the Fall Meeting of the Swiss Chemical Society, Zürich 11.9.2008; Abstract: *Chimia*, **2008**, *62*, 615.

Control and analysis of the functional group distribution on postsynthetically modified mesoporous silica

H. Ritter, J. H. Ramm, N. Gartmann, D. Brühwiler

Poster at the First International Conference on Multifunctional, Hybrid and Nanomaterials, Tours 15th -19th March 2009.

Curriculum Vitae

Surname	Ramm
First name	Jan Hinrich
	12.11.1979 in Otterndorf, Germany
Nationality	German

Education:

since 2005	Dissertation at the University of Zürich;
2003-2005	German Diploma at the TU Bergakademie Freiberg, Institute of Organic Chemistry; Thesis: "Metall-affine Tektone auf der Basis von 2-Hydroxymehtyl)pyridin"; ["Metal-affine tectones on the basis of 2-(hydroxymethyl)pyridine."]
March 2004	Internship at the Alfred-Wegener-Institute for Polar and Marine Research; "Determination of formaldehyde and hydrogen peroxide in arctic ice and snow samples."
1999-2003	Bachelor of Science at the TU Bergakademie Freiberg, Institute of Physical Chemistry; Thesis: "Phasenumwandlung von dotiertem und undotiertem Calciumcarbonat in Medien geringer Wasseraktivität"; ["Phase transition of calcium carbonate in media with low water activity."]
1986-1999	German Abitur at the grammar school Otterndorf.